

**SYNTHESIS AND CHARACTERISATION OF GALLIUM,
MOLYBDENUM AND GALLIUM-MOLYBDENUM DOPED
VANADIUM PHOSPHORUS OXIDE CATALYSTS FOR OXIDATION
OF N-BUTANE TO MALEIC ANHYDRIDE**

By

LING KUAN HOE

**A dissertation submitted to the Department of Chemical Engineering,
Faculty of Engineering and Science,
Universiti Tunku Abdul Rahman,
in partial fulfilment of the requirements for the degree of
Master of Science
March 2015**

ABSTRACT

SYNTHESIS AND CHARACTERISATION OF GALLIUM, MOLYBDENUM AND GALLIUM-MOLYBDENUM DOPED VANADIUM PHOSPHORUS OXIDE CATALYSTS FOR OXIDATION OF *n*-BUTANE TO MALEIC ANHYDRIDE

Ling Kuan Hoe

A series of gallium (Ga), molybdenum (Mo) and gallium-molybdenum (Ga-Mo) doped vanadium phosphate oxide catalysts were prepared via sesquihydrate route (VPOs). The undoped precursor was synthesized by refluxing vanadyl phosphate dihydrate ($\text{VOPO}_4 \cdot 2\text{H}_2\text{O}$) in 1-butanol. In first series, 0.1 mol%, 0.3 mol% and 0.5 mol% of gallium, while 1 mol%, 3 mol% and 5 mol% of molybdenum were added during the synthesis of $\text{VOHPO}_4 \cdot 1.5\text{H}_2\text{O}$ precursors. The key study of the first series is to study the effects of different mole percentage of Ga dopant and Mo dopant on the physicochemical, reactivity and catalytic properties of VPOs catalysts. The undoped, Ga doped and Mo doped precursors were calcined under a flow of 0.75% *n*-butane/air at 733K for 18 h to generate the active vanadyl pyrophosphate ($(\text{VO})_2\text{P}_2\text{O}_7$) catalysts. For second series, 0.1 mol% of Ga was added with 1 mol% of Mo during the synthesis of precursor and activated under different calcination durations, i.e. 18, 36, 54 and 72 h. The physical, reactivity and catalytic studies on the catalysts were performed by using XRD, SEM-EDX, BET, ICP-OES, redox titration, TPR in H_2 and catalytic reactor. The characteristic vanadyl

pyrophosphate phase $(VO)_2P_2O_7$ for the undoped, Ga doped, Mo doped and Ga-Mo doped VPOs catalysts has been confirmed by the XRD analyses for all catalysts, which showed similar diffraction patterns comprised of a well-crystallized $(VO)_2P_2O_7$ phase with three main peaks appeared at $2\theta = 22.8^\circ$, 28.4° and 29.9° corresponded to (0 2 0), (2 0 4) and (2 2 1) planes, respectively. The incorporation of Ga into the VPOs catalysts led the formation of V^{5+} phase, i.e. β -VOPO₄, while another V^{5+} phase, i.e. α -VOPO₄ was found in the Mo doped catalysts, as shown in XRD patterns. The increasing amount of Ga (0.1-0.5 mol%) and Mo (1-5 mol%) into the VPOs catalysts and prolong calcination duration from 18 to 72 h for Ga-Mo doped catalysts gave reducing trend in specific surface area. ICP-OES confirmed that the P/V atomic ratios for synthesised VPOs catalysts were in optimum range (P/V=1.05-1.33) of producing the active $(VO)_2P_2O_7$ catalysts. Catalytic tests revealed that the VPOs catalyst with 0.1 mol% of Ga induced higher activity towards the formation of *n*-butane to maleic anhydride (MA), without scarifying the selectivity of the catalyst, which provide a cleaner process with less by-products throughout the oxidation process. Whereby, the conversion of *n*-butane towards MA was gradually reduced with calcination duration for Ga-Mo doped VPOs catalyst.

ACKNOWLEDGEMENTS

I would like to thank everyone who had contributed to the successful completion of this project. Firstly, I would like to express my gratitude to my research supervisor, Asst. Prof. Dr. Leong Loong Kong of Universiti Tunku Abdul Rahman (UTAR) for his invaluable advice, guidance and his enormous patience throughout the development of the research. Thank you for your kind of helping hands in past and present times in supporting me throughout my doubt and darkness. I am grateful to him for encouraging me to my best and guiding me to the better path in life.

I would also like to express my gratitude to my loving parents who had given me encouragement throughout my ups and downs. Special thanks to my friends Kang Jo Yee and Catherine Loh Pei Xuan who had helped me with their kindness and given me encouragements and supports throughout my postgraduate's studies. Furthermore, I would like to thank my wonderful junior Mr. Prakas a/l Paranychamy for his helping hands and supports.

Great appreciation and truly thanks to Mr. Andy Guee Eng Hwa and Mr. Harry Hau Tien Boon of CNG Instruments Sdn. Bhd. for their kind of advices and technical assistances in running the TPDRO, BET and GC instruments.

In addition, I am grateful to UTAR for giving me this opportunity to carry out my research provided with necessary facilities. I would like to acknowledge that this research was funded by UTAR Research Fund.

Finally, I am indebted to my loving family members for their love, support and encouragement. Their unreserved contributions and patience have been critical to the successful completion of this research and the advancement of my education and future.

APPROVAL SHEET

This dissertation entitled “**SYNTHESIS AND CHARACTERISATION OF GALLIUM, MOLYBDENUM AND GALLIUM-MOLYBDENUM DOPED VANADIUM PHOSPHORUS OXIDE CATALYSTS FOR OXIDATION OF *n*-BUTANE TO MALEIC ANHYDRIDE**” was prepared by LING KUAN HOE and submitted as partial fulfilment of the requirements for the degree of Master of Science at Universiti Tunku Abdul Rahman.

Approved by,

(Asst. Prof. Dr. Leong Loong Kong)

Supervisor

Department of Chemical Engineering

Faculty of Engineering and Science

Universiti Tunku Abdul Rahman

Date: _____

FACULTY OF ENGINEERING AND SCIENCE
UNIVERSITI TUNKU ABDUL RAHMAN

Date: _____

SUBMISSION OF DISSERTATION

It is hereby certified that LING KUAN HOE (ID No: 09UEM09091) has completed this dissertation entitled **"SYNTHESIS AND CHARACTERISATION OF GALLIUM, MOLYBDENUM AND GALLIUM-MOLYBDENUM DOPED VANADIUM PHOSPHORUS OXIDE CATALYSTS FOR OXIDATION OF *n*-BUTANE TO MALEIC ANHYDRIDE"** under the supervision of Asst.. Prof. Dr. Leong Loong Kong from the Department of Chemical Engineering, Faculty of Engineering and Science, Universiti Tunku Abdul Rahman.

I understand that the University will upload softcopy of my dissertation in PDF format into UTAR Institutional Repository, which may be made accessible to UTAR community and public.

Yours truly.

(LING KUAN HOE)

DECLARATION

I hereby declare that this dissertation is based on my original work except for citations and quotations which have been duly acknowledged. I also declare that it has not been previously and concurrently submitted for any other degree or award at UTAR or other institutions.

(LING KUAN HOE)

Date _____

TABLE OF CONTENTS

ABSTRACT	ii
ACKNOWLEDGEMENTS	iv
APPROVAL SHEET	vi
SUBMISSION SHEET	vii
DECLARATION	viii
LIST OF TABLES	xiii
LIST OF FIGURES	xiv
LIST OF ABBREVIATIONS AND SYMBOLS	xvi

CHAPTER

1.0	INTRODUCTION	1
	1.1 History of Catalysts and Catalysis	1
	1.2 Definition of Catalyst	2
	1.3 Important Roles of Catalysis	3
	1.4 Types of Catalysis	4
	1.4.1 Homogeneous Catalysis	4
	1.4.2 Heterogeneous Catalysis	5
	1.5 Selective Oxidation of Light Hydrocarbon	6
	1.6 Essential Properties of Good Catalysts	8
	1.7 Problem Statement	9
	1.8 Objectives	10
2.0	LITERATURE REVIEW	12
	2.1 Maleic Anhydride	12
	2.1.1 The Use of Maleic Anhydride	12
	2.1.2 Worldwide Demand: Maleic Anhydride	13
	2.1.3 The Commercial Process for Maleic Anhydride	14
	2.1.4 Production Technologies of Maleic Anhydride	15
	2.2 VPO Catalyst	19
	2.2.1 The System of $(VO)_2P_2O_7$ Catalyst	20

2.2.2	The Mechanism of Selective Oxidation	23
2.2.3	The Origin of the Selective Oxidation to Maleic Anhydride	26
2.3	Modification of Vanadium Phosphate Catalyst	28
2.3.1	The Catalyst Precursor	29
2.3.2	Sesquihydrate Precursor for $(VO)_2P_2O_7$ Preparation	33
2.3.3	The Effect of Aqueous, Organic and Dihydrate routes on $(VO)_2P_2O_7$ Catalysts	34
2.3.4	Roles of the P/V Ratio	35
2.3.5	The Effect of Promoters	37
2.3.6	Activation Condition of Catalyst Precursor	45
2.3.7	The Effect of Calcination Duration/ Temperature	46
2.3.8	The Effect of Calcination Environment	48
3.0	MATERIALS AND METHODOLOGY	50
3.1	Gases and Materials	50
3.2	Methodology	50
3.2.1	Preparation of Bulk Catalysts via Sesquihydrate Precursor Route (VPOs)	51
3.2.2	Series 1: Preparation of Ga-doped and Mo-doped VPOs Catalysts	52
3.2.3	Series 2: Preparation of Ga-Mo doped VPOs Catalysts with Different Calcination Duration	53
3.3	Characterization of Vanadyl Pyrophosphate Catalysts	55
3.3.1	Gases and Materials	55
3.3.2	Instrumentations and Characterisation Technique	56
3.4	Methodology	57
3.4.1	X-ray Diffraction (XRD) Analyses	57
3.4.2	Scanning Electron Microscopy (SEM) and Energy-Dispersive X-ray (EDX) Spectroscopy	58

3.4.3 Brunauer-Emmett-Teller (BET) Surface Area Measurements	59
3.4.4 Inductively Coupled Plasma-Optical Emission Spectroscopy (ICP-OES)	61
3.4.5 Redox Titration Analyses	62
3.4.6 Temperature-Programmed Reduction (TPR in H ₂) Analyses	63
3.4.7 Catalytic Tests	64
4.0 RESULTS AND DISCUSSION	66
4.1 Series 1: Effect of Ga and Mo dopants on the Physico-chemical and Catalytic Properties of Vanadyl Pyrophosphate Catalysts	66
4.1.1 Series 1: XRD Analyses	66
4.1.2 Series 1: SEM Analyses	71
4.1.3 Series 1: BET Surface Area Measurements and Chemical Analyses	73
4.1.4 Series 1: Temperature-Programmed Reduction (TPR in H ₂) Analyses	77
4.1.5 Series 1: Catalytic Oxidation of <i>n</i> -Butane to Maleic Anhydride	83
4.1.6 Series1: Conclusions	86
4.2 Series 2: Effect of Different Calcination Duration on the Physico-chemical and Catalytic Properties of Ga-Mo Doped Vanadyl Pyrophosphate Catalysts	86
4.2.1 Series 2: XRD Analyses	87
4.2.2 Series 2: SEM Analyses	89
4.2.3 Series 2: BET Surface Area Measurements and Chemical Analyses	91
4.2.4 Series 2: Temperature-Programmed Reduction (TPR in H ₂) Analyses	92
4.2.5 Series 2: Catalytic Oxidation of <i>n</i> -Butane to Maleic Anhydride	97
4.2.6 Series 2: Conclusions	99

5.0	CONCLUSIONS	100
5.1	The Effects of Ga, Mo doped and Different Calcination Duration for the Ga-Mo doped VPOs catalysts	100
	LIST OF REFERENCES	102
	APPENDICES	126

LIST OF TABLES

TABLE	TITLE	PAGE
2.1	Industrial technologies for maleic anhydride production from <i>n</i> -butane	16
2.2	Selected promoted VPO catalysts studies in selective oxidation of <i>n</i> -butane to maleic anhydride	42
3.1	Gases and materials used for the preparation of vanadyl pyrophosphate catalysts	50
3.2	Chemicals and Gases	56
3.3	The instrumentations and characterisation technique used	57
4.1	XRD data of undoped, Ga-doped and Mo-doped VPOs catalysts	70
4.2	Specific BET surface area, chemical compositions, average oxidation number and percentages of V ⁴⁺ and V ⁵⁺ oxidation states present for undoped, Ga-doped and Mo-doped VPOs catalysts	80
4.3	Total amount of oxygen atoms removed and values of reduction energies for undoped, Ga doped and Mo doped catalysts	82
4.4	Catalytic performances of undoped, Ga doped and Mo doped VPOs catalysts	85
4.5	XRD data of Ga-Mo doped VPOs catalysts	89
4.6	Specific BET surface area, chemical compositions, average oxidation number and percentages of V ⁴⁺ and V ⁵⁺ oxidation states present for Ga-Mo doped VPOs catalysts	93
4.8	Total amount of oxygen atoms removed and values of reduction energies for Ga-Mo doped catalysts	96
4.8	Catalytic performances of Ga-Mo doped VPOs catalysts	99

LIST OF FIGURES

FIGURE	TITLE	PAGE
1.1	Energy profile of catalysed and non-catalysed reactions	3
1.2	Partial oxidation of <i>n</i> -butane to maleic anhydride	6
2.1	Structure of maleic anhydride	12
2.2	Chemical reaction for selective oxidation of <i>n</i> -butane to MA	15
2.3	DuPont transported-bed reactor	18
2.4	The idealized layered structure of $(VO)_2P_2O_7$	20
2.5	Idealized structure of $(VO)_2P_2O_7$ (vanadyl group) in (0 2 0) plane	21
2.6	Catalytic oxidation of <i>n</i> -butane on the surface of $(VO)_2P_2O_7$ crystal	22
2.7	Selective and non-selective oxidation site on crystal faces of $(VO)_2P_2O_7$	22
2.8	Conjectured steps in the oxidation of <i>n</i> -butane to maleic anhydride	24
2.9	A non-selective reaction pathway for oxidation of <i>n</i> -butane to maleic anhydride	26
2.10	Schematic representation of Mars and van Krevelen mechanism	27
2.11	Mechanism of the activation of oxygen over metal oxides	28
3.1	(a) First stage reflux; (b) Colour transformation of mixture during stage 1 reflux; (c) Centrifugation and (d) $VOPO_4 \cdot 2H_2O$ intermediate	54
3.2	(a) Colour transformation of solution during second stage reflux; (b) Centrifugation and (c) $VOHPO_4 \cdot 1.5H_2O$ precursor after oven drying	55
3.3	Thermal activation of $(VO)_2P_2O_7$ catalysts	55
3.4	Shimadzu XRD-6000 Diffractometer	58

3.5	Hitachi S-3400N electron microscope coupled with EDAX software	59
3.6	Thermo Finnigan Sorptomatic 1990	60
3.7	Perkin Elmer Optima 2000 DV optical emission spectrometer	61
3.8	Thermo Electron TPDRO 1100	64
3.9	Fixed-bed microreactor with on-line Thermo Scientific TRACE GC Ultra™	65
4.1	Powder XRD patterns for undoped and Ga-doped VPOs catalysts	67
4.2	Powder XRD patterns for undoped and Mo-doped VPOs catalysts	68
4.3	SEM micrograph for (a) VPOs-Undoped; (b) VPOs-0.1%Ga; (c) VPOs-0.3%Ga; (d) VPOs-0.5%Ga	72
4.4	SEM micrograph for (a) VPOs-Undoped; (b) VPOs-1%Mo; (c) VPOs-3%Mo and (d) VPOs-5%Mo	73
4.5	TPR in H ₂ profiles for undoped and Ga doped VPOs catalysts	78
4.6	TPR in H ₂ profiles for undoped and Mo doped VPOs catalysts	78
4.7	Catalytic performances of undoped, Ga doped and Mo doped VPOs catalysts	85
4.8	Powder XRD patterns for Ga-Mo doped VPOs catalysts	88
4.9	SEM Micrographs for (a) VPOs-0.1%Ga1%Mo-18; (b)VPOs-0.1%Ga1%Mo-36; (c)VPOs-0.1%Ga1%Mo-54 and (d) VPOs-0.1%Ga1%Mo-72	90
4.10	TPR in H ₂ profiles of Ga-Mo doped VPOs catalysts	94
4.11	Catalytic performances of Ga-Mo doped VPOs catalysts	98

LIST OF ABBREVIATIONS AND SYMBOLS

ΔH_r	Change in enthalpy of reaction
$^{\circ}\text{C}$	Degree Celcius
A_r	Pre-exponential factor
K	Absolute temperature in Kelvin
E_a	Activation Energy
$o\text{-H}_3\text{PO}_4$	<i>ortho</i> -Phosphoric acid
P/V	Phosphorus-to-vanadium ratio
ppm	Part-per-million
t	Crystallite size for $(h\ k\ l)$ phase
T	Temperature
T_{max}	Temperature of the peak maximum
$\alpha\text{-}, \beta\text{-}, \gamma\text{-VOPO}_4$	Vanadyl phosphate in α (alpha), β (beta), and γ (gamma) phases
$\beta\text{-}, \gamma\text{-}(\text{VO})_2\text{P}_2\text{O}_7$	Vanadyl pyrophosphate in α (alpha), β (beta), and γ (gamma) phases
β_{hkl}	Full-width at half maximum (FWHM) at $(h\ k\ l)$ phase
$\theta_{h\ k\ l}$	Diffraction angle for $(h\ k\ l)$ phase
T_{max}	Peak maximum temperature
$(\text{VO})_2\text{P}_2\text{O}_7$	Vanadyl pyrophosphate
Al	Aluminium
B	Boron
BET	Brunauer-Emmett-Teller
Bi	Bismuth
Bi_2O_3	Bismuth(III) oxide
BiPO_4	Bismuth(III) phosphate

Ce	Cerium
Co	Cobalt
Cr	Chromium
EDX	Energy-dispersive x-ray
EHT	Extra-high tension acceleration voltage
Fe	Iron
$\text{Fe}(\text{acac})_3/\text{Fe}(\text{C}_5\text{H}_7\text{O}_2)_3$	Iron(III) acetylacetonate
FWHM	Full-width at half maximum
Ga	Gallium
$\text{Ga}(\text{acac})_3/\text{Ga}(\text{C}_5\text{H}_7\text{O}_2)_3$	Gallium(III) acetylacetonate
Ga_2O_3	Gallium(III) oxide
GaPO_4	Gallium phosphate
GHSV	Gas hourly space velocity
H_3PO_4	Phosphoric acid
HNO_3	Nitric acid
HRTEM	High-resolution transmission electron microscopy
ICP-OES	Inductive coupled plasma-optical emission spectrometry
In	Indium
JCPDS	Joint Committee on Powder Diffraction Standards
LVBP	Lamellar vanadyl benzylphosphate
MA	Maleic anhydride
Mo	Molybdenum
N_2	Nitrogen
O_2	Oxygen
PO_4	Phosphate

Sb	Antimony
SEM	Scanning electron microscopy
STP	Standard temperature and pressure
TAP	Temporal analysis products
TCD	Thermal conductivity detector
TEM	Transmission electron microscopy
TeO ₂	Tellurium dioxide
Ti	Titanium
TOF	Turnover frequency
TON	Turnover number
TPDRO	Temperature-programmed desorption/reduction/oxidation
TPR	Temperature-programmed reduction
V ₂ O ₅	Vanadium(V) pentoxide
VOHPO ₄ ·0.5H ₂ O	Vanadyl(IV) hydrogen phosphate hemihydrate
VOHPO ₄ ·1.5H ₂ O	Vanadyl(IV) hydrogen phosphate sesquihydrates
VOPO ₄ ·2H ₂ O	Vanadyl phosphate dihydrates
VPA	Vanadium phosphorus oxide catalyst prepared via aqueous method
VPD	Vanadium phosphorus oxide catalyst prepared via dihydrates route
VPH	Vanadium phosphorus oxide catalyst prepared via hemihydrates route
VPO	Vanadium phosphorus oxide catalyst prepared via organic method
VPOs	Vanadium phosphorus oxide catalyst prepared via sesquihydrate route
VPOs-0.1%Ga	Vanadium phosphorus oxide catalyst prepared via sesquihydrate route doped with 0.1 mol% of gallium

VPOs-0.1%Ga1%Mo-18	Vanadium phosphorus oxide catalyst prepared via sesquihydrate route doped with 0.1 mol% of gallium, 1 mol% of molybdenum and calcined for 18 h
VPOs-1%Mo	Vanadium phosphorus oxide catalyst prepared via sesquihydrate route doped with 1 mol% of molybdenum
W	Tungsten
XPS	X-ray photoelectron spectroscopy
XRD	X-ray diffraction
Zr	Zirconium

LIST OF APPENDICES

APPENDIX	PAGE
APPENDIX A	126
APPENDIX B	128
APPENDIX C	131
APPENDIX D	139
APPENDIX E	140
APPENDIX F	143
APPENDIX G	146
APPENDIX H	147
APPENDIX I	149
APPENDIX J	155

CHAPTER 1

INTRODUCTION

1.1 History of Catalysts and Catalysis

The term "catalysis" was first introduced by Berzelius in 1836 who defined catalysis as "the ability of substances to awaken affinities, which are asleep at a particular temperature, by their mere presence and not by their own affinity". Then, catalysis has been brought into attention during the early of 1800s where catalysts were identified and studied thoroughly by other researches. (Hartley, 1985).

Ostwald (1894) proposed a definition as catalyst being a substance that accelerates the rate of chemical reaction without being consumed itself and does not affect the thermodynamic equilibrium of the reactions. Even before Berzelius devised the word 'catalysis' in its modern connotation in 1835, applied catalysis already existed in 8th century. According to the Arabic alchemist, Jabir Ibn. Haiyan (Geber), he reveals that mineral acid was used as a catalyst to produce ether by the dehydration of alcohol even reverse it then. The main objective of catalyst is to use as an active, selective and stable material for a determined catalytic process to develop a desired product (Gonzalez-Cortes and Imbert, 2013).

1.2 Definition of Catalyst

A catalyst is defined as a substance which accelerates the rate of chemical reaction by forming bonds with the reacting molecules, allowing these to react to form products, which detaches from the catalyst, and leaves without being consumed or altered in the end of each catalytic cycle (Chorkendoff and Niemantsverdriet, 2007).

As the catalyst is not consumed and is recovered in the catalytic process, each catalyst molecules can participate in many consecutive cycles, so only relatively small amount of catalyst is needed for the substrate to react. The efficiency of the catalyst is shows by the substrate-to-catalyst ratio, which is measured as turnover number (TON) or turnover frequency (TOF) (Rothnberg, 2008).

The catalyst offers an alternative route for the reaction by reducing the energy barrier or so called the activation energy (E_{act}). Therefore, the activation energy of the catalytic reaction is significantly smaller than that of uncatalysed reaction. Hence, the rate of catalytic reaction is higher (Figure 1.1).

The catalyst lowers the activation barrier by providing a surface or active site for adsorption and dissociation of the reactants, in which readily transformed to products. The overall change in free energy for the catalytic reaction equals that of the uncatalysed reaction. Hence, the catalyst does not affect the equilibrium constant for the overall reaction of reactants to products.

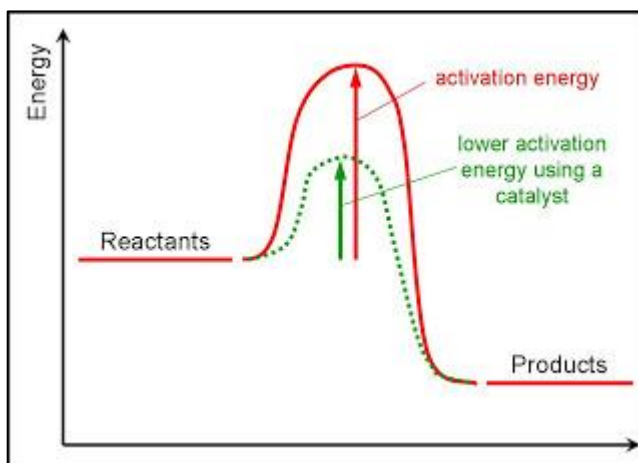


**Figure 1.1: Energy profile of catalysed and non-catalysed reactions
(Arrhenius Equation, 1889)**

1.3 Important Roles of Catalysis

Catalysis plays a main role in the development of sustainable processes, which are primary importance to present and future worldwide production based on energy and chemicals, i.e. the power, petroleum, chemicals and food industries while avoiding negative consequences for the environment. Future global energy prosperity will depend on new or improved processes that economically and environmentally sustainable which driven by the threat of climate change and scarcity of non-renewable raw material (Bartholomew and Farrauto, 2006).

Catalysts are widely used in several sectors including petrochemicals, pharmaceutical, polymer production, agricultural production and chemicals industries. In the industrialised world, 20-25% of gross national products involved heterogeneous catalysis and this perhaps the best to illustrate the economic impact of catalysis to the industries. Industrial society was

encountering major problems such as the aid to create production with environmental balanced, better efficiency of fuels, energy-saving production, and reduction of CO₂ and greenhouse gasses. All these will require solutions where catalysts play an important role. Furthermore, the development of new catalysts and catalytic processes gives opportunities for new selective chemical processes which may lead to a considerable reduction of by-products and waste products (Taufiq-Yap, 2009).

1.4 Types of Catalysis

Catalysts generally exist in multitude of forms, varying from atoms and molecules to larger structure such as zeolites or enzymes. Catalysts may employed in different surrounding i.e. liquids, gases or at the surface of solids (Chorkendorff and Niemantsverdriet, 2007). Traditionally, catalytic systems are classified as homogeneous or heterogeneous catalysis.

1.4.1 Homogeneous Catalysis

In homogeneous catalysis, the catalysts are molecularly dispersed with the reactants in same phase. The reactants initially bind to the catalysts and transform to products, and finally release from the catalysts. Typically, homogeneous catalysts are dissolved in a solvent with the reactants. This provides easy access to the catalytic site since it does not subject to the diffusion limitation but can make the separation of catalysts and products difficult. Homogeneous catalysis is in industrial applications, as it increases in

the rate of reaction without rising the reaction temperature For example, the esterification of carboxylic acids with methanol catalysed by (H⁺) ions (Fischer and Speier, 1895).

1.4.2 Heterogeneous Catalysis

A catalytic system that refers to all the cases where the catalyst and the reactants are in different phases is classified as heterogeneous catalysis. In heterogeneous catalysis, the reactants being adsorbed onto the surface of solid catalyst are activated by chemical interaction with the catalyst surface and selectively transformed to adsorbed products, which finally desorbed from the catalyst surface (Figure 1.2). Lastly, the catalyst itself being regenerated to its original form at the end of each cycle (Ertl, 2002).

Heterogeneous catalysis is normally referred to a system where the catalysts are usually in solids, which are in a different phase from gases or liquid reactants. The working with solid catalysts and gaseous reactants are often the best selection for petrochemicals and bulk chemicals industry which favour continuous processes at high temperatures due to reactivity and process size considerations. The primary advantage of heterogeneous catalysis is that the catalysts are in solid phase and thus can easily be separated and recycled from the gas and/or liquid reactants and products. Thus, the catalysts can be regenerated and reused as long as four years before being disposed, depending mainly on the operating temperature, interference-free operation and the purity of raw materials (Boudart, 1991).

In heterogeneous catalysis, the catalytic reaction of CO on the surface of noble metals such as platinum, palladium and rhodium in automotive catalytic converter. In this research, the partial oxidation of *n*-butane to maleic anhydride with the assist of solid vanadyl pyrophosphate catalyst is defined as a heterogeneous catalysis (Cavani and Trifiro, 2004).

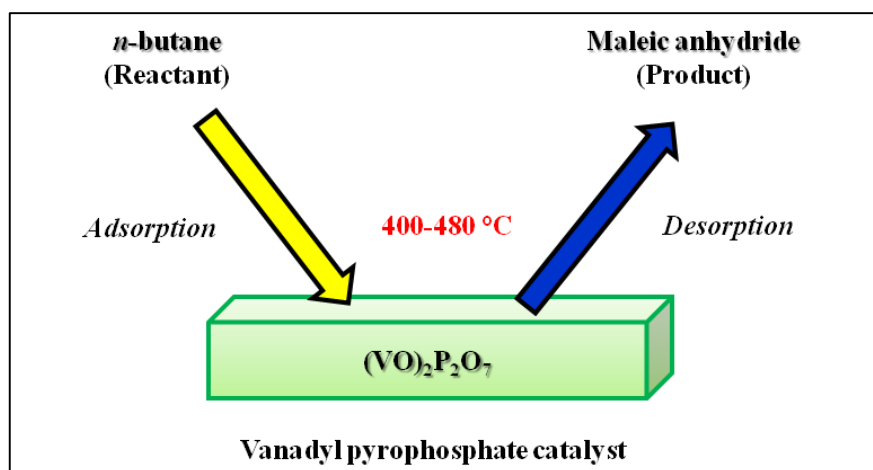


Figure 1.2: Partial oxidation of *n*-butane to maleic anhydride

1.5 Selective Oxidation of Light Hydrocarbon

The possibility of developing new environmental friendly and lower cost processes has generated interest in selective oxidation of light alkanes to valuable oxygenated compounds and alkenes (Centi et al., 2001a). This is due to the abundance and low cost of light alkanes such as ethane, propane and butane (Centi, 1993a). Selective oxidation has extremely fast in rate of reactions and highly selective which replace the older slow processes with high efficiency energy processes (Centi and Perathoner, 2001b).

Industrial processes have now moved towards more efficient use of resources and improvement in selectivity which both corresponds to an improvement in the process economics. The synthesis of maleic anhydride (MA) is one of the examples. The catalytic process was substituted with that using butane instead of benzene for the following reasons:

- i. The loss of two carbon atoms by using benzene is avoided
- ii. Carbon oxides and small amount of acetic acid are the only by-products
- iii. The toxicity aspects to the use of benzene is avoided, which reducing costs related to safety system and benzene handling

The oxidation of *n*-butane to maleic anhydride is as yet the only industrial process of selective oxidation of paraffin and *n*-butane selective oxidation on vanadium phosphorus oxide catalyst is a much studied reaction in heterogeneous catalysis (Centi, 1993b). Vanadyl pyrophosphate catalysts have been studied extensively for selective oxidation of *n*-butane to maleic anhydride (Asghar et al., 2010). Vanadyl pyrophosphate, $(VO)_2P_2O_7$ is known to be the active and selective catalyst phase of the *n*-butane oxidation to maleic anhydride. The use of highly active catalysts makes it possible to increase selectivity and conversion of *n*-butane to maleic anhydride (Centi, 1993b)

The butane process fully implements the principles of green chemistry in the reasons of use of non-toxic reactants, improved atom economy, simplified a complex multistep transformation and minimised waste formation.

1.6 Essential Properties of Good Catalysts

The suitability of a catalyst for an industrial process depends mainly on three properties: stability (lifetime), activity and selectivity (Hartley, 1985). The chemical, thermal and mechanical stability of a catalyst determines the catalyst lifetime in industrial reactors. A good catalyst must possess with long lifetime, which capable to regenerated as many times after the loss of activity during a process, and able to sustain the desired ion over prolonged period. The total catalyst lifetime is of crucial importance for the economics of industrial processes.

Activity is a measure of how fast one or more reactions proceed in the presences of the catalyst. Activity of a catalyst can be defined as the rate which the chemical reaction reaches the equilibrium, or in terms of thermodynamic quantity that measure the effective concentration or intensity of a particular substance in a given chemical system (Sharp, 2003). In this case, activity is defined as the amount of reactants transformed into product per unit of time and unit of reactor volume. In other words, catalysts must have reasonable activity per unit reactor volume, where high activity gives rise of high conversion of end product. The cost of the catalyst per unit of product being produced should be low, which in turn implies a high turnover number (TON) (Hartley, 1985).

The selectivity is of great importance in industrial catalysis, as defined as the fraction of the starting material that is converted to the desired products

(Somorjai, 2008). A catalyst with low selectivity may favor to unavoidable side reactions and form undesired by-products, thus the cost of separating the products from will be prohibitive. Therefore, a good catalyst must have high selectivity to produce a cleaner reaction.

Selectivity usually depends on reaction condition of temperature, pressure, reactants composition and the catalyst used (Fadoni and Lucarelli, 1999). Therefore, the catalyst used must be able to affect the desired reaction at an acceptable rate under practicable conditions of temperature and pressure. The use of high temperature and pressure usually produce good yields but it is proved to be very costly. Hence, it is essential to synthesise a catalyst which can be operated under the mildest conditions with minimum side reactions (Bond 1987; Cavani and Trifiro, 1994).

1.7 Problem Statement

The possible utilization of alkanes feedstock undergoes selective oxidation reactions requires the discovery of a selective catalyst for the reaction (Centi et al., 2001a). The selective oxidation of alkanes thus requires the development of novel concepts and catalytic system to fulfil the strict requirements of controlled surface reactivity that necessary for the selective behaviour (Centi, 1993a). The major challenges in selective oxidation of light hydrocarbon are (Bartholomew and Farrauto, 2006):

- i. Discovering the catalysts that contain high selectivity for the partially oxidised product and low selectivity for complete combustion
- ii. High precision in controlling reaction condition, mainly temperature, to avoid loss of selectivity as a result of high exothermicity of the reactions involved

Maleic anhydride, MA is found majorly used in unsaturated polyester and butanediol production by the activation of light alkanes with a redox catalyst, where VPO catalyst is applied during the oxidation process. However, it is often being claimed that the selectivity and activity of VPO catalyst are low by using dihydrate precursor method ($\text{VOPO}_4 \cdot 2\text{H}_2\text{O}$). The best performance reported for a fixed-bed reactor only able to reach not more than 82% selectivity and 65% activity towards the formation of MA (Ballarini et al., 2006). High formation of by-products is reported during the oxidation of *n*-butane to maleic anhydride using catalysts. Therefore, further studies and investigations on modified VPO catalyst shall be carried out to obtain better performances of VPO catalysts toward better conversion of MA with cleaner process.

1.8 Objectives

The objective of my research is to synthesise VPO catalysts with higher *n*-butane conversion and the least amount of by-products toward the formation of maleic anhydride.

The other objectives of this research are set as follows:

- i. To study the effect of different mole percentages of Ga dopant on the physico-chemical, reactivity and catalytic properties of VPO catalysts prepared via sesquihydrate precursor ($\text{VOHPO}_4 \cdot 1.5\text{H}_2\text{O}$) route.
- ii. To study the effect of different mole percentages of Mo dopant towards the physico-chemical, reactivity and catalytic properties of modified VPOs catalysts
- iii. To study the effect of calcination durations on physico-chemical, reactivity and catalytic properties of Ga-Mo doped VPOs catalysts.

CHAPTER 2

LITERATURE REVIEW

2.1 Maleic Anhydride

Maleic anhydride (MA), $C_4H_2O_3$, is chemically known as 2,5-furandione, dihydro-2,5-dioxofuran, toxilic anhydride or *cis*-butenedioic anhydride (Felthouse et al., 2001). It crystallises as orthorhombic crystalline needles and also available in the form of molten liquid or briquettes. MA has a cyclic structure in which carboxylic acid groups attached next to each other in the *cis* form with a ring containing four carbon and one oxygen atoms (Figure 2.1). It was first produced 150 years ago by the dehydration of maleic acid (Trivedi and Culbertson, 1982).

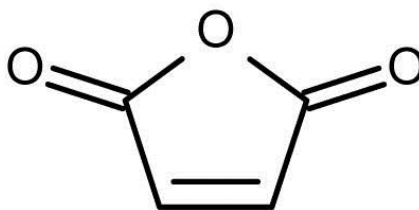


Figure 2.1: Structure of maleic anhydride

2.1.1 The use of Maleic Anhydride

Maleic Anhydride (MA) is an essential intermediate that used as a co-monomer for the production of unsaturated polyester resins, which are involved in the construction and electrical industries, and in pipeline and

marine construction. Other applications for MA are used as a chemical intermediate in the synthesis of fumaric acid and tartaric acid, specific agricultural chemicals, resins in numerous products, dye intermediate and pharmaceuticals (Trivedi and Culbertson, 1982). Some other end products of MA are in miscellaneous uses including assorted copolymer which make thickeners and dispersants, alkenyl succinic anhydrides, alkydic resins, lube oil additives, plasticisers, detergents, certain chemicals and organic intermediates (Centi et al., 2001a; Greiner, 2011).

2.1.2 Worldwide Demand: Maleic Anhydride

The worldwide consumptions for MA has continuously increased throughout the years. Back to year 1978, an estimation of 341 million pounds of MA were produced. In 1995, the global demand for MA has grown to an estimated 1.8 billion pounds, with a value of about 700 million U.S. dollars. In 2007-2013, the world MA capacity has increased at average by annum of 6-7% to 1.5 million tons in 2013, where the average annual MA market growth rate in the USA and Western Europe was 2.8% and 3.5%, respectively while, in Japan it dropped by 1.4%. The MA consumption is predicted that it will be grow at around 3% annually up to 2016. MA market was impacted by the production of 1,4-butanediol (BDO), one of the world's fastest growing chemicals used in the production of polybutylene terephthalate (PBT) resins, thermoplastic polyurethanes, elastane and many other products is used as an intermediate for the production of copolymers. (Kirk and Othmer, 2013).

2.1.3 The Commercial Process for Maleic Anhydride

The first commercial process for producing MA was introduced by National Aniline and Chemical in 1928 using the Weiss and Downs process (Lawrie, 2011), which the formation of MA by the catalytic partial oxidation of benzene in air. However, beginning from 1974, other feedstock, from C₄ hydrocarbon including 1-butene and 2-butene, subsequently *n*-butane, have been primarily replacing benzene to produce MA. The primary reasons for replacing benzene with *n*-butane were (Centi et al., 2001a):

- i. Lower cost of butane as compared to benzene: *n*-butane present in natural gas which also can be produced by steam cracking of oil
- ii. Better yield by weight (the relevant industrial parameter)
- iii. Lower environmental impact: benzene is classified as a carcinogen and involves severe and costly process control for safety monitoring and environment
- iv. Low cost of MA purification and separation: *n*-butane oxidation provides a very clean reaction with minimum by-products (CO and acetic acid) instead of benzene produces some heavy compounds (such as phthalic anhydride and benzoquinone) and large amount of CO_x

The advantages of C₄ hydrocarbon oxidation encouraged the development of industrial processes involving the partial oxidation of *n*-butane to MA and the first commercial process starting with *n*-butane was operated by Mosanto in 1974. The butane process was now being adopted worldwide due to the better economics and environmental protection. The oxidation of *n*-

butane to MA was successful after vanadyl pyrophosphate catalysts had been discovered, which posed unique characteristics of activity and selectivity. The reaction was carried out at 673 K in gas phase catalysed by vanadium and phosphorus mixed oxide, used in bulk phase (Figure 2.2).

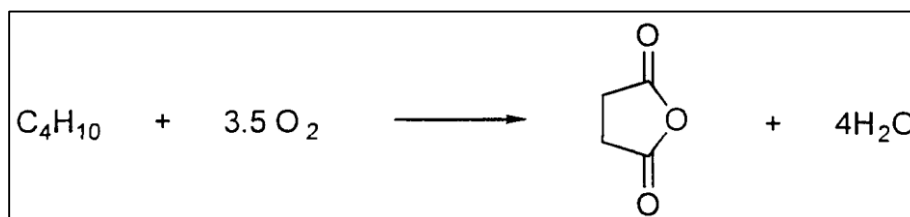


**Figure 2.2: Chemical reaction for selective oxidation of *n*-butane to MA
(Cavani and Trifiro, 1992; Centi et al., 2001a)**

In this reaction, eight hydrogen atoms are abstracted from *n*-butane, and three oxygen atoms are added to form maleic anhydride. This is an extensive oxidation process involving the cleavage of eight C-H bonds and the insertion of three oxygen atoms with multistep poly-functional reaction mechanism, entirely occurs on the adsorbed phase yet provided selectivity of desired products (Felthouse et al., 1995).

2.1.4 Production Technologies of Maleic Anhydride

The advantages of replacing benzene with *n*-butane as the feedstock compensated the higher cost due to some of the reasons:

- i. The reduce in productivity: using *n*-butane is about 15% more expensive than that using benzene for similar production due to lower catalyst conversion and lower limit of hydrocarbon-oxygen explosion

- ii. The steam production: butane require higher heat of reaction as compared to benzene
- iii. Lower selectivity

All these problem statements are dependent on the choice of the reactor which is greatly affecting the conversion-yield relationship, the control of the heat of reaction and the feasibility of catalyst regeneration.

The production of MA is depending on the employed technologies (fixed-bed or fluidised-bed). The selectivity to maleic anhydride is around 65-70% under typical industrial conditions (673-723 K, less than 2 molar % of *n*-butane in air) with conversion from 70-85%. Table 2.1 summarised the industrial technologies for the oxidation processes from *n*-butane to MA.

Table 2.1: Industrial technologies for maleic anhydride production from *n*-butane (Centi et al., 2001a).

Process	Type of reactor	Recovery Method
ALMA (Lonzagroup, Lummus)	Fixed-bed	Anhydrous
BP (Sohio)-UCB	Fixed-bed	Anhydrous
Denka Scientific Design	Fixed-bed	Anhydrous
DuPont	Transported-bed	Anhydrous
Lonzagroup	Fixed-bed	Anhydrous/ aqueous
Mitsubishi Chemicals	Fixed-bed	Anhydrous
Monsanto	Fixed-bed	Anhydrous

In almost all MA processes, the fixed-bed reactor was normally employed with multi-tubular reactor concept due to the high exothermic reactions. The typical reactor contained a bundle of 10-15 thousand tubes,

enclosed by a jacket through which circulated by cooling medium to prevent hotspots and destroy of catalyst. Agitated commercial molten salt or heat-transfer fluid was used to maintain the temperature of the reaction zone within the desired range (Centi et al., 1988; Mota et al., 2000).

Whereby, the fluidised-bed reactor offers the possibility of controlling the reaction temperature more uniformly by passing through a granular catalyst in a fluid (gas or liquid) with high velocity to suspend the solid. The advantages of the fluidised-bed reactor as compared to the fixed-bed reactor included (Centi et al., 2001a):

- i. Excellent rates of heat and mass transfer
- ii. Higher degree of catalyst performance (reduce downtime for catalyst replacement)
- iii. Higher of product yields (gases can be fed directly into the reactor rather than pre-mixed)

However, there are two major disadvantages for this overwhelming preference (Johnsson et al., 1987; Centi et al., 2001a):

- i. Lower maleic anhydride selectivity (over-oxidation of MA to carbon dioxide due to backmixing)
- ii. Necessary of discovering hard catalyst particle (high attrition rate of catalyst caused by constant motion)

Comparatively, transported-bed reactor is the most recent reactor developed by DuPont for MA production (Figure 2.3). It is generally operates

with an attrition-resistant vanadium phosphorus oxide (VPO) catalyst by redox cycle (Mars and van Krevelen, 1954) over the feed (*n*-butane in inert gas virtually absence of oxygen) in a transport bed reactor. The spent catalyst is carried overhead where it is separated and regenerated with air in a conventional bubbling fluidised bed reactor. After regeneration, it is re-introduced onto transport bed reactor where the re-oxidised catalyst is exposed again to the *n*-butane rich process feed gas (Contractor and Sleight, 1987; Contractor, 1999). However, the transported-bed reactor was discontinued as DuPont's plant has been shut down.

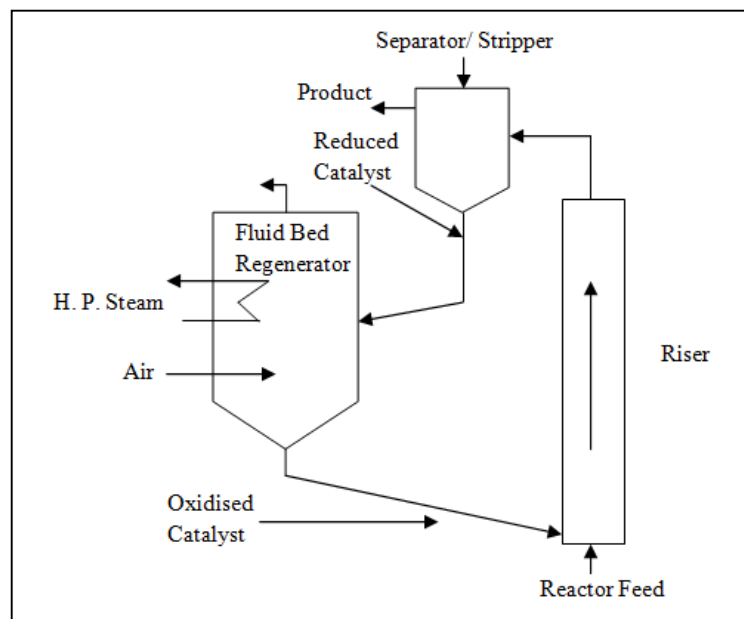


Figure 2.3: DuPont transported-bed reactor (Contractor, 1999)

2.2 VPO Catalyst

The vanadium phosphorus oxide (VPO) has a remarkable and interesting complex catalytic system, which has been widely studied along the past few decades by many researches.

Several of distinct compounds and well-characterised crystalline vanadium phosphate phases can be formed (Borders, 1987; Sananes et al., 1995). The transformation of vanadium phosphate phases including V^{5+} vanadyl orthophosphates *e.g.* α_I , α_{II} , β -, γ -, δ -, ϵ -, and ω -VOPO₄, and VOPO₄·2H₂O (Ladwig, 1965; Gopal and Calvo, 1972; Borders et al., 1984; Borders, 1987), the V^{4+} vanadyl hydrogen phosphates *e.g.* VOHPO₄·4H₂O, VOHPO₄·0.5H₂O, VO(H₂PO₄)₂, vanadyl pyrophosphate ((VO)₂P₂O₇), and the V^{3+} vanadyl metaphosphate ((VO(PO₃)₂) (Johnson et al., 1984; Torardi and Calabrese, 1984; Leonowicz et al., 1985; Bordes, 1987). However, the V^{3+} vanadyl metaphosphate was rarely present in *n*-butane oxidation (Centi, 1993b).

In the past academic literatures, the vanadyl hydrogen phosphate hemihydrate, VOHPO₄·0.5H₂O has been found to be used as a catalyst precursor, which gives a catalyst mainly composed of (VO)₂P₂O₇ phase after the activation. The (VO)₂P₂O₇ phase has been identified as the most active and selective in *n*-butane oxidation to maleic anhydride, which has been applied in industry since 1960 (Bordes and Courtine, 1979; Centi, 1993b; Hutchings, 1993; Hutchings, 2004).

2.2.1 The System of $(VO)_2P_2O_7$ Catalyst

The structure of vanadium phosphate oxide, VPO catalyst is dependent on several factors, including P/V composition, thermal treatment duration, activation condition and gas phase composition, which can greatly affect the catalyst properties. The variety of crystallite phases can be obtained by using a high-resolution transmission electron microscopy (HRTEM) that allows for direct imaging of the atomic structure of the catalyst (Kiely et al., 1996).

Vanadyl pyrophosphate, $(VO)_2P_2O_7$ phase plays an important role in the oxidation of *n*-butane to MA. $(VO)_2P_2O_7$ has a layered structure with two VO_6 octahedral pairs share edges and subsequently connected by PO_4 tetrahedral (Figure 2.4) which gives a layer structure in a (0 2 0) plane (Hutchings, 1991). The double vanadyl groups which perpendicular to the (0 2 0) plane are present in *trans* position to each other within a pair of edge sharing octahedral (Figure 2.5) (Cavani et al., 1985).

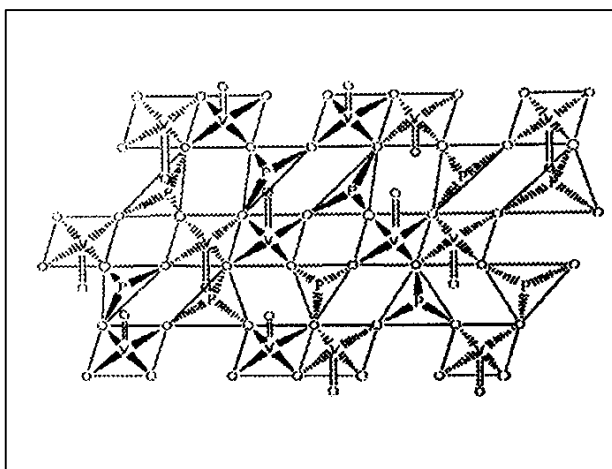
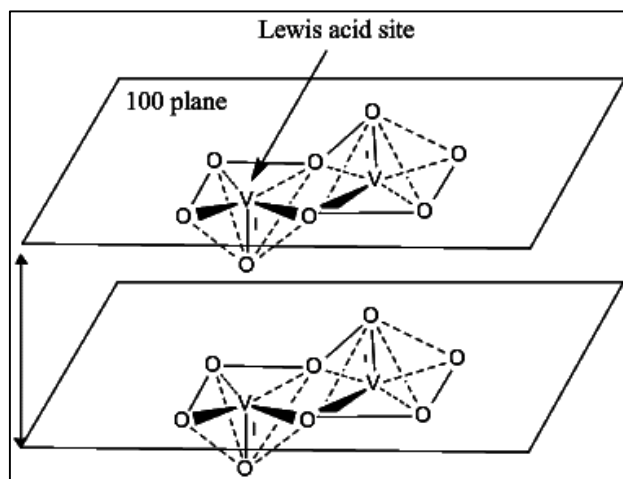


Figure 2.4: The idealised layered structure of $(VO)_2P_2O_7$

(Cavani et al., 1985)



**Figure 2.5: Idealised structure of $(VO)_2P_2O_7$ in $(0\ 2\ 0)$ plane
(Cavani et al., 1985)**

It has been widely accepted that the performance of $(VO)_2P_2O_7$ is directly related to the exposure of $(0\ 2\ 0)$ facets, which is related to the $(0\ 0\ 1)$ facet of $VOHPO_4 \cdot 0.5H_2O$ (O'Mahony et al., 2005). Both phases possess similar crystal structures, which the $(VOHPO_4)$ layers are hydrogen bonded through HPO_4^{2-} groups in the precursor phase and become covalently bonded via pyrophosphate ($P_2O_7^{4-}$) group during the thermal transformation to vanadyl pyrophosphate (Gulians et al., 2001). The $(0\ 2\ 0)$ basal plane of $(VO)_2P_2O_7$ where V-O-V pair sites are located (Figure 2.6). The selective oxidation of *n*-butane to MA was takes place on the basal plane and deep oxidation on the $(0\ 2\ 0)$ side planes (Misono, 2002).

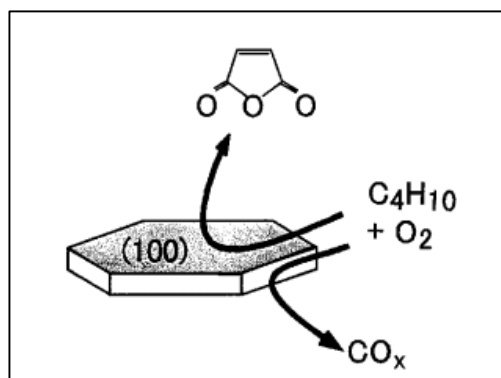


Figure 2.6: Catalytic oxidation of *n*-butane on the surface of $(VO)_2P_2O_7$ crystal (Misono, 2002)

The catalytic behaviour of $(VO)_2P_2O_7$ with respect to different crystal planes has been studied by exposing it individually. The $(VO)_2P_2O_7$ was deactivated by surface deposition of SiO_2 and the crystallites were then fractured to expose the side faces of $(0\ 2\ 1)$ and $(0\ 0\ 1)$ planes (Figure 2.7). The side planes were found to be non-selective, where MA was formed on the $(1\ 0\ 0)$ plane (Inumaru et al., 1997; Misono, 2002).

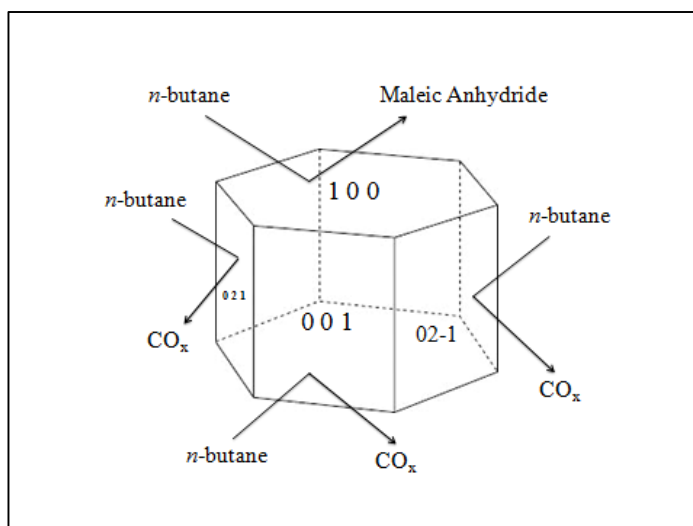


Figure 2.7: Selective and non-selective oxidation site on crystal faces of $(VO)_2P_2O_7$ (Misono, 2002)

2.2.2 The Mechanism of Selective Oxidation

The selective oxidation of *n*-butane to maleic anhydride in the presence of VPO catalyst involves the abstraction of eight hydrogen atoms, insertion of three oxygen atoms and transfer of fourteen electrons. The reaction undergoes a redox mechanism (Mars and van Krevelen, 1954) in which the catalyst oxidises the adsorbed reactant with lattice oxygen, the spent lattice oxygen is then replenished by surface oxygen species derived from gaseous oxygen, thus regenerating the reduced catalyst for the new catalytic cycle (Mars and van Krevelen, 1954). The reaction has high MA selectivity at low *n*-butane conversion with only CO_x as by-product (Centi et al., 1988).

Cavani and Trifiro (1994) proposed a reaction pattern for the formation of maleic anhydride from *n*-butane (Figure 2.8). The process was suggested that none of the intermediates has been observed among the reaction products. The absence of any of these intermediates under normal reaction conditions is justified simply on the basis of kinetics. The initial rate of oxidation of *l*-butene has been found 60 times higher than that of *n*-butane (Centi et al., 1984). Comparatively, other researchers have found that the initial oxidation rate of *l*-butene was 20 times more than that of *n*-butane (Misono et al., 1990). The differences in reactivity have justified the fast transformation of all intermediates (formed by the activation of *n*-butane) to the final product before any desorption from the catalyst surface can be occurred.

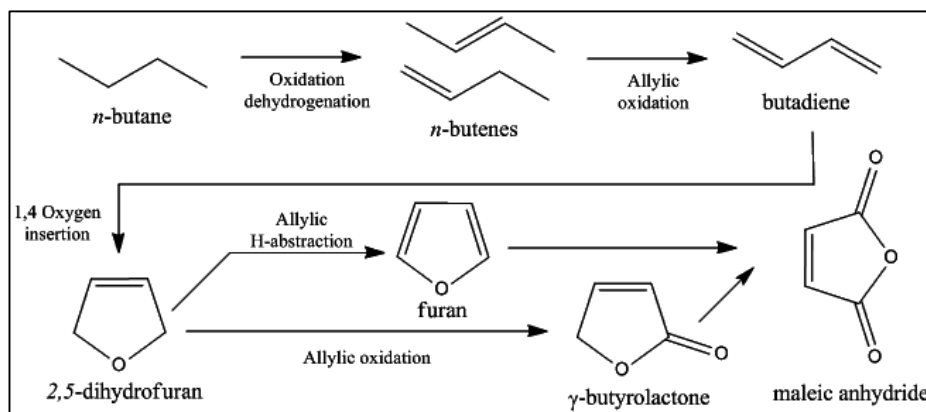


Figure 2.8: Conjectured steps in the oxidation of n -butane to maleic anhydride (Cavani and Trifiro, 1994)

Cavani and Trifiro (1994) proposed the reaction steps for two reasons:

- i. Butene, butadiene and furan have been detected in the oxidation of n -butane with vanadium phosphorus catalysts under selected conditions (such as a deficiency of oxygen at a very high n -butane concentration) (Centi et al., 1988)
- ii. In the oxidation of butenes, butadiene and furan at the same conditions as for n -butane oxidation, maleic anhydride and all the intermediates have been observed (with exception of 2,5-dihydrofuran and lactone) (Centi et al., 1988)

The oxidation of 2,5-dihydrofuran to furan occurs at a low temperature (473 K) with high selectivity which has explained the absence of the hypothesised intermediate in the oxidation of butene and butadiene (Cavani and Trifiro, 1994).

The mechanism is specially executed by the use of $(VO)_2P_2O_7$ catalyst. A main property of the catalyst is its ability to carry out the first step, the activation of *n*-butane with high selectivity, which can be separate to two types: C-H bond activation and C-C bond activation. However, focus has been mainly on C-H bond activation since C-C bond activation has led to cracking and non-selective products (Pepera et al., 1985). By contrast, other phosphate catalysts or molybdenum oxide catalysts are active and selective in the oxidation of butenes and butadiene to MA (Trifiro, 1993).

The second key feature of the $(VO)_2P_2O_7$ catalyst is related to the fact that the rate of dehydrogenation is higher than the rate of oxygen insertion into butenes, which is important for achieving high selectivity (Fumagalli et al., 1993). The insertion reaction has constituted a route parallel to the formation of butadiene which is selective route. The oxygen insertion is responsible for the formation of crotoaldehyde, methyvinylketone, and the products of the oxidative cleavage of C=C bond (Cavani and Trifiro, 1994).

However, with all the intermediates transformed before the desorption can occur, side reaction are precluded. Therefore, lack of desorption is the key feature for the achievement of high selectivity to MA. Other byproducts can be formed in the individual intermediates as result of the unselective reactions of oxidation, which include acids, ketones, aldehydes and others from acid-catalysed reaction such as oligomerization, isomerization, and hydration. There are two different sites responsible for the formation of carbon oxides (Figure 2.9) which including the direct oxidation of *n*-butane, and the decomposition of

the MA (Centi et al., 1989a; Bej and Rao, 1991; Bej and Rao, 1992a), where X_i stands for all possible intermediates compounds formed at the catalyst surface and CO_x is the only byproduct that formed only from *n*-butane and maleic anhydride. These sites are different from those involved in the selective reaction pathway (Lashier et al., 1990).

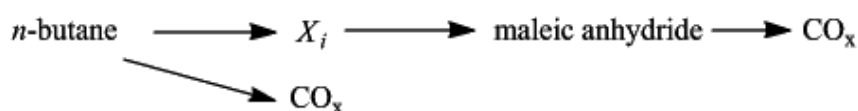


Figure 2.9: A non-selective reaction pathway for oxidation of *n*-butane to maleic anhydride (Centi et al., 1989a)

2.2.3 The Origin of the Selective Oxidation to Maleic Anhydride

The oxidation of *n*-butane to maleic anhydride has involved seven of oxygen atoms and fourteen electron. Aerobically, the selectivity of ~65% was obtained for the oxidation of butane to MA over a $(VO)_2P_2O_7$ catalyst. However, by anaerobic process, the selectivity has increased to ~80% (Taufiq-Yap et al., 1997a; Taufiq-Yap et al., 1997b; Sakakini et al., 2000). Mars and van Krevelen (1954) has postulated that the oxidizing species in hydrocarbon oxidation was attributed by the lattice O atoms of the oxide (Figure 2.10).

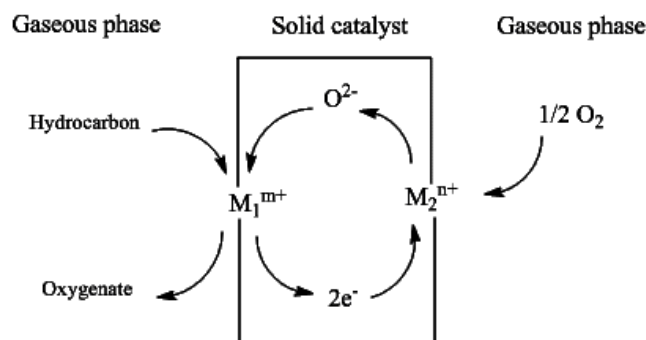


Figure 2.10: Schematic representation of Mars and van Krevelen mechanism (Mars and Krevelen, 1954)

The primary important of vanadyl pyrophosphate, $(VO)_2P_2O_7$ catalyst is to perform the removal of hydrogen atoms from and oxygen insertion towards the four carbon chain. Therefore, the types of oxygen species that involved in the complex nature of the redox mechanism play an important role in terms of how various factors affect the oxygen properties.

From earlier study, researchers Che and Tench (1982) have characterised the activation of oxygen on the metal oxides and proposed a mechanism as illustrated in Figure 2.11. The gas phase oxygen is initially undergoes chemisorption to form an activated species, $[O_a]$. This active species can be formed as molecular surface species (O_2^{2-} or O_2^-), or dissociative adsorbed as monoatomic anions (O^{2-} or O^-). These anions, O^{2-} and O^- are claimed to be highly reactive for the oxidative dehydrogenation and activation of lower alkane (Kung, 1986). The activated oxygen species may possibly react with the hydrocarbon to form hydrocarbon-oxygen complex or replenish the surface layer oxygen, $[O_{a1}]$. Alternatively, the surface lattice oxygen can further replenish the bulk oxygen $[O_1]$, or react with the hydrocarbon. These

surface layer oxygen and bulk oxygen are occurred to be the surface lattice oxygen of the catalyst (Che and Tench, 1982).

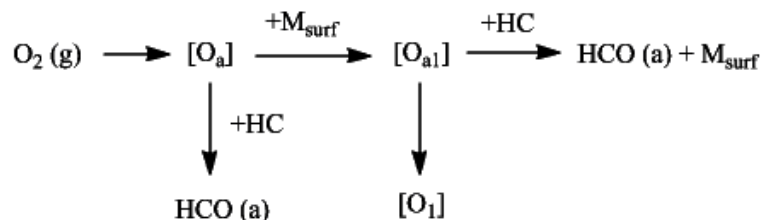


Figure 2.11: Mechanism of the activation of oxygen over metal oxides

(Che and Tench, 1982)

where $[\text{O}_a]$ = chemisorbed oxygen, O_x^{y-}
 $[\text{O}_{a1}]$ = surface layer oxygen
 $[\text{O}_1]$ = bulk oxygen
 M_{surf} = metal oxide surface vacancy
 HC = hydrocarbon
 HCO (a) = hydrocarbon-oxygen complex

Furthermore, previous study has focused on the roles of lattice and surface oxygen in selective oxidation of *n*-butane via temporal analysis of products (TAP) reactor. This study has proposed that the initial activation is performed mainly by surface oxygen, while the intermediate oxidation steps are performed by lattice oxygen (Ebner and Gleaves, 1988).

2.3 Modification of Vanadium Phosphate Catalyst

Catalytic performance is a key feature in the selective oxidation of *n*-butane to maleic anhydride. Due to the dissatisfactions of selectivity to MA, several aspects of further improvement in the catalytic behavior of $(\text{VO})_2\text{P}_2\text{O}_7$ catalyst have been shown, which included:

- i. The method of active phase precursor preparation

- ii. Phosphorus-to-vanadium (P/V) composition
- iii. Addition of promoters
- iv. Activation condition for catalyst precursor

2.3.1 The Catalyst Precursor

Vanadium /Phosphorus /Oxide based catalyst (VPO) can be prepared via different routes. Generally, V_2O_5 is used as a source of vanadium, and H_3PO_4 is used as a source of phosphorus. By using different reducing agents, different kind of precursors can be used, which these precursors will transform to vanadyl pyrophosphate catalyst after calcination process.

Vanadyl hydrogen phosphate hemihydrate ($VOHPO_4 \cdot 0.5H_2O$) is the catalyst precursor for $(VO)_2P_2O_7$. The activation of the precursor in the reaction feedstock yields vanadium phosphate catalyst. After the pretreatment process, the catalyst is equilibrated and the catalytic activity remains consistent throughout the lifetime of the catalyst. The activated catalysts are formed topotactically from the precursor (Johnson et al., 1984). Védrine et al. (2013) proposed that by controlling the morphology of the precursor, we can control the morphology of the final catalyst. This phenomenon has gained a great interest of research, which based around the preparation methods of the catalyst precursor. The methods for the preparation of the catalyst precursor are generally classified into few methods i.e. aqueous, organic, dihydrate (Taufiq-Yap et al., 2002; Hutchings 2009) and hydrothermal (Taufiq-Yap et al., 2006a),

which usually involve reacting agent, V_2O_5 and H_3PO_4 in the presence of reducing agent.

The vanadium phosphorus oxide catalyst prepare via aqueous method, VPA was used in early literature (Equation 2.1). This was the original preparation method for the VPO catalysts, which involved reducing V_2O_5 in an aqueous solution of hydrochloric acid, followed by addition of the phosphorus component, usually as 85% *ortho*- H_3PO_4 (Poli et al., 1981; Batis et al., 1991; Lombardo et al., 1992; Cornaglia et al., 1993; Hutchings et al, 1997). The solid precursor was isolated by evaporation of the solvent.

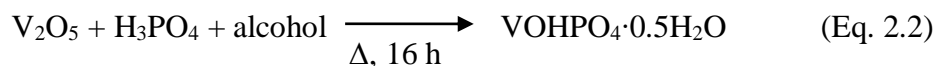


The VPA has gave disadvantage to present engineering, which the presence of traces of chloride is corrosive to reactors. Meanwhile, a significant amounts of impurity $VO(H_2PO_4)_2$ was obtained (Hutchings, 2004) and this method produced catalysts with very low in surface area (Taufiq-Yap et al., 2002).

Other than the traditional mineral acid (HCl), there have been alternative aqueous routes used by other research groups such as oxalic acid, , lactic acid and phosphoric acid, and $NH_2OH \cdot HCl$ as reducing agents (Poli et al., 1981; Hutchings and Higgins, 1997; Shimoda et al., 1985). On the other hand, several of alternative sources have been investigated to have further catalytic improvement. Poli et al. (1981) has replaced V_2O_5 with NH_4VO_3 as the source

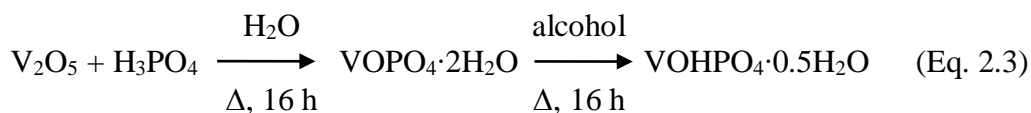
of vanadium in conjunction with H₃PO₄ and oxalic acid, whereas, Batis et al. (1991) used a VCl₃/V₂O₅ mixture instead of V₂O₅. The synthesis method by using vanadium metal to reduce V₂O₅ and the direct reaction of V₂O₅ and H₃PO₄ have also been reported by Mizuno et al. (1997) and Shimoda et al. (1985), respectively. The VPO catalysts prepared via aqueous medium are tend to have low surface area where directly affect the catalyst activity, therefore the catalysts exhibit poor performance for butane oxidation.

In the 1970s, due to the major disadvantage of the VPA method, an improved method has been developed which substitutes both the acid and water needed in aqueous method with organic solvents (Equation 2.2). The most common route which using alcohol as both the solvent and reducing agent:



The precursor, VOHPO₄·0.5H₂O was prepared by reduces the V₂O₅ by an alcohol to a partially soluble V⁴⁺ complex or suspension, followed by the addition of *ortho*-H₃PO₄, and isolation by precipitation (Hodnett, 2000). Isobutanol is the most common organic solvent that used in the preparation (O'Connor et al., 1990) other than the mixture of isobutanol and benzyl alcohol (Cornaglia et al., 1999). Further investigations on other organic solvents have been carried out by researchers such as 2-butyl alcohol, which also gives the VOHPO₄·0.5H₂O catalyst precursor (Johnson et al., 1984). The organic method (VPO) is found to be much better in terms of surface area, reducibility and mobility of oxygen species (Taufiq-Yap et al., 2002).

The vanadium phosphorus oxide catalyst prepared via dihydrate method, VPD was first discovered by Johnson et al. (1984), who described the preparation method for $\text{VOHPO}_4 \cdot 0.5\text{H}_2\text{O}$ precursor by the reduction of $\text{VOPO}_4 \cdot 2\text{H}_2\text{O}$ with alcohol (Equation 2.3). The method has continued to be investigated by Horowitz et al. (1988) and Ellison et al. (1994) for short-chain and longer chain alcohols, respectively. In this method, an intermediate of V^{5+} dihydrate phase, $\text{VOPO}_4 \cdot 2\text{H}_2\text{O}$ is prepared by reacting V_2O_5 and H_3PO_4 using water as solvent before being dried and reduced by isobutyl alcohol to $\text{VOHPO}_4 \cdot 0.5\text{H}_2\text{O}$.



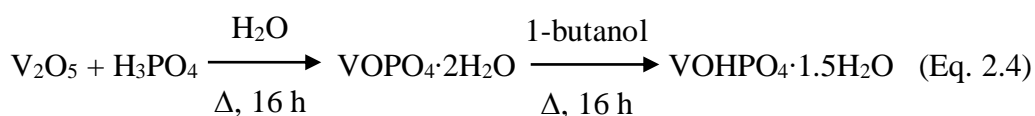
By using primary alcohol, the catalyst produced in form of rosette cluster where high surface area of $40 \text{ m}^2\text{g}^{-1}$ was obtained in a thin hemihydrate (Sananes et al., 1996). Taufiq-Yap et al. (2004b and 2006b) have revealed a high amount of lattice oxygen removed from the VPD catalyst. This phenomenon explains the higher activity of the catalyst was due to the larger amount of active oxygen species removed from the catalyst especially those linked to the V^{4+} phase (Taufiq-Yap et al., 2009a).

In hydrothermal method, the process involves the chemistry of hot water under desired pressure to carry out precipitation reactions. It is the most recent method in preparing $\text{VOHPO}_4 \cdot 0.5\text{H}_2\text{O}$ precursor by reacting V_2O_5 and *o*- H_3PO_4 with water and oxalic acid in an autoclave machine at 383 K (Taufiq-Yap and Hasbi, 2005; Taufiq-Yap et al., 2006a). Taufiq-Yap et al.

(2006a) reported that hydrothermal method catalysts exhibited only the highly crystalline pyrophosphate phase and TPR studies indicated that the oxygen species originating from V^{4+} phase are difficult to be removed. Apparently, the hydrothermal synthesised catalysts have lower activity as compared to VPO and VPD preparation methods.

2.3.2 Sesquihydrate Precursor for $(VO)_2P_2O_7$ Preparation

An alternative precursor, vanadyl hydrogen phosphate sesquihydrate ($VOHPO_4 \cdot 1.5H_2O$) was designed to produce $(VO)_2P_2O_7$ catalyst (Matsuura et al., 1995) and has continued to be investigated by few groups of researchers (Ishimura et al., 2000; Taufiq-Yap et al., 2004a). The precursor was prepared by the reduction of $VOPO_4 \cdot 2H_2O$ suspended in refluxed 1-butanol (Equation 2.4). The $VOPO_4 \cdot 2H_2O$ intermediate is similarly synthesised as in VPD route and subjected to reflux in less reductive *l*-butanol. This method is denoted as VPOs route:



Ishimura et al. (2000) have reported that higher specific activity was observed by the bulk catalyst derived from sesquihydrate precursor as compared from hemihydrate precursor even though with lower surface area. The structure of sesquihydrate route catalyst has formed by layers of wide spacing which capable to intercalate additives to improve catalytic performances (Ishimura et al., 2000; Leong et al., 2011).

By increasing the pretreatment duration of the sesquihydrate precursor in butane/air mixture at 673 K has induced the formation of new V^{5+} phase and reduce of the surface area of the catalysts. The morphology of VPOs catalysts was shown to be in rosette shape. However, by increasing the pretreatment duration, significant changes were observed where the surface of the crystal platelet were cracked and getting rougher. The reactivity studies have showed that more lattice oxygen can be removed for the shortest period of pretreatment which in contrast with the similar catalyst prepared by organic method (VPO) (Taufiq-Yap et al., 2004a).

2.3.3 The Effects of Aqueous, Organic and Dihydrate routes on $(VO)_2P_2O_7$ Catalysts

Many of researches have been done over decades mainly on the effects of different preparation route to the final catalyst in terms of physico-chemical characterizations, reactivity and reactivity studies.

From previous study of Batis et al. (1991) and Hutchings et al. (1997), it was found that the $(VO)_2P_2O_7$ catalyst, which synthesised via aqueous and organic routes had a similar trend in specific activities. However, organic routes for catalyst has obtained higher surface area and better in catalytic performance, as compared to that prepared in aqueous solution.

Comparatively, in morphology, the VPA catalysts have showed a cubic morphology with low surface area while VPO catalysts have platelet structure.

VPD catalysts prepared by primary alcohols have obtained a higher surface area that attributed by a rosette-shape structure and XRD characterization showed only one peak corresponding to the (2 2 0) reflection plane. By using secondary alcohol, it also shown that the VPD catalysts have a similar morphology and surface area with VPO catalysts and consist of characteristic peaks in XRD pattern, where (0 0 1) reflection plane is predominant. These findings have suggested that the catalysts with rosette-shape structure exhibit higher activity than the catalysts in platelets, which attributed by the increasing of surface area as all the catalysts synthesised via hemihydrate precursor are reported to have similar specific activities (Hutchings et al., 1997).

In contrast, Horowitz et al. (1988) have reported that platelets catalysts were more selective than that in rosette-shaped. The catalysts prepared by VPD method with isobutanol and straight chain alcohol; preparation by VPO method using mixture of benzyl alcohol and isobutanol in 1:10 ratio, both have exhibited in rosette-shape structure with low selectivity. This proposed that rosette structure tend to obscure the active planes of the catalyst, where thick platelets give greater in selectivity (Okuhara and Misono, 1993).

2.3.4 Roles of the P/V Ratio

Phosphorus plays an important role in the VPO system although it has been reported that no correlation was observed between the P/V atomic ratio and the catalytic activity (Geem and Nobel, 1987). However, Ruiz et al. (1993)

has proposed that P/V ratio can be an important factor in determining the activity and selectivity of the catalyst.

The optimal catalyst composition is characterised by a slight excess of phosphate with respect to the empirical formula of the $\text{VOHPO}_4 \cdot 0.5\text{H}_2\text{O}$ precursor (Horowitz et al., 1998; O' Connor et al., 1990; Cornaglia et al., 1991). Previous literatures have proposed a considerable excess of surface phosphate, P/V ratio from 1.50 to 3.00 by XPS data (Ebner and Thompson, 1993) in prevent the bulk oxidation of $(\text{VO})_2\text{P}_2\text{O}_7$ to VOPO_4 phases (Centi et al., 1988; O' Connor et al., 1990; Guilhoume et al., 1992). Matsuura and Yamazaki, (1990) reported that the excess of phosphate terminates the side faces of (2 0 0) plane of $(\text{VO})_2\text{P}_2\text{O}_7$ (001, 021, 02-1..., etc) in form of the surface $\text{VO}(\text{PO}_3)_2$ phase which prevents the oxidation of vanadyl pyrophosphate due to lower oxidisability of $\text{VO}(\text{PO}_3)_2$.

However, Cavani et al. (1992) reported that with a slight deficiency of phosphate (P/V=0.95) in the catalyst, the rates of V^{4+} oxidation and reduction are high. The increase of V^{5+} content leads to more active but less selective catalyst, vice versa, low reducibility of V^{4+} in VPO catalysts with high surface phosphate concentration results in low catalytic activity. Therefore, catalysts with a slight excess of phosphate (P/V=1.05) show the good correlation between the reducibility and oxidisability to obtain high activity and selectivity in *n*-butane oxidation.

High surface phosphate concentration ($P/V \geq 2.0$) is the important factor for the selectivity of the catalyst by isolating the V^{4+} active site on the surface (Hodnett et al., 1983; Hodnett and Delmon, 1984). This is further supported by Garbassi et al. (1986), they found the presence of β -VOPO₅ phases were detected at P/V ratio that less than 1.0, whereas the excess of phosphate is proposed to prevent the oxidation of V^{4+} to V^{5+} during the calcination process.

However, Morishige et al. (1990) found that the industrial catalysts which had prepared with bulk P/V ratio of 0.95 to 1.20, surface enrichment of phosphate was obtained ($P/V = 1.6 - 1.8$). They suggested that a phosphate-rich layer was supported on the surface of $(VO)_2P_2O_7$, which responsible for the oxidation of *n*-butane to MA.

Satsuma et al. (1989) studied a series of catalysts with P/V ratio of 1.0 to 2.0. They proposed that a number of vanadium sites are remained inactive at P/V ratio less than 1.0, whereby at higher P/V ratio, all active surface sites are observed.

2.3.5 The Effect of Promoters

One of the key areas of studied in VPO catalysts is the promotion effect of compounds, known as dopants or promoters. A promoter defined as a small amount of material added to the catalyst, which in itself it is of low activity or inactivity, but in the reaction it enhances the activity, stability or selectivity of

the active component (Bartholomew and Farrauto, 2006). The industrial employed VPO catalysts are usually promoted with metal compounds purposely to improve the catalytic performance in terms of activity and selectivity (Centi et al., 2001a). The nature, the location and the roles of metal promoters in the VPO system have been previously reviewed (Hutchings, 1991; Hutchings and Higgins, 1996). The catalytic performance of both doped and undoped catalysts is frequently studied and claimed at low *n*-butane conversion of 15% to 50%.

Several methods have been used in the past to incorporate promoters in the VPO lattice (Hutchings, 1991):

- i. The incorporation of promoters during the synthesis of $\text{VOHPO}_4 \cdot 0.5\text{H}_2\text{O}$ precursor
- ii. The wetness impregnation of the $\text{VOHPO}_4 \cdot 0.5\text{H}_2\text{O}$ precursor with the promoters prior to the formation of final catalyst by heat treatment
- iii. Promoter impregnation into final VPO catalysts

In Kourtakis et al. (2010) studies, they proposed a method in which promoter cations are incorporated into the precursors by cation substitution during its synthesis. During the calcination process, the promoter cations migrate into the bulk and lattice of the catalyst in varying degrees to form new microstructures which showed improvements in catalytic performance. Promoter compounds can be added either together with the vanadium and phosphorus compounds prior to preparation of the catalyst precursor; or by

impregnation of the catalyst precursor prior to formation of the final catalyst by heat treatment (Hutchings, 1991).

Several studies have been reported concerning the synthesis of VPO precursors as well as the role that promoters can play in improving catalytic performance. A wide range of cation metals have been added to vanadium phosphate catalysts and beneficial effects have been reported. For example, great efforts have been made by researchers that found that Zr, Zn and Cr could be used as structural promoter, while Fe, Cs and Ag can enhance the activity of VPO catalysts (Ye et al., 1990; Sananes et al., 1992; Hutchings and Higgins, 1996; Gulians et al., 1999b; Ji et al., 2002; Liang and Ye, 2005). The incorporation of promoters were considered to act in two ways; structural promoter, effects due to an enhancement in the surface area of the activated catalyst, and electronic promoter, which has been demonstrated in very few systems to date (Sartoni et al., 2004)

The incorporation of alkali and alkaline-earth metal ions in the VPO lattice was studied and reported by Zazhigalov et al. (1996). They found that the presence of different concentration of Li, Na, K, Cs, Be, Mg, Ca and Ba cations can easily donate electrons to the VPO lattice, thus increase the electronegativity of lattice oxygen thus enhancing the rate of *n*-butane oxidation. The similar series of promoters was reported by Brutovsky et al. (1997). He found that the incorporation of Mg, Ca and Ba salts with VPO catalysts provided a higher product yield and selectivity of MA as compared to the unpromoted catalyst which derived from aqueous method.

There has been very little interest shown in doping by group 13 elements such as (B, Al, Ga, In). However, Sanchez et al. (2001) have found that these promoters are able to change the morphology of the $\text{VOHPO}_4 \cdot 0.5\text{H}_2\text{O}$ precursor from its characteristic platelet-like to rosette-like structure. They realised that only Ga- and In- promoted catalysts improved the catalytic performance in *n*-butane oxidation to maleic anhydride. On the other hand, Holmes et al. (2000) have reported that Al- promoted VPO catalysts during the synthesis of $\text{VOHPO}_4 \cdot 0.5\text{H}_2\text{O}$ precursor improved the catalytic performance for the selective oxidation of *n*-butane, at the same time shortened the equilibration period as compared to the conventional VPO catalysts. They found that the morphology of the precursor was affected by the incorporation of aluminum phosphate. Both of the $(\text{VO})_2\text{P}_2\text{O}_7$ and amorphous aluminum phosphate were crystallised during the equilibration of the promoted $\text{VOHPO}_4 \cdot 0.5\text{H}_2\text{O}$ precursor.

Low levels of Ga- promoted VPO catalysts displayed improved the catalytic performance during the *n*-butane oxidation and increased the surface area as compared to the unpromoted VPO catalyst (Sartoni et al., 2004). The source of Ga was found to be and experiments were carried out with Ga_2O_3 , GaPO_4 and $\text{Ga}(\text{acac})_3$ during the synthesis of $\text{VOHPO}_4 \cdot 0.5\text{H}_2\text{O}$ precursor. $\text{Ga}(\text{acac})_3$ was found to give significant improvement in *n*-butane conversion, but neither Ga_2O_3 nor GaPO_4 gave an enhancement in surface area. A series of Ga doped (0.1 - 1.5 mol%) catalysts prepared using $\text{Ga}(\text{acac})_3$ had been tested in the study. The 0.1 mol% of Ga produced using $\text{Ga}(\text{acac})_3$ shown to have the best activity, with 73 % *n*-butane conversion. It is believed that further

modification of Ga-doped VPO catalyst could improve overall performances of catalyst.

Typically, there is an ideal concentration of the promoter at which its favourable effect reaches its maximum, this latter being observed within a narrow range of promoter concentration only. For instance, the low level of molybdenum (Mo) introduced to the VPO catalysts (Hutchings, 1996) is found to increase both activity and selectivity whereas the low level of Co affects mainly the activity (Abdelouahab et al., 1995; Mota et al., 2000). Due to the reason of considerably increased activity, smaller amounts of expensive active dopant are necessary. Hence, the catalyst can become more economic.

Some of the results of recent studies are summarised and briefly discussed in Table 2.2 which demonstrate the beneficial effects of promoters on VPO system for selective oxidation of *n*-butane to maleic anhydride.

Table 2.2: Selected promoted VPO catalysts studies in selective oxidation of *n*-butane to maleic anhydride

Promoter	Doping level	Synthesis	Catalytic performance (Promoted)	Catalytic performance (Unpromoted)	Promoter location or function	Reference
Cr, Mo, W	Cr/Mo=0.5-5% wt. W=1.7-10.5% wt. P/V=1.3	Wetness impregnation with *VHP, salts and isobutyl alcohol	Ψ S(MA) = 22% - 84% at Ψ C = 80% at 631 K	S(MA) = 50% at C = 80% at 718 K	Structural modifier	Pierini and Lombardo, 2005
Cr, Mo, W	Cr/Mo=1-5% wt. W=2.5-10.5% wt. P/V=1.3	Co-precipitate with *VHP, salts, isobutyl alcohol and phosphoric acid during phosphatation	S(MA) = 9% - 80% at C = 80% at 683 K	S(MA) = 50% at C = 80% at 718 K	Not reported	Pierini and Lombardo, 2005
Ce-Fe	VPO/Ce-Fe=1:3, 1:1, 4:1 at 5% wt. P/V=1.1	Ce-Fe oxide mixture precipitated from nitrates added to V ₂ O ₅ , isobutyl alcohol and benzyl alcohol under co-precipitation	Ψ Y(MA) = 39.7% - 42.7% at 673 K	Y(MA) = 27.4% at 673 K	Increase lattice oxygen activity	Shen et al., 2002

Table 2.2 (continued)

Bi-Fe	Bi-Fe/V=1% wt.	Bi and Fe nitrates with VPD under reflux	S(MA) = 64% at C = 43% at 673K	S(MA) = 63% at C = 83% at 673K	No effect Likely	Goh et al., 2008
	Bi-Fe/V=1% wt.	Co-precipitation of Bi-Fe complex with isobutanol	S(MA) = 61% at C = 72% at 673K		surface Bi- Fe oxide	
	Bi-Fe/V=1% wt.	Ball-milling of Bi-Fe oxide with ethanol	S(MA) = 55% at C = 57% at 673K		Increase surface area	
Ga	Ga/V=0.1% - 1.0% mol	Ga([#] acac) ₃ , Ga ₂ O ₃ and GaPO ₄ added to VHP and H ₃ PO ₄ under reflux	S(MA)= 45%- 62% at C = 24%-73% at 673K	S(MA) = 55% at C = 22% at 673K	Structural and electronic promoter	Sartoni et al., 2004
Bi	Bi/V=0.1	Ball-milling of BiPO ₄ and organic VHP	S(MA)= 74% at C = 88% at 713K	S(MA)= 67% at C = 73% at 713K	Bulk BiPO ₄	Haber et al., 1997
	Bi/V=0.1	Ball-milling of Bi ₂ O ₃ and organic VHP	S(MA)= 71% at C = 83% at 713K		Surface BiPO ₄	

Table 2.2 (continued)

Co	Co/V=4% wt.	Impregnation of VHP with Co acetate or acac	S(MA)= 60% at C = 80% at 703K	S(MA)= 30% at C = 80% at 713K	Co phosphate phase	Cornaglia et al., 1999; 2000
----	-------------	---	-------------------------------	-------------------------------	--------------------	------------------------------

*VHP = $\text{VOHPO}_4 \cdot 0.5\text{H}_2\text{O}$ #acac = acetyl acetate Ψ C, S(MA) and Y(MA) are *n*-butane conversion, MA selectivity and yield of MA, respectively

2.3.6 Activation Condition of Catalyst Precursor

Activation conditions and duration of catalyst precursor play an important role in obtaining the active site of VPO catalysts for *n*-butane oxidation to maleic anhydride. Several number of crystalline VPO phases can be observed during the transformation of precursor to the active VPO catalyst. The active phase can be affected by the temperature, time and atmosphere of activation, precursor morphology, P/V ratio and the presence of defects in the structure (Ruiz et al., 1987; Centi et al., 1993).

Generally, the activation procedure has been reported in two types of method which included:

- i. Activation in air at temperature lower than 673 K, which followed by introduction of reactant mixture. As the precursor is heated at 553 K, the trapped alcohol is being released, which cause disruption of the structure, microcracks and increases the surface area. The precursor is first decomposed and transformed to an amorphous phase consist of V^{5+} and V^{4+} . Then, the amorphous phase was dehydrated and transformed to $(VO)_2P_2O_7$ active phase by the reactant mixture (Horowitz et al., 1988; Cornaglia et al., 1991)
- ii. Activation in oxygen-free atmosphere at temperature higher than 673 K, which followed by introduction of hydrocarbon-air mixture (*n*-butane in air). Pure crystalline $(VO)_2P_2O_7$ is being formed at first and partial oxidation are likely to occur after the introduction of hydrocarbon-air mixture (Horowitz et al., 1988; Cavani and Trifirò, 1994)

2.3.7 The Effect of Calcination Duration/ Temperature

Calcination process involves high temperature at which its purpose is to decompose and volatilise the catalyst precursors into the final catalyst. It has been known that the calcination temperature, duration and environment can affect the transformation of precursor to active phase (Taufiq-Yap et al. 2001).

Hodnett and Delmon (1984) studied the effect of calcination duration and temperature on the formation of phases related to VPO catalysts synthesised via VPA method. They found that excess phosphorus has strongly stabilised the V^{4+} in the β^* phase which calcined at 773 K (Hodnett et al., 1983), and one of the related phases B, β or $(VO)_2P_2O_7$ during calcination at 923 K (Bordes and Courtine, 1979; Poli et al., 1981). Higher calcination temperatures claimed to be more favored to the formation of β -VPO₅ and resulted in lower surface area.

Ma et al. (2012) also reported that catalyst calcined at high temperature (above 1123 K), agglomeration occurred which decreased the surface area and pore volume. They proposed that the particle size of catalyst would remain stable at low temperature, however, high temperature causing the catalyst to become bulkier in crystallite size. High temperature calcination will lead to sintering structural change, as well as deactivation of surface area and reduce in pore volume. However, if the calcination process is performed at temperature lower than 573 K, the precursor will fail to transform to active phase $(VO)_2P_2O_7$. Therefore, the optimum calcination temperature range for VPO catalyst should be set at 673 – 753 K.

Waugh and Taufiq-Yap (2003) studied the effect of varying the calcination duration of the butane/air based on the morphology and reactivity of VPO catalysts. A series of catalysts had been prepared by calcine $\text{VOHPO}_4 \cdot 0.5\text{H}_2\text{O}$ for different duration (40, 100 and 132 h) in 0.75% *n*-butane/air mixture at 673 K. They reported that increasing the calcination duration with *n*-butane/air mixture displayed increased in total surface area and changed the surface and bulk morphologies into which more oxygen can be removed from the lattice structure.

Taufiq-Yap et al. (2004a), on the contrary, studied a series of catalysts which was derived from $\text{VOHPO}_4 \cdot 1.5\text{H}_2\text{O}$ which calcined at 10, 30 and 75 h with a reaction flow of 0.75% *n*-butane/air mixture. On the basis of comparison between surface area they found that the total surface area was decreased with the calcination duration. However, the amount of oxygen desorbed was increased as the length of calcination time prolonged.

Further study of VPO catalysts derived from $\text{VOHPO}_4 \cdot 0.5\text{H}_2\text{O}$ was carried out and reported by Taufiq-Yap et al. (2012). They reported that increasing the calcination duration of VPO catalysts prepared via VPO and VPD method, induced the formation of V^{5+} phase and led to a decrease in total surface area. They proposed that the shape of the catalysts was cracked and lost as the calcination time prolonged.

2.3.8 The Effect of Calcination Environment

Previous studies have shown that the calcinations atmospheres can affect the catalyst's morphology, activity, and selectivity towards the *n*-butane oxidation. In order to maintain the active phase (V^{4+}) VPO catalyst, the reducing property of *n*-butane is needed with the non-reactive environment by using inert gases (N_2/CO_2) to prevent oxidisation. However, this non-reactive environment required high calcination temperature that might causing sintering phenomenon. Therefore, the calcination atmosphere of VPO catalyst has been set at 0.75 % *n*-butane in air, which below the explosive limit (~ 1.75 %) (Cheng and Wang 1997).

Taufiq-Yap and Saw (2008) have discussed the effect of different calcination environments on VPO catalysts. The VPO catalysts were synthesised via dihydrate route and were calcined in *n*-butane/air and propane/air, respectively. They found that both catalysts exhibited well crystalline with characteristic peaks of pyrophosphate phase. The *n*-butane/air calcined catalysts gave higher in surface area and oxygen species associated with V^{4+} as compared to the propane/air calcined catalysts.

The effect of water vapor on the transformation of $VOHPO_4 \cdot 0.5H_2O$ to $(VO)_2P_2O_7$ was investigated by Ryumon et al. (2006). The precursor was transformed into a single-phase of well-crystallised $(VO)_2P_2O_7$ within 5 h with presence of 40% water vapor under a reactant gas (0.9% *n*-butane, 10% O_2 in He), whereas the transformation took more than 100 h in reactant gas without water vapor. They found that water vapor has accelerated two processes in calcination process

under the reaction conditions: the crystallization of the amorphous vanadium pyrophosphate phase containing V^{4+} and V^{5+} to $(VO)_2P_2O_7$ and β - $VOPO_4$, respectively, and the transformation of β - $VOPO_4$ to $(VO)_2P_2O_7$. They suggested that the water vapor inhibited the topotactic transformation of $VOHPO_4 \cdot 0.5H_2O$ to $(VO)_2P_2O_7$.

CHAPTER 3

MATERIALS AND METHODOLOGY

3.1 Gases and Materials

The gases and materials for the preparation of vanadyl pyrophosphate catalysts are prepared accordingly to the grade and purity as tabulated in Table 3.1.

Table 3.1: Gases and materials for the preparation of vanadyl pyrophosphate catalysts

Chemicals	Supplier	Purity (%)
0.75% <i>n</i> -Butane in air, <i>n</i> -C ₄ H ₆ /air	MOX	0.75
Vanadium(V) oxide, V ₂ O ₅	Merck	99
<i>ortho</i> -phosphoric acid, <i>o</i> -H ₃ PO ₄	Merck	85
Gallium(III) acetyl acetonate, Ga(C ₅ H ₇ O ₂) ₃	Sigma Aldrich	99.99
Molybdenum(IV) oxide, MoO ₂	Sigma Aldrich	99.99

3.2 Methodology

The synthesis of vanadyl pyrophosphate catalyst has been developed by Matsuura et al. (1995) via vanadyl hydrogen phosphate sesquihydrate precursor (VOHPO₄·1.5H₂O). In this research, the sesquihydrate route was employed due to the usage of more environmental friendly reducing agent (1-butanol). From the studies of Sartoni et al. (2004), 0.1 mol% of gallium was reported to increase the activity of VPO catalyst, while 1 mol% of molybdenum has enhanced the selectivity

towards the formation of maleic anhydride, studied by Beatriz and Lombardo, (2005). Thus, gallium(III) acetyl acetonate, $\text{Ga}(\text{C}_5\text{H}_7\text{O}_2)_3$ and molybdenum(IV) oxide, MoO_2 were respectively used as dopant to modify the VPOs catalysts with the expectation to increase the conversion rate of *n*-butane to maleic anhydride and reduce the formation of by-products. The 0.1 mol% of Ga with 1 mol% of Mo doped VPOs catalysts will be used and undergo different calcination durations in Series 2, with expectation to further improve the catalytic performances. The synthesis methods of VPOs catalyst in this research are based on the previous studies by Sartoni et al. (2004), Beatriz and Lombardo, (2005), Leong et al. (2012) and Taufiq-Yap et al. (2012). By using their researches as references, at least 3 repetition of experimental set were prepared in order to obtain more accurate results.

3.2.1 Preparation of Bulk Catalysts via Sesquihydrate Precursor Route (VPOs)

The synthesis of vanadyl hydrogen phosphate sesquihydrate precursor ($\text{VOHPO}_4 \cdot 1.5\text{H}_2\text{O}$) is a two-steps procedure, which involving vanadyl hydrogen phosphate dihydrate ($\text{VOPO}_4 \cdot 2\text{H}_2\text{O}$), as the intermediate before obtaining the sesquihydrate precursor.

In the first stage (Figure 3.1), 15.0 g of Vanadium(V) oxide, V_2O_5 was suspended with 90 ml of aqueous *ortho*-phosphoric acid, *o*- H_3PO_4 in 360 ml of distilled water. The mixture was then stirred under reflux at 393 K for 24 h. The brownish solid solution had gradually changed to yellow colour. The resulting yellow solid ($\text{VOPO}_4 \cdot 2\text{H}_2\text{O}$) was recovered by centrifugation and washed sparingly

with distilled water. The sample was then dried in oven at 358 K for 72 h and finally identified by x-ray diffraction (XRD) technique.

In the second stage (Figure 3.2), 10.0 g of synthesised $\text{VOPO}_4 \cdot 2\text{H}_2\text{O}$ was added in 150 ml of 1-butanol and refluxed with continuous stirring at 393 K for 24 h. After being cooled to room temperature, the resulting light blue solid ($\text{VOHPO}_4 \cdot 1.5\text{H}_2\text{O}$ precursor) was then recovered by centrifugation, washed sparingly with small amount of acetone and finally oven-dried at 358 K for 72 h. The precursor was denoted as PreVPOs-Undoped.

The undoped precursor was then calcined in a reaction flow of 0.75% *n*-butane in air mixture at 723 K for 18 h to generate the active phase of catalyst $(\text{VO})_2\text{P}_2\text{O}_7$ (Figure 3.3). The activated catalyst was denoted as VPOs-Undoped and it acts as bulk reference catalyst.

3.2.2 Series 1: Preparation of Ga-doped and Mo-doped VPOs Catalysts

The synthesis of Ga and Mo doped catalysts precursor at first stage were similar to the preparation of the undoped catalyst as shown in section 3.2.1.

In the second stage (Figure 3.2), 0.1 mol% of gallium (III) acetylacetonate, $\text{Ga}(\text{acac})_3$ was added into 10 g of $\text{VOPO}_4 \cdot 2\text{H}_2\text{O}$ precursor for the preparation of 0.1% Ga doped VPOs catalyst. The mixture was dissolved in 1-butanol (150 ml) and refluxed with stirring at 393 K for 24 h. The step was repeated with difference concentration of gallium dopant (0.3 and 0.5 mol%).

After being cooled to room temperature, the resulting light blue solid ($\text{VOHPO}_4 \cdot 1.5\text{H}_2\text{O}$ precursor) was then recovered by centrifugation, washed sparingly with small amount of acetone and finally oven-dried at 358 K for 72 h. The Ga doped precursor was denoted as PreVPOs-X%Ga ($X = 0.1, 0.3$ and 0.5). The above steps were repeated with molybdenum dopant, Mo (1, 3 and 5 mol%), where molybdenum (VI) oxide, MoO_2 was used as Mo dopant source.

Both Ga doped and Mo doped precursor were then calcined in a reaction flow of 0.75% *n*-butane in air mixture for 18 hours 723 K. The activated Ga and Mo doped catalysts after calcined for 18 h were denoted as VPOs-X%Ga ($X = 0.1, 0.3$ and 0.5 mol%) and VPOs-X%Mo ($X = 1, 3$ and 5 mol%), respectively.

3.2.3 Series 2: Preparation of Ga-Mo doped VPOs Catalysts with Different Calcination Duration

In Stage 1 synthesis, the catalysts precursor were prepared as shown in section 3.2.1. For the second stage of reflux, 0.1 mol% of gallium (III) acetylacetonate, $\text{Ga}(\text{acac})_3$ and 1 mol% of molybdenum (VI) oxide were added into 10.0 g of $\text{VOPO}_4 \cdot 2\text{H}_2\text{O}$. The mixture was dissolved in 150 ml of 1-butanol and refluxed with continuous stirring at 393 K for 24 h.

After being cooled to room temperature, the resulting light blue solid ($\text{VOHPO}_4 \cdot 1.5\text{H}_2\text{O}$) was then recovered by centrifugation and washed sparingly with small amount of acetone, then oven-dried at 358 K for 72 h. The Ga-Mo doped precursors were denoted as PreVPOs-0.1%Ga1.0%Mo.

The Ga-Mo doped precursor was calcined in a reaction flow of 0.75% *n*-butane in air mixture at 723 K for 18, 36, 54 and 72 hour, respectively (Figure 3.3). The activated Ga-Mo doped catalysts after different calcination duration were denoted as VPOs-0.1%Ga1%Mo-X (X = 18, 36, 54 and 72 h), respectively. The activated Ga-Mo doped catalyst calcined for 18 h was acts as the reference catalyst in Series 2.

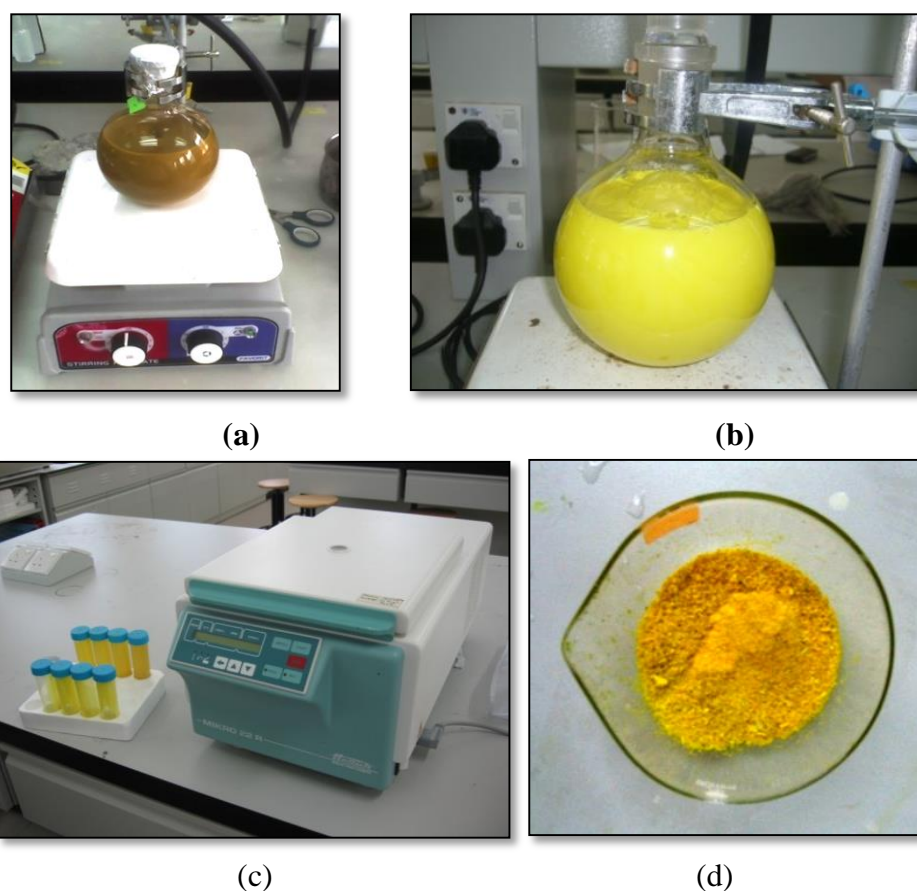
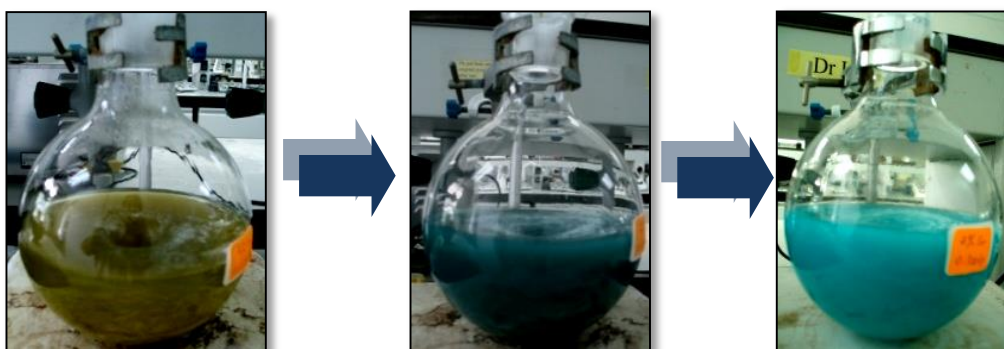


Figure 3.1: (a) First stage reflux; (b) Colour transformation of mixture during stage 1 reflux; (c) Centrifugation and (d) $\text{VOPO}_4 \cdot 2\text{H}_2\text{O}$ intermediate



(a)



(b)



(c)

Figure 3.2: (a) Colour transformation of solution during second stage reflux; (b) Centrifugation and (c) $\text{VOHPO}_4 \cdot 1.5\text{H}_2\text{O}$ precursor after oven drying

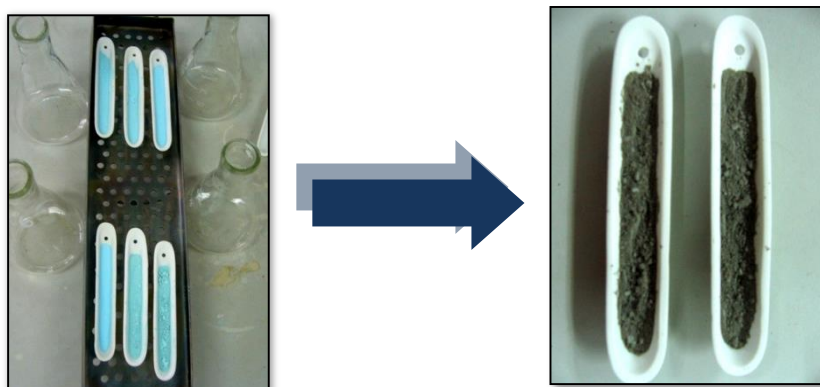


Figure 3.3: Thermal activation of $(\text{VO})_2\text{P}_2\text{O}_7$ catalysts

3.3 Characterisation of Vanadyl Pyrophosphate Catalysts

3.3.1 Gases and Materials

The gases and materials for the characterisation of vanadyl pyrophosphate catalysts are prepared as shown in Table 3.2.

Table 3.2: Chemicals and Gases

Methodology		Supplier	Purity (%)
BET surface area measurements			
Chemicals	Liquid Nitrogen, N ₂	MOX	
Gases	Purified Nitrogen, N ₂	MOX	99.999
	Purified Helium, He	MOX	99.999
ICP-OES			
Chemicals	Nitric acid, HNO ₃	Merck	69-70
	Vanadium (V) pentoxide, V ₂ O ₅	UNI Chem	
	Gallium(III)Acetylacetonate, Ga(C ₅ H ₇ O ₂) ₃	Aldrich	99.99
	Molybdenum (IV) Oxide, MoO ₂	Aldrich	99
	<i>ortho</i> -Phosphoric acid, <i>o</i> -H ₃ PO ₄	MERCK	85
Redox titration			
Chemicals	Potassium Permanganate, KMnO ₄	Fisher Scientific	
	Sulphuric acid, H ₂ SO ₄	Merck	95-97
	Ammonia Dihydrogen Orthophosphate, NH ₄ H ₂ PO ₄	Ajax chemicals	
	Diphenylamine, (Ph) ₂ NH	Acros Organics	
	Ammonium Metavanadate, NH ₄ VO ₃	BDH Chemicals	
	Ammonium Iron(II) Sulphate, (NH ₄) ₂ Fe(SO ₄) ₂ ·6H ₂ O	System	
Temperature Programmed Reduction (TPR in H₂ / Ar)			
Gases	Hydrogen in Argon, H ₂ /Ar	MOX	5.23
	Purified Argon, Ar	MOX	99.999
Fixed-Bed microreactor			
Gases	<i>n</i> -Butane in air	MOX	1.0
	Purified Helium, He	MOX	99.999

3.3.2 Instrumentations and Characterisation Technique

A series of instruments and characterisation technique were used throughout the entire research for catalysts characterisation as shown in Table 3.3.

Table 3.3: The instrumentations and characterisation technique used

Instrumentations and Characterisation Technique	Specification
<u>Physical Characterisation</u>	
X-ray diffractometer	Shinadzu XRD-6000
Scanning electron microscopy	Hitachi S-3400N
Brunauer-Emmet-Teller surface area measurements	Thermo Finnigan Sorptomatic 1990
<u>Chemical Characterisation</u>	
Energy-dispersive x-ray analyses	EDAX and Oxford software
Inductive coupled plasma-optical emission spectrometry	Perkin Elmer Optima 2000 DV optical emission spectrometer
Redox titration	Niwa and Murakami (1982) method
<u>Reactivity Study</u>	
Temperated-programmed reduction	TPDRO 1100 series
Catalytic Test	Fixed-bed microreactor with on-line Thermo Scientific TRACE GC Ultra™

3.4 Methodology

3.4.1 X-ray Diffraction (XRD) Analyses

XRD analyses for the catalysts were performed by using a Shimadzu XRD-6000 diffractometer (Figure 3.4) employed with Cu K α radiation ($\lambda = 1.54 \text{ \AA}$) at 40 kV generated by a copper x-ray tube (Toshiba, A-40-Cu) at normal focus 2.0 kW type at ambient temperature. Small amount of sample solid is prepared and packed into an aluminium shallow plate holder. The high quality XRD patterns of precursor

and catalysts were obtained with a continuous scanning range of $2\theta = 2.0000\text{--}60.0000^\circ$ at the rate of $2.000^\circ\text{min}^{-1}$. The diffractogram obtained will then be matched up with the Joint Committee on Powder Diffraction Standards (JCPDF) PDF1 database version 2.6 to verify the precursor and catalyst phases. The values of the unique distance (d-spacing), intensity and FWHM were obtained by using Basic Process version 2.6 software by Shimadzu.



Figure 3.4: Shimadzu XRD-6000 Diffractometer

3.4.2 Scanning Electron Microscopy (SEM) and Energy-Dispersive X-Ray (EDX) Spectroscopy

The images of surface morphologies of catalysts were captured on a Hitachi S-3400N scanning electron microscope (Figure 3.5). A small amount of fresh catalyst was prepared and placed on the surface of a carbon tape, which had been fixed on an aluminium stub (diameter = 10 mm). Then, the stub was coated with gold in a sputter coater and followed by imaging process. The EDX analyses were continued by using EDAX and Oxford software coupled with the SEM machine

(Hitachi S-3400N). The surface P/V atomic ratio of catalysts were obtained quantitatively by manipulating parameters (process time, live time, dead time, current probe and accelerating voltage) which can affect the final x-ray spectrum.



Figure 3.5: Hitachi S-3400N electron microscope coupled with EDAX software

3.4.3 Brunauer-Emmett-Teller (BET) Surface Area Measurements

The Brunauer-Emmett-Teller (BET) surface area, involving nitrogen adsorption-desorption at 77 K has been used for the determination of the surface area of the catalysts by using a Thermo Finnigan Sorptomatic 1990 analyser (Figure 3.6). Prior to analysis, approximately 0.5 g of catalyst was degassed at 423 K for overnight as the pre-treatment stage. The analysis method is based on non-specific physisorption of a N_2 gas onto a solid close to the condensation temperature of the desorbing gas. The adsorption is characterised by an isotherm, which represents the equilibrium amount of N_2 gas adsorbed on a solid at given temperature, as a function of pressure. The specific surface area is calculated by the BET equation (Equation 3.1) (Brunauer et al., 1938):

$$\frac{p}{V(p_o - p)} = \frac{1}{V_m C} + \frac{(C-1)p}{CV_m p_o} \quad (\text{Eq. 3.1})$$

where V is the volume, reduced to standard conditions, i.e. the standard temperature and pressure (STP) of gas adsorbed per unit mass of adsorbent at given pressure, p and constant temperature; p_o is the saturation pressure at the measurement temperature; V_m is the volume of gas required to form a complete monolayer adsorbed layer at STP per unit mass of adsorbent, when the surface is covered by monolayer of adsorbate; and C is a constant related to free energy of adsorption which is represented by Equation 3.2.

$$C = A_r \exp\left[\frac{(\Delta H_1 - \Delta H_2)}{RT}\right] \quad (\text{Eq. 3.2})$$

where A_r is the pre-exponential factor; ΔH_1 is the heat of adsorption of first layer; ΔH_2 is the heat of liquefaction; R is the gas constant; and T is the absolute temperature (K). All the VPOs catalysts in this research shown a mesoporous adsorption curve in BET analysis, indicated that the produced catalysts are consisted of mesoporous texture of Type IV isotherm. The graph were attached in Appendix I.



Figure 3.6: Thermo Finnigan Sorptomatic 1990

3.4.4 Inductively Coupled Plasma-Optical Emission Spectrometry (ICP-OES)

The bulk chemical composition of catalysts were obtained by using an inductively coupled plasma-optical emission spectrometry (ICP-OES) using a sequential scanning Perkin Elmer Optima 2000 DV optical emission spectrometer as shown in Figure 3.7. Initially, a known amount of catalyst (0.025 g) was digested in 10 ml of HNO₃ (8 M) with slightly heated and stirred continuously. The resulting solutions were diluted with deionised water to obtain nominal concentration of 100 ppm. The standard solutions of phosphorus and vanadium were both prepared at concentration 6.25, 12.5 and 25.0 ppm, while the standard solution of Ga³⁺ and Mo⁴⁺ were both prepared at concentration 0.03125, 0.125, 0.5, 2 and 5 ppm, respectively. Deionised water was used as a blank solution, also known as a control. All the standard solutions and blank solutions were added with 10 mL of HNO₃ (8 M) in order to be consistent with the sample solutions.



Figure 3.7: Perkin Elmer Optima 2000 DV optical emission spectrometer

3.4.5 Redox Titration Analyses

Redox titration was carried out to determine the average vanadium valence (V_{AV}) of the VPO catalyst according to the method developed by Niwa and Murakami (1982). A known amount of catalyst (0.1 g) was dissolved in 100 ml sulphuric acid (2 M) at 353 K and cooled to room temperature before being titrated. Then, 20 ml of this solution was first titrated with potassium permanganate solution (0.01 N). This titrant was functioned as to oxidise both V^{3+} and V^{4+} in the solution to V^{5+} with the colour changed from original greenish-blue to pale purple where the end point was obtained. The volume of potassium permanganate used was recorded as V_1 . Then the oxidised solution was treated with ammonium iron (II) sulphate solution (0.01 N) with diphenylamine as redox indicator. The end point was observed by the colour of solution changed from purple to colourless, indicated that all the V^{5+} was reduced to V^{4+} . The volume of ammonium iron (II) sulphate used was denoted as V_2 . A fresh 20 ml of the original solution was titrated with ammonium iron (II) sulphate solution (0.01 N) with diphenylamine as redox indicator to determine the V^{5+} content in the original solution. The end point was indicated by the colour changed from purple to greenish-blue. The amount of ammonium iron (II) sulphate solution used was recorded as V_3 . According to Niwa and Murakami (1982), the relative amount of V^{3+} , V^{4+} and V^{5+} can be determined by the following equations:

$$\begin{aligned}V^{4+} + 2V^{3+} &= 20 [\text{MnO}_4^-] V_1 \\V^{5+} + V^{4+} + V^{3+} &= 20 [\text{Fe}^{2+}] V_2 \\V^{5+} &= 20 [\text{Fe}^{2+}] V_3\end{aligned}\tag{Eq.3.3}$$

where $[\text{MnO}_4^-]$ is the concentration of potassium permanganate solution; $[\text{Fe}^{2+}]$ is the concentration of ammonium iron (II) sulphate solution; V_1 is the volume of potassium permanganate solution used' and both V_2 and V_3 are the volumes of ammonium iron (II) sulphate solution used.

The average oxidation state of vanadium (VAV) can be determined by solving the equation below (Niwa and Murakami, 1982):

$$V_{AV} = \frac{5V^{5+} + 4V^{4+} + 3V^{3+}}{(V^{5+} + V^{4+} + V^{3+})} \quad (\text{Eq. 3.4})$$

3.4.6 Temperature-programmed Reduction (TPR in H₂) Analyses

TPR in H₂ analyses were performed by using Thermo Electron TPDRO 1100 (Figure 3.8). The TPR analysis started with a two stages pre-treatment process on the catalyst to eliminate the possible contaminants and oxidise the metal portion of the catalyst which involved two stages. In the first stage, a catalyst (~0.0200 g) was cleaned by using a purified argon flow (1 bar, 20 cm³ min⁻¹) held for 5 min at room temperature. Subsequently, the catalyst was cleaned by heating (10 K min⁻¹) from room temperature to 473 K in a purified argon flow (1 bar, 20 cm³ min⁻¹) for 45 min before cooling to room temperature. After the pre-treatment process, the flow was switched to 5.23% hydrogen in argon (1 bar, 25 cm³ min⁻¹) stream with a linear raise of temperature (5 K min⁻¹) from room temperature to 1000 K. A TPR in H₂ profile was plotted in hydrogen consumed as a function of temperature by using TPDRO Version 2.3 software.



Figure 3.8: Thermo Electron TPDRO 1100

3.4.7 Catalytic Tests

The partial oxidation of *n*-butane to maleic anhydride (MA) was carried out in a laboratory-scaled fixed-bed microreactor (Figure 3.9). A standard amount of catalyst (0.25 g) was held in place by plugs of quartz wool in a reactor tube and fixed into a furnace. A thermocouple was located in the centre of the catalyst bed and the reaction temperature was controlled typically at ± 1 K. Reactant gas *n*-butane and air were fed into the reactor via calibrated mass flow controllers to provide a feedstock composition of 1% *n*-butane in air. The product (0.5 ml) was then fed via heated line to an on-line gas chromatograph for analysis. The gas composition was analysed by an Thermo Scientific TRACE GC Ultra™ gas chromatograph (Figure 3.9) equipped with a Hyesp-R (1 m, 1/8 ") packed column and a Molecular Sieve 5A column (3 m, 1/8 ") which the TCD allows to detect the fixed gases of O₂, N₂, CO, CO₂... *etc.* The flame ionisation detector (FID) allows the detection of all hydrocarbon gases included C₁ to C₄ and maleic anhydride where this channel was equipped with a RTX-1701 wide bore capillary column (30 m × 0.54 mm). The catalyst was heated

in situ in the reactor at 673 K with gas hourly space velocity (GHSV = 2400 h⁻¹) during the time where *n*-butane conversion and selectivity of MA were observed to be stabilised. Carbon mass balances of $\geq 95\%$ were observed.



Figure 3.9: Fixed-bed microreactor with on-line Thermo Scientific TRACE GC

Ultra™

CHAPTER 4

RESULTS AND DISCUSSION

4.1 Series 1: Effects of Ga and Mo dopants on the Physico-chemical and Catalytic Properties of Vanadyl Pyrophosphate Catalysts

The effects of Ga and Mo dopants on the physico-chemical and catalytic properties of VPOs catalysts were investigated. In the synthesis of vanadyl pyrophosphate catalysts, the undoped, Ga and Mo doped $\text{VOHPO}_4 \cdot 1.5\text{H}_2\text{O}$ precursors were activated under the reaction flow of 0.75% *n*-butane in air at 723 K for 18 h. The activated $(\text{VO})_2\text{P}_2\text{O}_7$ catalysts were denoted as VPOs-Undoped, VPOs-X%Ga ($X = 0.1, 0.3$ and 0.5 mol%) and VPOs-X%Mo ($X = 1, 3,$ and 5 mol%), respectively, where VPOs represents the vanadyl pyrophosphate catalyst prepared via sesquihydrate route.

4.1.1 Series 1: XRD Analyses

X-Ray diffraction (XRD) analysis is used to determine the phase composition of the catalysts. Figures 4.1 and 4.2 showed the XRD patterns for Ga and Mo doped VPOs catalysts, respectively, together with their undoped counterpart. The XRD patterns of the undoped, Ga doped and Mo doped VPOs catalysts were found to exhibit similar characteristic reflection peaks, which consist of well-crystallised vanadyl pyrophosphate phase, $(\text{VO})_2\text{P}_2\text{O}_7$. The characteristic peaks appeared at $2\theta =$

22.9°, 28.4° and 29.9° (JCPDS File No. 34-1381), which corresponded to (0 2 0), (2 0 4) and (2 2 1) reflection planes, respectively.

As observed in Figure 4.1, there was an additional weak peak emerged at around $2\theta = 21.5^\circ$ for Ga doped VPOs catalysts, which peak is corresponded to V^{5+} phase, i.e. β -VOPO₄ (JCPDS Files No. 27-0948). It has shown that the peaks that assigned as the V^{5+} phases (β -VOPO₄) were found to be more intense as the doping percentage of Ga increased. This indicated that the addition of Ga into the VPOs catalysts had promoted the formation of V^{5+} phases, where one β -VOPO₄ peak was found in 0.1, 0.3 and 0.5 mol% Ga doped VPOs catalysts. Ga doped catalysts have higher intensity of three major characteristic reflection planes of (VO)₂P₂O₇ phase as compared to the undoped counterpart. However, the addition of higher concentrations leads to a slightly decrease in the intensity of the (0 2 0) reflection and (2 0 4) reflection, as it induced the formation of V^{5+} phases. This is in agreement with the findings reported by Sartoni et al. (2004), which showed that the addition of higher concentrations of Ga(acac)₃ in catalyst prepared via hemihydrates, leads to a significant decrease in the intensity of the (0 0 1) reflection relative to the (2 2 0) reflection (Sartoni et al., 2004).

As shown in Figure 4.2, a β -VOPO₄ peak was found in 1, 3 and 5 mol% Mo doped VPOs catalysts. The peaks were found to be more intense as the mol% of Mo increased. Besides, an α_{II} -VOPO₄ peak was appeared when Mo dopant (1 mol%) was added into the VPOs catalysts. The peak was observed to be more intense as the mol% of Mo increased. As the doping of Mo increased to 5 mol% into the VPOs catalyst, an additional peak of α_{II} -VOPO₄ peak was to be induced at around

$2\theta = 30.0^\circ$. Previous studies had proposed that crystallite size is inversely proportional to the activity of the VPOs catalysts due to smaller crystallite size contributed better active phase for the *n*-butane oxidation. The formation of extra peak (α_{II} -VOPO₄) had increased the crystallinity of the VOPO₄ phases of the VPOs catalysts (Ruiz et al., 1987; Centi et al., 1988; Centi, 1993), at the same time suppressed the linewidth of the V⁴⁺ phases and caused increased in the crystallite size. When the amount of Mo increased from 1 mol% to 5 mol%, the V⁵⁺ phase intensity increased. The additional of Mo gave a slightly decreased in the intensity of the reflection peaks at the characteristic peaks ($2\theta = 22.9^\circ$, 28.4° and 29.9°) corresponded to (0 2 0), (2 0 4), and (2 2 1) reflection planes. The same phenomenon also been reported by Taufiq-Yap et al. (2009) indicated that the incorporation of other dopants such as Bi and Fe into VPO catalysts has caused the formation of V⁵⁺ phases, which displayed an increase in the average oxidation state of vanadium.

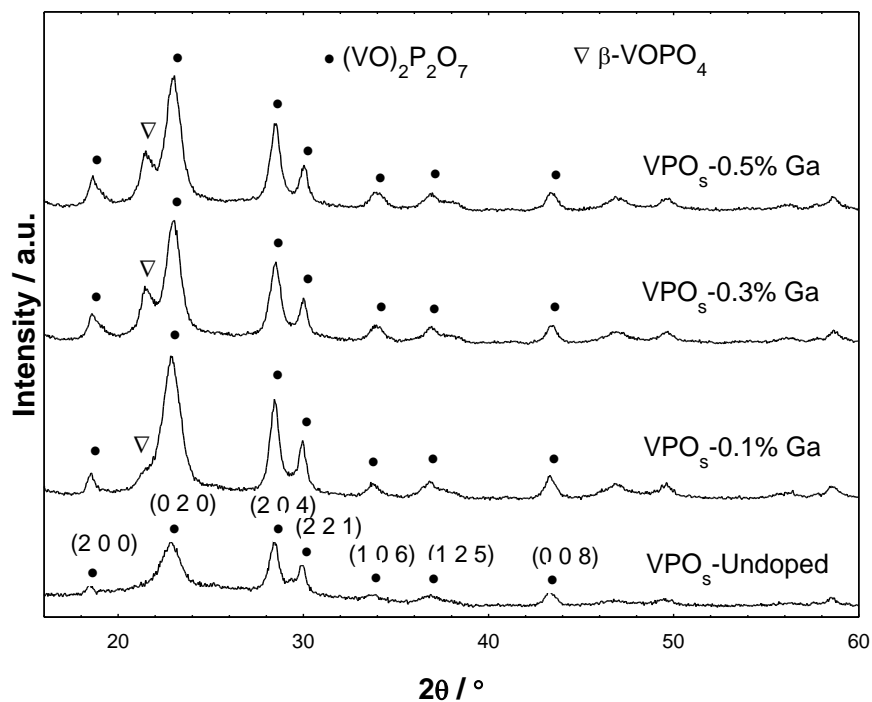


Figure 4.1: Powder XRD patterns for undoped and Ga doped VPOs catalysts

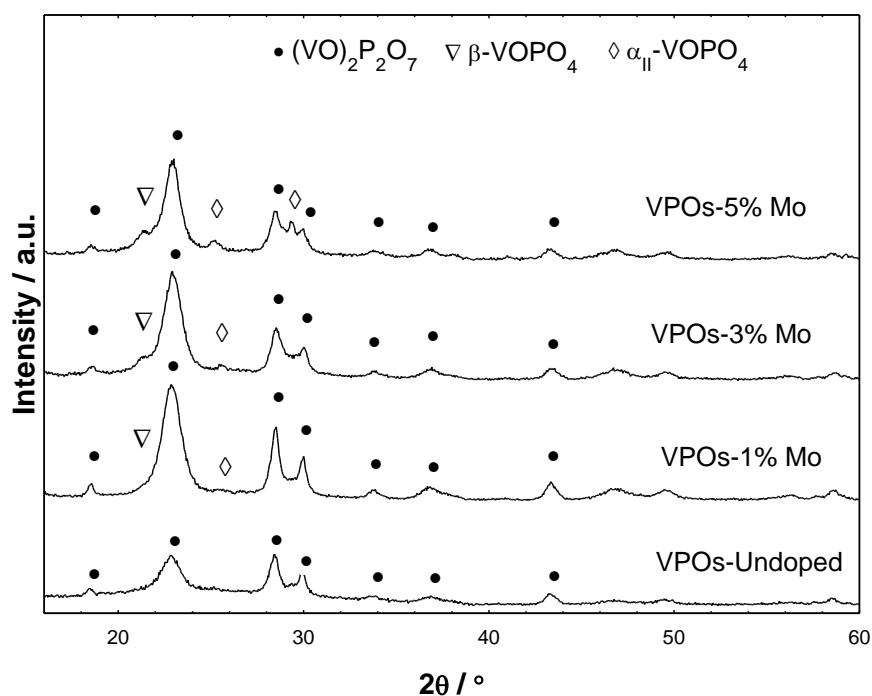


Figure 4.2: Powder XRD patterns for undoped and Mo-doped VPOs catalysts

The full-width half maximum (FWHM) of the (0 2 0) and (2 0 4) reflection planes were used to determine the crystallite sizes of the catalysts. It has been widely accepted that the best performance of VPO catalyst is directly related to the presence and extent of the exposed (0 2 0) facets (O'Mahony et al., 2005). Table 4.1 shows that the crystallite sizes of the (0 2 0) reflection plane for undoped, VPOs-0.1%Ga, VPOs-0.3%Ga, VPOs-0.5%Ga were calculated as 58.49, 68.16, 82.10, and 78.47 Å, respectively, while the crystallite sizes of the (2 0 4) reflection plane for the catalysts were 108.12, 109.74, 106.71 and 108.37 Å. The incorporation of Ga into the VPOs catalysts has shown to produce catalysts with larger crystallite sizes in the (0 2 0) direction but with a limited development in the (2 0 4) direction as compared to the undoped catalyst. These results were in agreement with the same analysis done on Ga doped $(VO)_2P_2O_7$ catalysts prepared via hemihydrate route in previous research (Sartoni et al., 2004).

Table 4.1 shows the incorporation of Mo into the VPOs catalysts had limited improvement of crystallite sizes in the (0 2 0) direction but significantly induced larger crystallite sizes in the (2 0 4) direction, as compared to the undoped counterpart. The crystallite sizes of the (0 2 0) reflection plane for VPOs-undoped, VPOs-1%Mo, VPOs-3%Mo and VPOs-5%Mo were calculated as 58.49, 65.23, 68.03 and 77.00 Å, respectively, while the crystallite sizes of the (2 0 4) reflection plane for the catalysts were 108.12, 112.26, 111.41 and 112.83 Å, respectively.

Table 4.1: XRD data of undoped, Ga doped and Mo doped VPOs catalysts

Catalyst	Line width ^a (°)		Crystallite size ^c (Å)	
	(0 2 0)	(2 0 4)	(0 2 0)	(2 0 4)
VPOs-Undoped	1.3697	0.7492	58.49	108.12
VPOs-0.1% Ga	1.1754	0.7382	68.16	109.74
VPOs-0.3% Ga	0.9760	0.7592	82.10	106.71
VPOs-0.5% Ga	1.0212	0.7476	78.47	108.37
VPOs-1% Mo	1.2283	0.7217	65.23	112.26
VPOs-3% Mo	1.1779	0.7274	68.03	111.41
VPOs-5% Mo	1.0406	0.7180	77.00	112.83

^aFWHM of (020) reflection plane.

^bFWHM of (204) reflection plane.

^cCrystallite thickness by means of Debye-Scherrer's formula.

4.1.2 Series 1: SEM Analyses

The surface morphologies of the undoped, Ga and Mo doped VPOs catalysts were obtained by Scanning Electron Microscopy (SEM) Analysis and showed in Figure 4.3 and 4.4.

The principal secondary structure of the undoped and doped VPOs catalysts were found to be the same, consisting different sizes of plate-like crystals, which were agglomerated into cluster. These plate-like crystals were comprised of agglomerates of $(VO)_2P_2O_7$ platelets that preferentially exposed the (1 0 0) crystal plane (Kiely et al., 1995). However, the crystal platelets formed exhibited folded edges, which is deemed as an important characteristic of VPO catalysts produced via sesquihydrate route (Leong et al., 2011). Similar type of platelet arrangement was also found from the $(VO)_2P_2O_7$ catalysts obtained via conventional organic and dihydrate methods (Kiely et al, 1995; Abon et al., 2001; Taufiq-Yap et al., 2001; Taufiq-Yap et al., 2004b).

The Ga and Mo doped catalysts were observed to be more layered plate-like crystals and more compact structures with further agglomeration among the platelet cluster as compared to the undoped counterpart. As the amount of Ga added into the VPOs catalysts increased from 0.1 mol% to 0.5 mol%, the platelet of the catalysts became smaller and had more compact agglomeration, respectively. The VPOs-0.3%Ga and VPOs-0.5%Ga appeared to have some bulky structure of crystals which could be assigned to the presence of the V^{5+} phase i.e. β -VOPO₄.

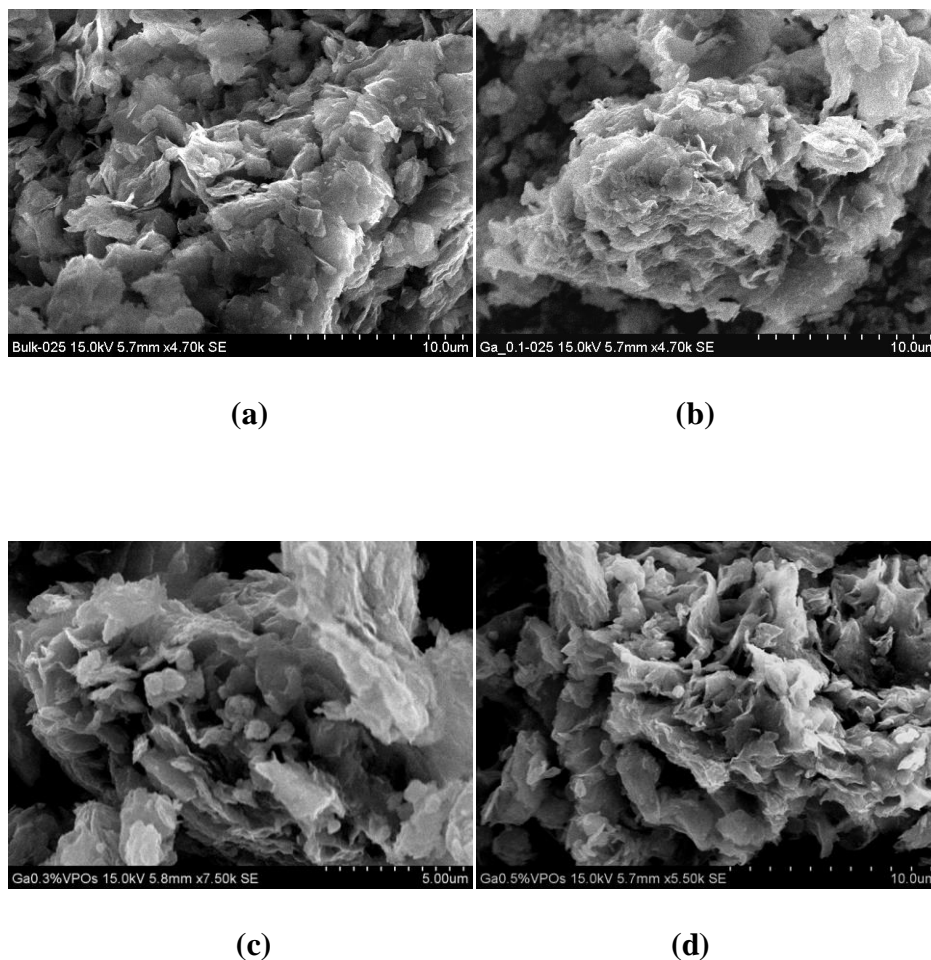


Figure 4.3: SEM micrograph for (a) VPOs-Undoped; (b) VPOs-0.1%Ga; (c) VPOs-0.3%Ga; (d) VPOs-0.5%Ga

Same phenomenon was observed for Mo doped catalysts. As the amount of Mo increased from 1 mol% to 5 mol%, the plate-like crystals became smaller and agglomerated into bulkier structure. This could be explained by the formation of the two V^{5+} phases i.e. α_{II} - and β -VOPO₄, which appeared in bulky properties (Kiely et al., 1996).

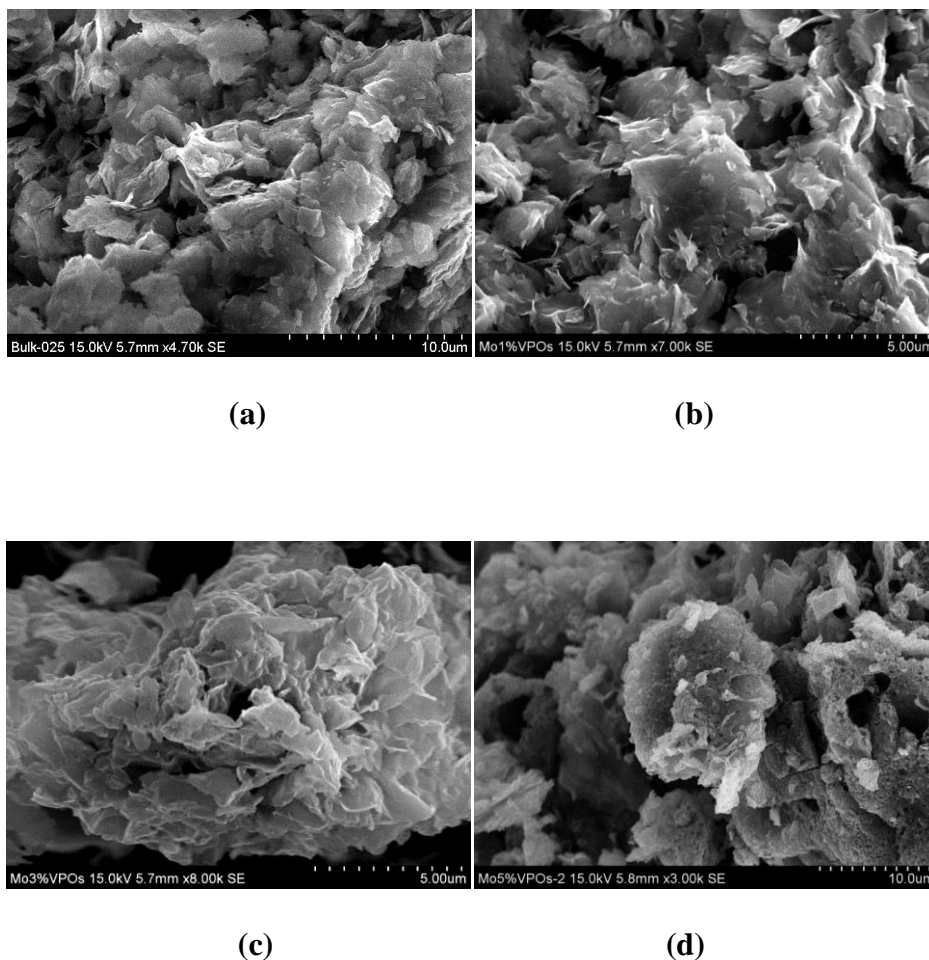


Figure 4.4: SEM micrograph for (a) VPOs-Undoped; (b) VPOs-1%Mo; (c) VPOs-3%Mo and (d) VPOs-5%Mo

4.1.3 Series 1: BET Surface Area Measurements and Chemical Analyses

The BET surface areas of the undoped and doped VPOs catalysts are tabulated in Table 4.2. The specific surface area obtained for the undoped catalyst was $17.3 \text{ m}^2\text{g}^{-1}$. As compared to the undoped catalyst, the incorporation of Ga showed higher specific surface area ($18.3 \text{ m}^2\text{g}^{-1}$) at low doping level VPOs-0.1%Ga but slightly reduced i.e. VPOs-0.3%Ga = $13.9 \text{ m}^2\text{g}^{-1}$ and VPOs-0.5%Ga = $12.5 \text{ m}^2\text{g}^{-1}$, as the mol% of Ga increased.

As compared to the undoped catalyst, 1 and 3 mol% of Mo-doped catalysts showed higher specific surface area, which obtained $20.4 \text{ m}^2\text{g}^{-1}$ and $19.7 \text{ m}^2\text{g}^{-1}$, respectively, while VPOs-5%Mo obtained only $16.4 \text{ m}^2\text{g}^{-1}$, which is lower than the undoped counterpart. The increment of specific surface area could be suggested that the incorporation of 0.1 mol% Ga, 1 and 3 mol% of Mo into the VPOs catalysts gave rise to the standard structural promotion as it had somehow intercalated in between the layers of the VPOs structure. It also altered the development of the (1 0 0) basal face of $(\text{VO})_2\text{P}_2\text{O}_7$, which led to the increase of specific surface area of the catalysts (Taufiq-Yap et al., 2006c). However, the reduction of specific surface area for VPOs-0.3%Ga, VPOs-0.5%Ga and VPOs-5%Mo could be due to the formation of α_{II} - and β - VOPO_4 peaks, which has caused the agglomerate of VPOs crystal appeared in bulky structure and led to the decreasing in specific surface area (Kiely et al., 1996), which was confirmed with XRD profile in section 4.1.1 and SEM in section 4.1.2, respectively.

The similar phenomena were observed in Ga and Mo doped VPO catalysts prepared via hemihydrate route, where 0.1 mol% of Ga and 1 mol% of Mo achieved higher specific surface area within their series of VPO catalysts (Sartoni et al., 2004; Pierini et al., 2005).

The chemical analyses using ICP-OES revealed that the incorporation of Ga into the VPOs catalysts increased the phosphorus content in the catalysts due to the increased in P/V atomic ratio (Table 4.2). The undoped catalyst had bulk P/V atomic ratio of 1.24 while Ga doped catalysts had bulk P/V atomic ratios of 1.31, 1.30 and 1.27 for VPOs-0.1%Ga, VPOs-0.3%Ga and VPOs-0.5%Ga, respectively.

Table 4.2: Specific BET surface area, chemical compositions, average oxidation number and percentages of V⁴⁺ and V⁵⁺ oxidation states present for undoped, Ga-doped and Mo-doped VPOs catalysts

Catalysts	Specific BET		ICP			V ⁴⁺ (%)	V ⁵⁺ (%)	Average oxidation number
	surface area (m ² g ⁻¹)	EDX	P/V	Ga/V	Mo/V			
VPOs-Undoped	17.3	1.12	1.24	-	-	85.25	14.75	4.1475
VPOs-0.1% Ga	18.3	1.18	1.31	0.0013	-	78.04	21.96	4.2196
VPOs-0.3% Ga	13.9	1.04	1.30	0.0034	-	65.62	34.38	4.3438
VPOs-0.5% Ga	12.5	1.24	1.27	0.0055	-	65.99	34.01	4.3401
VPOs-1% Mo	20.4	1.13	1.24	-	0.0120	58.33	41.67	4.4167
VPOs-3% Mo	19.7	1.10	1.24	-	0.0350	64.54	35.46	4.3546
VPOs-5% Mo	16.4	1.11	1.17	-	0.0561	67.32	32.68	4.3268

However, the incorporation of Mo into VPOs catalysts did not show significant changes to the bulk P/V atomic ratios. EDX analyses showed that the surface P/V atomic ratios ranged from 1.04 to 1.24 (Table 4.2). The results were in agreement with the optimal P/V ratio range (1.10 - 1.30) for producing active and selective $(VO)_2P_2O_7$ phase (Centi 1993). Furthermore, the chemical analyses confirmed the presence of Ga in the catalysts with Ga/V atomic ratios of 0.0013, 0.0034 and 0.0055 for VPOs-0.1%Ga, VPOs-0.3%Ga and VPOs-0.5%Ga, respectively and Mo in the catalysts with Mo/V atomic ratios of 0.0120, 0.0350 and 0.0561 for VPOs-1%Mo, VPOs-3%Mo and VPOs-5%Mo, respectively.

The average oxidation numbers of vanadium and the composition of V^{5+} and V^{4+} oxidation states are summarised in Table 4.2. The incorporation of Ga and Mo into the VPOs catalysts increased the average oxidation numbers of vanadium from 4.1475 for undoped catalyst to 4.2196, 4.3438 and 4.3401 for VPOs-0.1%Ga, VPOs-0.3%Ga and VPOs-0.5%Ga, respectively, and 4.4167, 4.3546 and 4.3268 for VPOs-1%Mo, VPOs-3%Mo and VPOs-5%Mo, respectively. These results reflected that an oxidised phase such as $VOPO_4$ exists in the Ga and Mo doped catalysts structure, which led to the increase of V^{5+} contribution, as compared to the undoped catalyst. This is in agreement with the XRD profiles as discussed in section 4.1.1, which the incorporation of Ga and Mo to the VPOs catalyst had induced the formation of V^{5+} phases.

4.1.4 Series 1: Temperature-Programmed Reduction (TPR in H₂) Analyses

TPR in H₂ analyses were performed in order to investigate the redox properties of the doped catalysts. The TPR in H₂ profiles of the undoped, Ga and Mo doped VPOs catalysts were shown in Figure 4.5 and Figure 4.6, respectively. The peak maxima temperatures, total amount removed oxygen in each peak and the derived activation energies for Ga and Mo doped catalysts are illustrated in Table 4.3 and Table 4.4.

The undoped, Ga doped (Figure 4.5) and Mo doped (Figure 4.6) catalysts gave two peak maxima in the reduction by H₂. The observation of two kinetically different reduction peaks for all the catalysts implies the presence of two types of oxygen species. The first peak at low temperature (~790-880 K) was assigned to the removal of the oxygen species associated to V⁵⁺ phase, whereas the second peak at high temperature (~820-1070 K) is due to the removal of oxygen species associated to V⁴⁺ phase (Rownaghi et al., 2009). The electrical conductivity investigation on VPO catalysts suggested that O²⁻ is related to V⁵⁺ phase, while O⁻ is associated with the V⁴⁺ phase (Herrmann and Raulin, 2005; Taufiq-Yap et al., 2006c). The reduction of V⁴⁺ species was the predominant species for the undoped, Ga doped and Mo doped catalysts, as in agreement with the redox titration results that discussed in section 4.1.3.

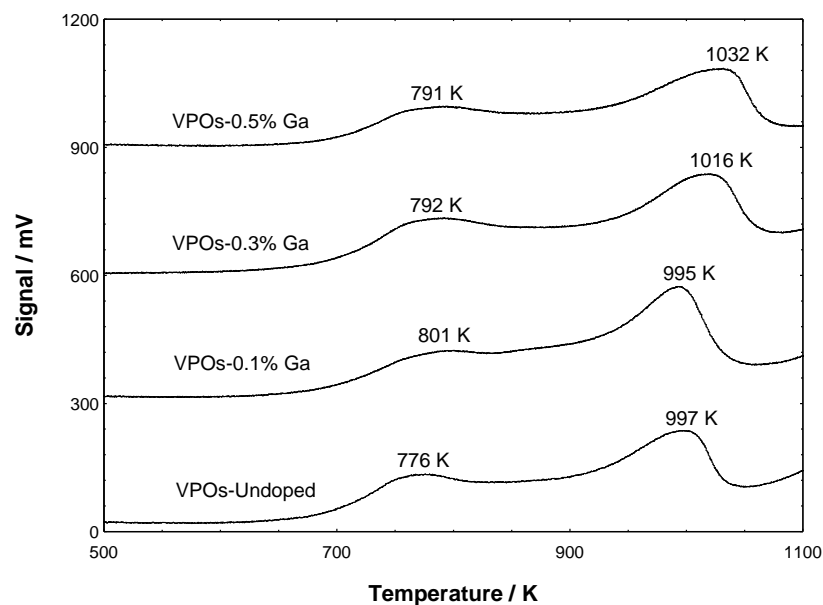


Figure 4.5: TPR in H₂ profiles for undoped and Ga doped VPOs catalysts

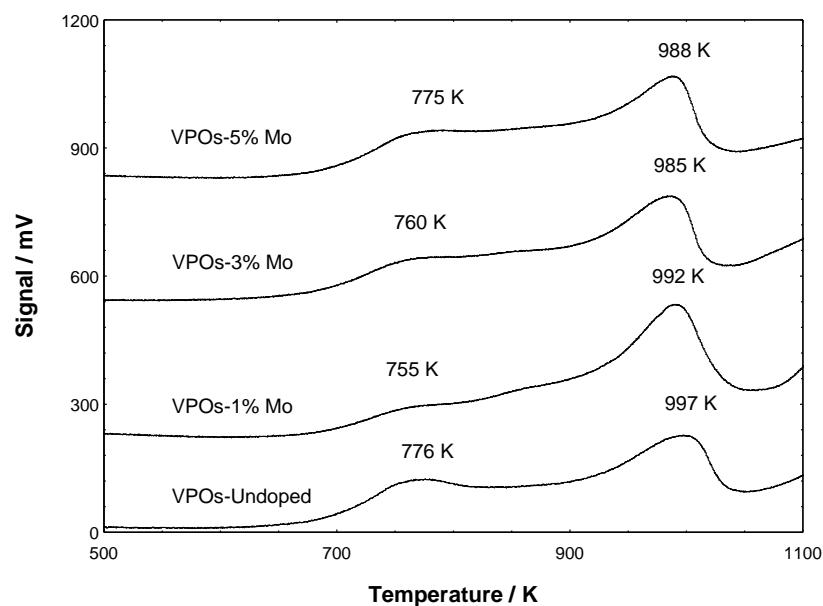


Figure 4.6: TPR in H₂ profiles for undoped and Mo-doped VPOs catalysts

As shown in Figure 4.5, the undoped catalyst gave two peak maxima in the rate of hydrogen consumption at 776 K and 997 K with the amount of oxygen removed for each peak were found to be 4.79×10^{20} and 1.17×10^{21} atom g⁻¹, as tabulated in Table 4.3. VPOs-0.1%Ga gave two similar reduction characteristic peaks

to the undoped catalyst. The first peak has shifted to higher temperature at 801 K while the second peak slightly remained at 995 K. The removal of oxygen species associated with V^{5+} from the first peak significantly increased to 5.44×10^{20} atom g^{-1} while the amount of oxygen removed from second peak which related to V^{4+} phase was slightly increased to 1.57×10^{21} atom g^{-1} , which exhibited the highest amount of oxygen removed from V^{4+} phase. The catalyst with higher amount of oxygen associated with V^{5+} gave higher availability of selective oxygen, which the catalyst could provide more selective reaction towards the desired product. This also implies to the catalyst with high amount of oxygen associated with V^{4+} , which could be more active towards the *n*-butane conversion (Borders, 1993).

Comparatively, VPOs-0.3%Ga gave two broader peak maxima as compared to the undoped catalysts. The first peak was appeared at lower temperature, i.e. 792K while the second peak shifted to higher temperature at 1016 K. The amount of oxygen removed from the first reduction peak associated with V^{5+} was greatly increased to 6.91×10^{20} atom g^{-1} . However, the amount of oxygen removed from V^{4+} phase was decreased to 1.13×10^{21} atom g^{-1} . Unlike the VPOs-0.1%Ga, VPOs-0.3%Ga gave higher oxygen species associated with V^{5+} phase, which suggested that the catalyst tend to give higher selectivity (Borders, 1993).

VPOs-0.5%Ga gave peak maxima which appeared at 791 and 1032 K. The amount of oxygen removed from both peak maxima were 5.18×10^{20} atom g^{-1} and 1.23×10^{21} atom g^{-1} , respectively. As compared to the undoped counterpart, these TPR in H_2 analyses results consequently indicated that the addition of Ga would

leads to the enhancement of the total amount of oxygen removed, i.e. O^-V^{4+} and O^-V^{5+} from bulk and lattice of the catalysts.

Figure 4.6 showed the TPR in H_2 profiles for the undoped and Mo-doped VPOs catalysts. The incorporation of Mo into VPOs catalysts gave two similar peak maxima as the undoped catalyst. For VPOs-1%Mo, the first reduction peak was shifted to lower temperature at 755 K, which assigned to the removal of O^{2-} species that associated with the V^{5+} phase, whereas the second reduction peak occurred at higher temperature, i.e. 992 K, which is related to the removal of lattice oxygen O^- from the V^{4+} active phase (Abon et al., 2001; Volta, 2000). The amount of oxygen removed which linked to V^{5+} phase was reduced to 3.97×10^{20} atom g^{-1} , whereas the oxygen removed from V^{4+} phase was slightly increased to 1.41×10^{21} atom g^{-1} .

VPOs-3%Mo gave lower intensity of the first reduction peak appeared at 760 K, the second reduction peak slightly reduced with broader width size at 985 K. The oxygen species linked to V^{5+} phase was decreased to 4.42×10^{20} atom g^{-1} and the amount of oxygen removed which is assigned to the reduction of V^{4+} phase was decreased to 1.07×10^{21} atom g^{-1} .

As the percentage of Mo increased to 5 mol%, the two characteristic reduction peaks for VPOs-5%Mo appeared at 775 K and 988 K, respectively. The removal of oxygen species associated with V^{5+} phase has increased to 5.45×10^{20} atom g^{-1} while the removal of oxygen species associated with V^{4+} phase had slightly decreased to 1.09×10^{21} atom g^{-1} , as compared to the undoped counterpart.

The reduction activation energies values (Tables 4.3) were calculated by using Redhead equation (Appendix H). The reduction activation energies for the undoped catalyst were obtained for the peak maxima as: 129.8 kJ mol⁻¹ at 776 K; and 163.4 kJ mol⁻¹ at 977 K. For the Ga doped catalysts, the calculated reduction activation energies were 134.0 kJ mol⁻¹ at 801 K and 166.4 kJ mol⁻¹ at 995 K for VPOs-0.1%Ga. The reduction activation energies for VPOs-0.3%Ga were 132.5 and 169.9 kJ mol⁻¹ at 792 K and 1016 K, respectively, while for VPOs-0.5%Ga were 132.3 and 172.6 kJ mol⁻¹ at 791 K and 1032 K, respectively. The increment in the reduction temperature indicated that gallium would strengthen the bonding between the oxygen species and the VPO matrix. This eventually increased the reduction activation energy of O⁻-V⁴⁺ and O²⁻-V⁵⁺ for Ga doped VPOs catalysts.

For the Mo-doped catalysts, the reduction activation energies calculated for VPOs-1%Mo were 126.3 and 165.9 kJ mol⁻¹ at 755 and 992 K, respectively. The reduction activation energies for VPOs-3%Mo were 127.1 and 164.7 kJ mol⁻¹ at 760 and 985 K, respectively. VPOs-5%Mo obtained similar reduction activation energies of 129.6 and 165.2 kJ mol⁻¹ at 775 and 988 K, respectively. The reduction activation temperatures for all peak maxima of Mo doped catalysts were found to be not affected by the concentration of the Mo. These results indicated that no excess of reduction activation energy is required for the oxygen species desorbed from the Mo doped VPOs catalysts throughout the selective oxidation of *n*-butane to maleic anhydride.

Table 4.3: Total amount of oxygen atoms removed and values of reduction energies for undoped, Ga doped and Mo doped catalysts

Catalyst	Peak	T_m (K)	Reduction activation energy, E_r (kJ mol ⁻¹)	Amount of oxygen removed (atom g ⁻¹)
VPOs-Undoped	1	776	129.8	4.79×10^{20}
	2	977	163.5	1.17×10^{21}
	Total			1.65×10^{21}
VPOs-0.1%Ga	1	801	134.0	5.44×10^{20}
	2	995	166.4	1.57×10^{21}
	Total			2.11×10^{21}
VPOs-0.3%Ga	1	792	132.5	6.91×10^{20}
	2	1016	169.9	1.13×10^{21}
	Total			1.82×10^{21}
VPOs-0.5%Ga	1	791	132.3	5.18×10^{20}
	2	1032	172.6	1.23×10^{21}
	Total			1.75×10^{21}
VPOs-1%Mo	1	755	126.3	3.97×10^{20}
	2	992	165.9	1.41×10^{21}
	Total			1.81×10^{21}
VPOs-3%Mo	1	760	127.1	4.42×10^{20}
	2	985	164.7	1.07×10^{21}
	Total			1.51×10^{21}
VPOs-5%Mo	1	775	129.6	5.45×10^{20}
	2	988	165.2	1.09×10^{21}
	Total			1.64×10^{21}

4.1.5 Series 1: Catalytic Oxidation of *n*-Butane to Maleic Anhydride

The catalytic performance of the undoped, Ga doped and Mo doped catalysts for selective oxidation of *n*-butane to maleic anhydride (MA) was tested at operating temperature (673 K), with gas hourly space velocity, GHSV of 2400 h⁻¹ (Leong et al., 2011). The catalytic performance data of the Ga and Mo doped catalysts are shown in Figures 4.7, respectively. The summary of the *n*-butane conversion, product selectivity and the turnover number (TON) of the catalysts were tabulated in Table 4.4.

The undoped catalyst gave an *n*-butane conversion of 4% with maleic anhydride, MA selectivity of about 61%. The incorporation of Ga into the VPOs catalysts gave slight increment on the catalytic performances for both *n*-butane conversion and selectivity towards MA. The *n*-butane conversion for Ga doped catalysts were 20 %, 15 % and 9 % for VPOs-0.1%Ga, VPOs-0.3%Ga and VPOs-0.5%Ga, respectively. These results indicated that higher amount of Ga will not further improve the activity of the catalysts, as 0.3 and 0.5 mol% of Ga added to the VPOs catalyst had respectively reduced the activity towards the oxidation of *n*-butane. The addition of Ga into the VPOs catalysts has slightly increased the MA selectivity to 64 %, 67 % for VPOs-0.1%Ga and VPOs-0.3%Ga, respectively. However, the addition of 0.5 mol% of Ga to VPOs catalyst has caused a slight reduction of MA selectivity to 66 %. As compared to the undoped counterpart, the presence of Ga dopant does resulted in slightly higher activity and selectivity. This is in agreement with the XRD analyses (section 4.1.1) and redox titration (section

4.1.3). The increment of the average oxidation number reflected that V^{5+} phase was obtained, as confirmed by the XRD profiles, thus, increased the MA selectivity.

Mo doped catalysts were shown to give its maximum activity and selectivity accordingly to the mol% added to the VPOs catalyst. As compared to the undoped counterpart, VPOs-1%Mo gives higher *n*-butane conversion and selectivity of MA, i.e. 10 % and 65 %, respectively. This is in agreement with Pierini and Lombardo (2005), reported for VPO catalysts doped at 1 mol% of Mo gave the best catalytic performance with 84 % selectivity at 80 % conversion towards maleic anhydride. By increasing the percentage of Mo doping to 3 mol% into the catalysts, the *n*-butane conversion and selectivity of MA remained same as the undoped catalyst with 4 % and 61 %, respectively. However, there is slightly increased of *n*-butane conversion and MA selectivity for VPOs-5%Mo, i.e. 8 % and 62 %, respectively.

The catalyst Turnover Number (TON) is quantitatively importance that used for comparing the catalyst efficiency. TON is the activity per unit area (intrinsic activity), which obtained as the number of particular mole of catalyst been converted before it becomes inactivated. The TON of VPOs-0.1%Ga was found to be the highest (1.09) among the Ga doped VPOs catalysts series with its highest value in activity. This is in agreement with the previous study of Sartoni et al. (2004), which proposed that lower Ga doping (0.1 mol%) produced using $Ga(acac)_3$ shown to have the best activity. Meanwhile, VPOs-1%Mo obtained 0.49 of TON number with the highest conversion towards MA and product selectivity among the tested Mo-doped VPOs catalysts.

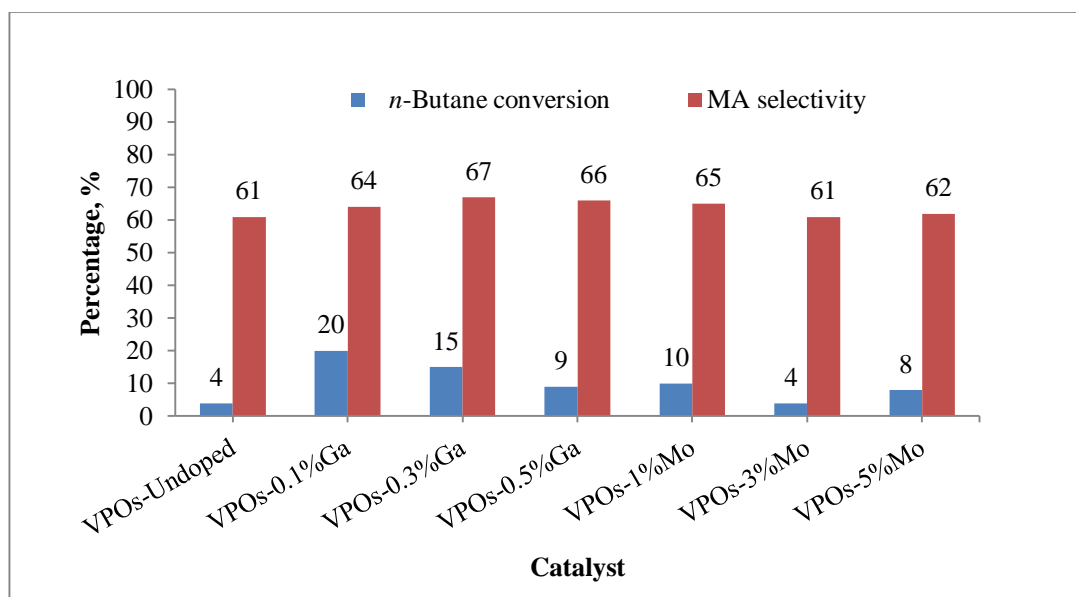


Figure 4.7: Catalytic performances of undoped, Ga doped and Mo doped VPOs catalysts

Table 4.4: Catalytic performances of undoped, Ga doped and Mo doped VPOs catalyst

Catalyst	Turnover number (TON)	n-Butane conversion (%)	Product selectivity (%)		
			MA	CO	CO ₂
VPOs-Undoped	0.23	4	61	3	36
VPOs-0.1%Ga	1.09	20	64	1	35
VPOs-0.3%Ga	1.08	15	67	2	31
VPOs-0.5%Ga	0.72	9	66	3	31
VPOs-1%Mo	0.49	10	65	2	33
VPOs-3%Mo	0.20	4	61	2	37
VPOs-5% Mo	0.49	8	62	2	36

4.1.6 Series 1: Conclusions

The increasing of gallium dopant and molybdenum dopant, respectively, in the catalysts prepared via sesquihydrate route was observed to induce the formation of V^{5+} phase and a significant change of the morphology of the catalysts. The presence of Ga has increase the removal of reducible oxygen species and TON value and activity with higher selectivity as compared to the undoped catalyst. The doping of 0.1 mol% Ga to VPOs catalyst has contribute the highest conversion of *n*-butane and selectivity toward the maleic anhydride formation. However, slight improvement only obtained from VPOs-1%Mo, out of the synthesised Mo doped VPOs catalysts.

4.2 Series 2: Effect of Different Calcination Durations on the Physico-chemical, Reactivity and Catalytic Properties of Ga-Mo Doped Vanadyl Pyrophosphate Catalysts

In the synthesis of vanadyl pyrophosphate catalysts, the Ga-Mo doped $VOHPO_4 \cdot 1.5H_2O$ precursors were activated under the reaction flow of 0.75% *n*-butane in air at 723 K for 18, 36, 54 and 72 h, respectively. The activated $(VO)_2P_2O_7$ catalysts were denoted as VPOs-0.1%Ga1%Mo-X (X = 18, 36, 54 and 72 h), where VPOs represents the vanadyl pyrophosphate catalyst prepared via sesquihydrate route. The effects of the different calcination durations on the physico-chemical, reactivity and catalytic properties of Ga-Mo doped VPOs catalysts were examined.

4.2.1 Series 2: XRD Analyses

The XRD patterns for VPOs-0.1%Ga1%Mo-18, VPOs-0.1%Ga1%Mo-36, VPOs-0.1%Ga1%Mo-54 and VPOs-0.1%Ga1%Mo-72 (Figure 4.8) showed similar characteristic reflections which comprised of a well-crystallised $(VO)_2P_2O_7$ phase with the three main peaks appeared at $2\theta = 22.9^\circ$, 28.4° and 29.9° which corresponded to the (0 2 0), (2 0 4), and (2 2 1) planes respectively (JCPDS File No. 34-1381).

The (0 2 0) reflection plane obtained at $2\theta = 22.9^\circ$ was shown to be more predominant as the Ga-Mo doped catalysts calcination duration increased from 18 to 72 h.. Similar width sizes of (2 0 4) and (2 2 1) planes of the catalysts were obtained as the calcination durations increased, which appeared at $2\theta = 28.4^\circ$ and 29.9° .

Surprisingly, the incorporation of Ga and Mo into the VPOs catalysts exhibited only the main characteristic peaks of $(VO)_2P_2O_7$ phase. The V^{4+} phase was found to be the only phase present in the XRD profile as the calcination duration increased. This phenomenon could be explained by the poorly crystalline and amorphous $VOPO_4$ phases present in the VPOs catalysts which unable to detect by XRD analysis (Ruiz et al., 1987; Centi et al., 1988; Centi, 1993). The peaks belonging to the $(VO)_2P_2O_7$ phase were shown to be more intense as the calcination durations of the Ga-Mo doped catalysts increased from 18 h to 72 h. The crystallinity of the catalysts as shown in the XRD patterns (Figure 4.8) had increased with the duration of calcination.

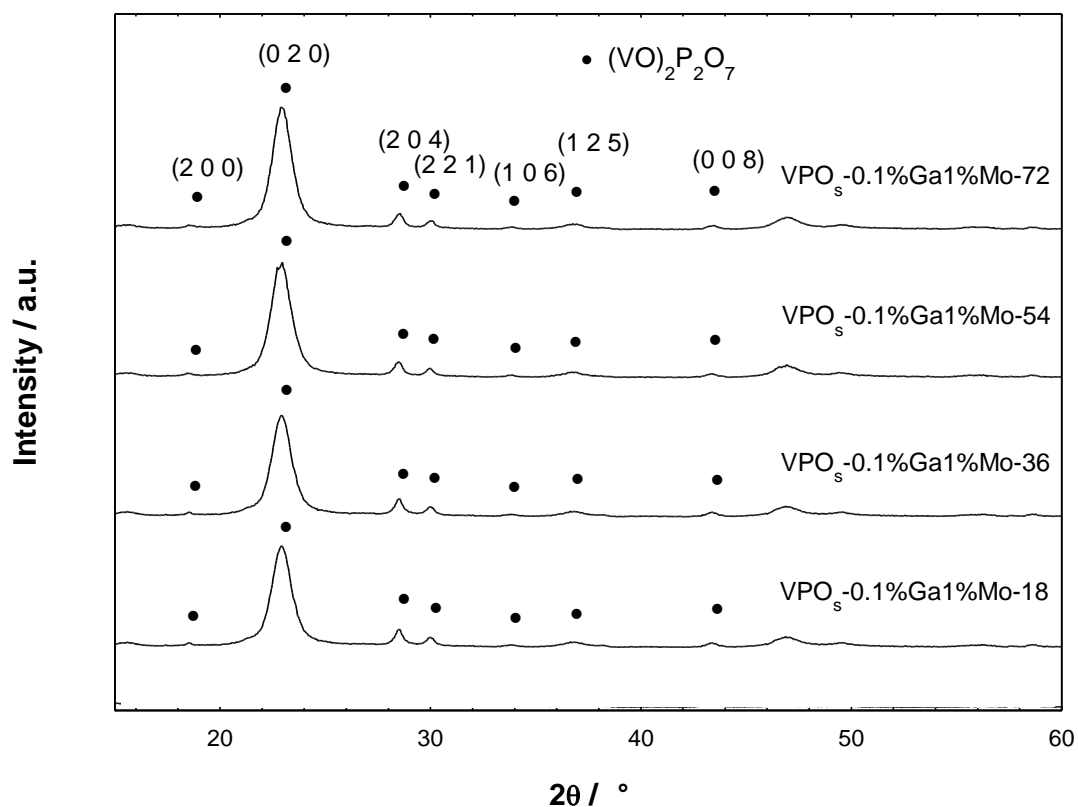


Figure 4.8: Powder XRD patterns for Ga-Mo doped VPOs catalysts

The estimation of the crystallite size for the Ga-Mo doped VPOs catalysts with different calcination duration was tabulated at Table 4.5. The crystallite sizes of (0 2 0) reflection plane for VPOs-0.1%Ga1%Mo-18, VPOs-0.1%Ga1%Mo-36, VPOs-0.1%Ga1%Mo-54, and VPOs-0.1%Ga1%Mo-72 were calculated as 44.89, 69.60, 66.99, and 68.64 Å, respectively, whereas the crystallite sizes of (2 0 4) reflection plane within the same series of catalysts produced were 114.40, 106.63, 103.27 and 111.62 Å, respectively.

The 0.1%Ga-1%Mo doped VPOs catalyst which calcined for 18 h has smaller crystallite size in (0 2 0) direction but larger crystallite size in (2 0 4) direction. However, as the calcination duration had increased to more than 18 h, the crystallite

size in (0 2 0) direction gradually increased, in contrary, smaller crystallite size was obtained in (2 0 4) direction.

Table 4.5: XRD data of Ga-Mo doped VPOs catalysts

Catalyst	Line width ^a (°)	Line width ^b (°)	Crystallite size ^c (Å)	
	(0 2 0)	(2 0 4)	(0 2 0)	(2 0 4)
VPOs-0.1%Ga1%Mo-18	1.1784	0.7081	44.89	114.40
VPOs-0.1%Ga1%Mo-36	1.1513	0.7598	69.60	106.63
VPOs-0.1%Ga1%Mo-54	1.1961	0.7845	66.99	103.27
VPOs-0.1%Ga1%Mo-72	1.1671	0.7257	68.64	111.62

^aFWHM of (020) reflection plane.

^bFWHM of (204) reflection plane.

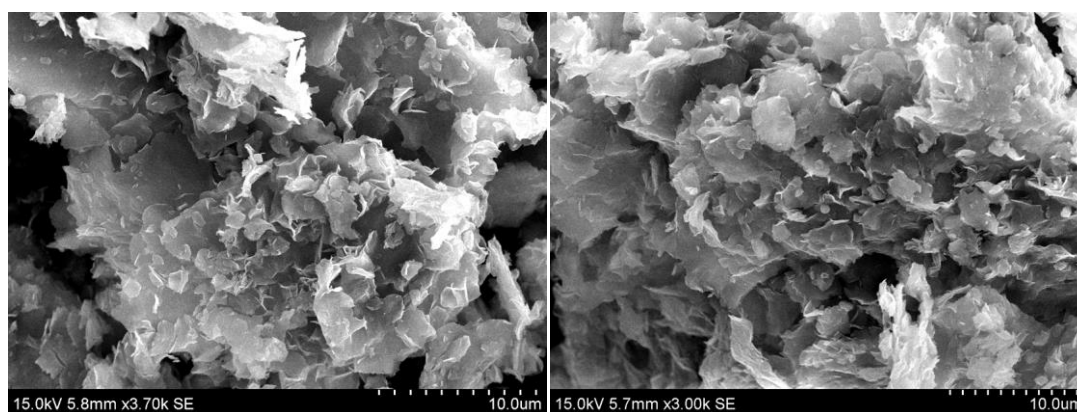
^cCrystallite thickness by means of Debye-Scherrer's formula.

4.2.2 Series 2: SEM Analyses

The results of the scanning electron microscopy (SEM) analyses showed the surface morphologies of the Ga-Mo doped catalysts obtained after different calcination times. All the catalysts showed their secondary principle structures, which consist of the different sizes of plate-like crystals. These plate-like crystals were comprised of agglomerates of (VO)₂P₂O₇ platelets that preferentially exposing the basal (1 0 0) plane of the catalyst (Kiely et al., 1995). However, the amounts of these plate-like agglomerates were shown different in all the catalysts, as shown in Figure 4.9.

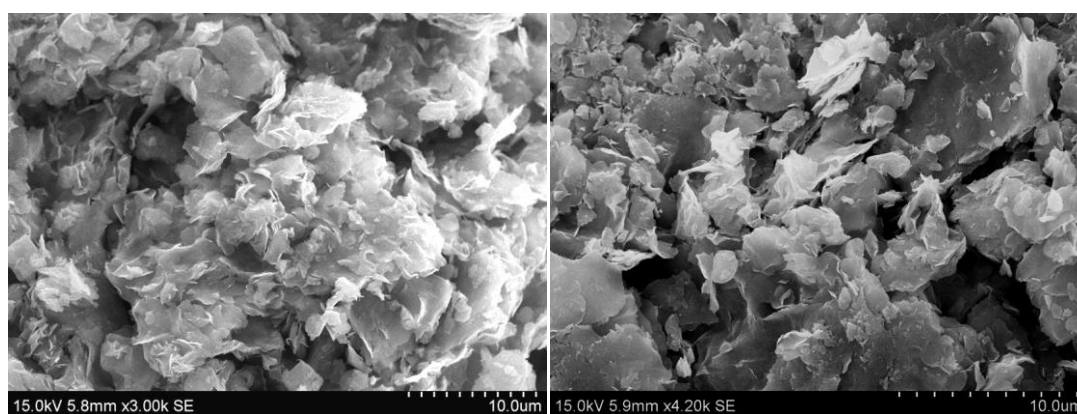
VPOs-0.1%Ga1%Mo-18 catalyst showed more uniform plate-like cluster than VPOs-0.1%Ga1%Mo-36. This should be the reason for higher specific surface

area obtained for VPOs-0.1%Ga1%Mo-18. The catalysts which had been calcined for the longer duration, i.e. VPOs-0.1%Ga1%Mo-54 and VPOs-0.1%Ga1%Mo-72, appeared to have agglomerates with bulky type of structures. The platelets obviously formed larger sizes of structure, as compared to its less calcined counterparts. This appeared to be a consistency whereby the plate-like agglomerates decreased with the rising of the calcination duration. These observation were also reported by Taufiq-Yap and his co-workers (2012), found that the specific surface area of VPO catalysts reduced with longer calcination duration.



(a)

(b)



(c)

(d)

Figure 4.9: SEM Micrographs for (a) VPOs-0.1%Ga1%Mo-18; (b) VPOs-0.1%Ga1%Mo-36; (c) VPOs-0.1%Ga1%Mo-54; and (d) VPOs-0.1%Ga1%Mo-72

4.2.3 Series 2: BET Surface Area Measurements and Chemical Analyses

The specific BET surface areas of the Ga-Mo doped catalysts are obtained as in Table 4.6: 23.5 m² g⁻¹ for VPOs-0.1%Ga1%Mo-18; 21.6 m² g⁻¹ for VPOs-0.1%Ga1%Mo-36; 20.0 m² g⁻¹ for VPOs-0.1%Ga1%Mo-54; and 20.4 m² g⁻¹ for VPOs-0.1%Ga1%Mo-72. The incorporation of Ga-Mo into the VPOs catalyst had increased the specific surface area, however, raising the calcination duration had reduced the specific surface area of the catalysts. The slight reduction of specific surface area for the Ga-Mo doped catalysts with longer calcination duration could be due to the fact that less platelets per cluster catalyst are formed as discussed earlier in Section 4.4.2.

Chemical analyses using ICP-OES showed that the bulk P/V atomic ratio for VPOs-0.1%Ga1%Mo-18, VPOs-0.1%Ga1%Mo-36, VPOs-0.1%Ga1%Mo-54 and VPOs-0.1%Ga1%Mo-72 were 1.35, 1.39, 1.32, and 1.60, respectively. The EDX analyses indicated that the surface P/V atomic ratios were ranged from 1.12 to 1.14. These results showed that the P/V atomic ratio were slightly higher than the optimal P/V atomic ratio range (1.10-1.30) reported for producing the active (VO)₂P₂O₇ phase (Centi, 1993).

The average oxidation states of the vanadium and the percentages of V⁵⁺ and V⁴⁺ oxidation states are summarised in Table 4.6. Apparently, the valence state of vanadium plays an important role on the selective oxidation of *n*-butane to MA (Abon et al., 2001; Abon and Volta, 1997). The mixture of V⁵⁺ and V⁴⁺ are an essential to provide highly reactive and selective catalyst, where the final oxidation

state of the activated catalysts is fall between +4.00 to +4.40. This finding was adhering to the literature by Abon and Volta (1997). Evidence was shown by the XRD patterns, which have been discussed that no V^{5+} was obtained from the Ga-Mo doped catalysts under different calcination durations.

4.2.4 Series 2: Temperature-Programmed Reduction (TPR in H_2) Analyses

The information of the behaviour, type of reducible species and the forms and amount oxygen species available from the catalysts were obtained by TPR analyses in H_2/Ar stream (5.23% H_2 in Argon, 1 bar, $25\text{ cm}^3\text{ min}^{-1}$) of a fresh catalyst raising the temperature from room temperature to 1273 K at 5 K min^{-1} in that stream as shown in Figure 4.10. The peak maxima temperatures, total amount of reducible oxygen atoms and reduction energies were summarised in Table 4.7.

There are several important points were observed from the TPR in H_2 profiles. The Ga-Mo doped catalysts gave three peak maxima in the reduction of H_2 (Figure 4.10). The first two peaks are assigned based on the lower temperature region within the range of the reduction of V^{5+} phase, whereas the third peak is assigned based on the higher temperature region within the range of lattice oxygen removed from the active V^{4+} phase. It was suggested that the peaks from V^{5+} is related to the O^{2-} while the peak attributed to V^{4+} is associated with the removal of O^- from the catalysts (Abon et al., 2001; Volta, 2000).

Table 4.6: Specific BET surface area, chemical compositions, average oxidation number and percentages of V⁴⁺ and V⁵⁺ oxidation states present for Ga-Mo doped VPOs catalysts

Catalysts	Specific BET surface area (m ² g ⁻¹)	EDX	ICP			V ⁴⁺ (%)	V ⁵⁺ (%)	Average oxidation number
			P/V	Ga/V	Mo/V			
VPOs-0.1%Ga1%Mo-18	23.5	1.12	1.35	0.0013	0.0122	85.85	14.15	4.1415
VPOs-0.1%Ga1%Mo-36	21.6	1.14	1.39	0.0015	0.0121	86.21	13.79	4.1379
VPOs-0.1%Ga1%Mo-54	20.0	1.13	1.32	0.0012	0.0121	83.93	16.07	4.1607
VPOs-0.1%Ga1%Mo-72	20.4	1.11	1.60	0.0013	0.0124	84.65	15.35	4.1535

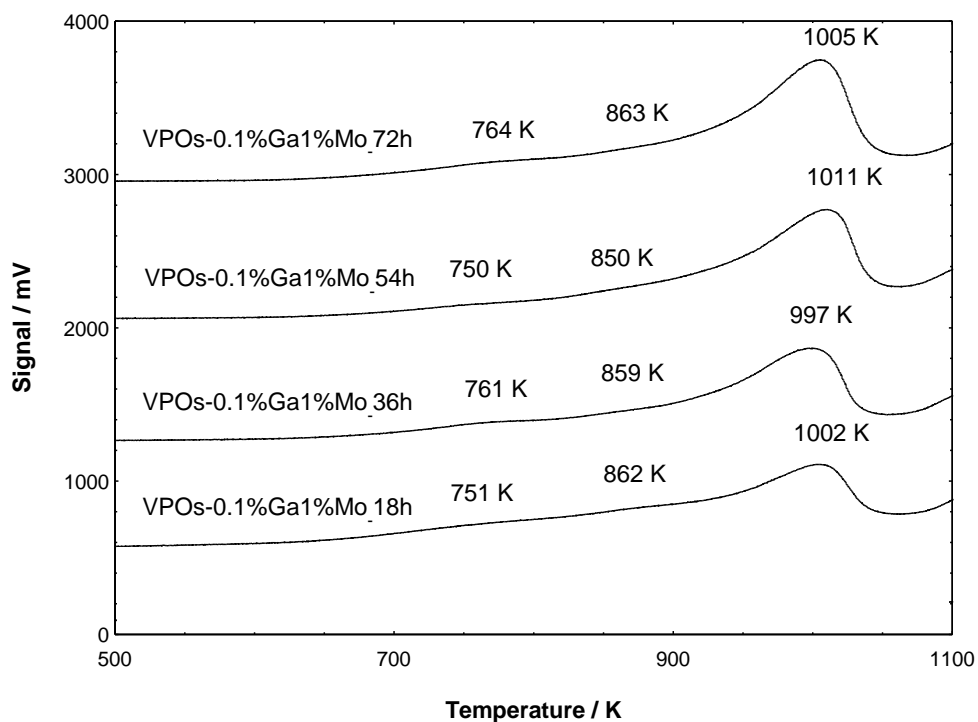


Figure 4.10: TPR in H₂ profiles of Ga-Mo doped VPOs catalysts

VPOs-0.1%Ga1%Mo-18 catalyst gave characteristic of three reduction peaks which occurred at 751, 862 and 1002 K with the amount of oxygen removed in each peak were 2.75×10^{20} , 3.67×10^{20} and 8.06×10^{20} atom g⁻¹, respectively.

VPOs-0.1%Ga1%Mo-36 also gave three peak maxima, which occurred at 761, 859 and 991 K. The reduction temperature remained similar, with the reduction of the V⁵⁺ and V⁴⁺ species appeared to be slightly affected as the calcination duration of Ga-Mo doped catalyst increased. The removal amount of oxygen species associated to V⁵⁺ decreased to 4.45×10^{20} atom g⁻¹, however, the amount of oxygen removed from the third peak which is assigned to the reduction of V⁴⁺ phase increased to 1.05×10^{21} atom g⁻¹.

VPOs-0.1%Ga1%Mo-54 gave similar three peak maxima appeared at 750, 850 and 1011 K. The removal amount of oxygen species related to V^{5+} phase was further decreased to 3.35×10^{20} atom g^{-1} . However, the amount of oxygen species removed from the V^{4+} phase was slightly increased to 1.09×10^{21} atom g^{-1} .

As the length of calcination period increased to 72 h, the three reduction peaks in H_2 which assigned to the reduction of V^{5+} and V^{4+} species for VPOs-0.1%Ga1%Mo-72 occurred at 764, 863 and 1005 K, respectively. As shown in the TPR- H_2 profile (Table 4.7), the total amount of oxygen removed from V^{4+} phase is shown to be dominant with 1.09×10^{21} atom g^{-1} compared to only 4.02×10^{20} atom g^{-1} oxygen species removed from V^{5+} phase.

From these results, the amount of oxygen removed of lower temperature region ($V^{5+}-O^{2-}$), for the Ga-Mo doped catalysts were not significantly affected by the duration of calcination. Whereby, the total removal of oxygen associated with V^{4+} was increased at least 30%, as the calcination duration had increased from 18 h to 36 h and above. This could be suggested that longer calcination duration has changed the surface and bulk morphologies into which more oxygen can be removed from the lattice structure (Waugh and Taufiq-Yap, 2003; Taufiq-Yap et al., 2004).

Furthermore, the reduction activation temperatures for all peak maxima that shown in TPR- H_2 profiles (Figure 4.10) were found not significantly affected by the calcination duration during the activation of the VPOs catalysts. These indicated that no additional energy is required for the reducible oxygen desorbed from the catalysts throughout the catalytic reaction.

Table 4.7: Total amount of oxygen atoms removed and values of reduction energies for Ga-Mo doped catalysts

Catalyst	Peak	T _m (K)	Reduction activation energy, E_r (kJ mol ⁻¹)	Amount of oxygen removed (atom g ⁻¹)
VPOs-0.1%Ga1% Mo-18	1	751	125.6	2.75×10^{20}
	2	862	144.3	3.67×10^{20}
	3	1002	167.6	8.06×10^{20}
	Total			1.45×10^{21}
VPOs-0.1%Ga1% Mo-36	1	761	127.3	2.42×10^{20}
	2	859	143.7	2.03×10^{20}
	3	997	166.7	1.05×10^{21}
	Total			1.50×10^{21}
VPOs-0.1%Ga1% Mo-54	1	750	125.4	1.61×10^{20}
	2	850	142.2	1.74×10^{20}
	3	1011	169.1	1.09×10^{21}
	Total			1.43×10^{21}
VPOs-0.1%Ga1% Mo-72	1	764	127.8	2.33×10^{20}
	2	863	144.3	1.69×10^{20}
	3	1005	168.1	1.09×10^{21}
	Total			1.49×10^{21}

4.2.5 Series 2: Catalytic Oxidation of *n*-Butane to Maleic Anhydride

The influence of calcination durations for Ga-Mo doped catalysts on the catalytic performance was investigated and tabulated in Figure 4.11 and summarised in Table 4.8. The *n*-butane conversion for VPOs-0.1%Ga1%Mo that calcined for 18 h, 36 h, 54 h and 72 h are 30 %, 31 %, 25 % and 23 %, respectively. Whereas, the selectivity for the same series of catalysts are in the range of 68 % - 69 %. Apparently, the Ga-Mo doped VPOs catalyst with 36 h calcination duration shown to give the highest conversion and selectivity towards the formation of MA among the prolonged calcination durations of the Ga-Mo doped catalysts.

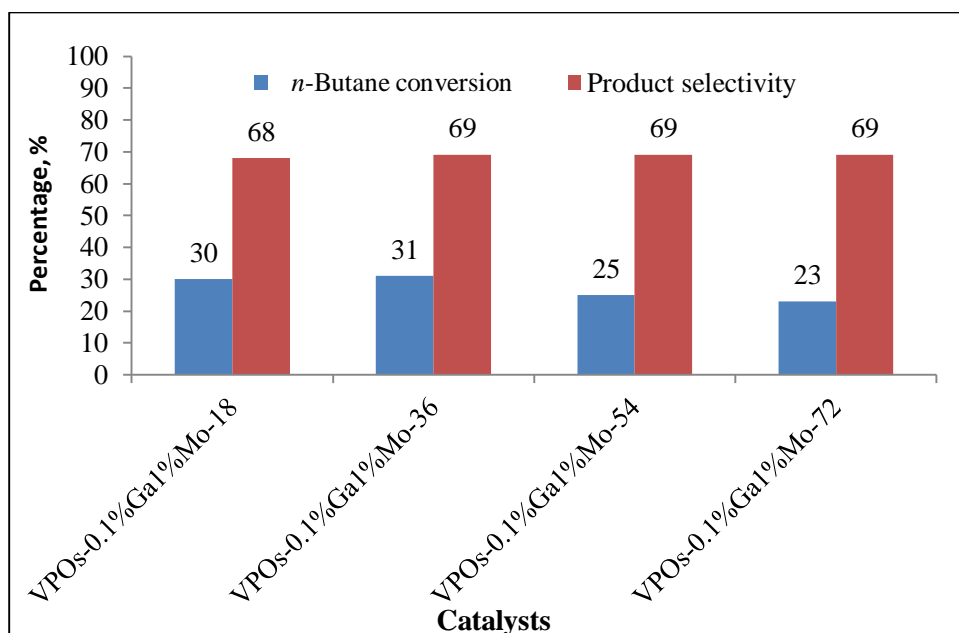


Figure 4.11: Catalytic performances of undoped and Ga-Mo doped VPOs catalysts

The turnover number (TON) of the Ga-Mo doped VPOs catalysts showed that VPOs-0.1%Ga1%Mo-36 has the highest value among the same series of catalysts. This showed that Ga-Mo doped catalyst calcined for 36 h gave better catalytic performances with the increment in *n*-butane conversion and selectivity toward the MA formation, which is in agreement with most of the results obtained.

Table 4.8: Catalytic performances of Ga-Mo doped VPOs catalysts

Catalyst	<i>n</i> -Butane conversion (%)	Turnover number (TON)	Product selectivity (%)		
			MA	CO	CO ₂
VPOs-0.1%Ga1% Mo-18	30	1.28	68	0	32
VPOs-0.1%Ga1% Mo-36	31	1.44	69	0	31
VPOs-0.1%Ga1% Mo-54	25	1.25	69	0	31
VPOs-0.1%Ga1% Mo-72	23	1.13	69	0	31

4.2.6 Series 2: Conclusions

The calcination duration has played an important role for the 0.1 mol% Ga and 1 mol% Mo doped vanadium phosphorus oxide catalysts prepared via sesquihydrate method, which has caused the structural disorder of the catalysts, affected the crystallite sizes in (0 2 0) and (2 0 4) directions and lowered the specific surface areas of the catalysts. The morphology of all the Ga-Mo doped catalysts is shown to be in plate-like crystals agglomeration, however, the platelets were getting bulkier as the calcination duration increased.

The TPR in H₂ profile shows that more lattice oxygen can be removed for 36 h calcined Ga-Mo doped catalyst which synthesised via sesquihydrate route. Besides, the catalyst shows higher TON, *n*-butane conversion and more selective toward the formation of maleic anhydride, although it had slightly smaller in specific surface area.

CHAPTER 5

CONCLUSIONS

5.1 The Effects of Ga, Mo doped and Different Calcination Duration for the Ga-Mo doped VPOs catalysts

The synthesised VPOs catalyst included the undoped, Ga doped and Mo doped were shown to exhibit good crystalline with three main characteristic peaks of $(VO)_2P_2O_7$ phase at $2\theta = 22.8^\circ$, 28.4° and 29.9° corresponded to (0 2 0), (2 0 4) and (2 2 1) planes, respectively. Generally, the Ga doped and Mo doped catalysts showed more intense peaks corresponded to the $(VO)_2P_2O_7$ active phase with additional V^{5+} phases as compared to the undoped counterpart. The SEM micrographs showed their morphologies found to be in plate-like crystals with folded edges, which deemed to be an important feature of VPO catalysts produced via sesquihydrate route. The consumption H_2 in TRP profiles have showed that more lattice oxygen can be removed from VPOs catalysts that incorporated with Ga and Mo, somehow 0.1 mol% of Ga achieved the highest amount of oxygen removed among all the same series of catalysts. However, high amount of Mo doped into the VPOs catalyst system (i.e. 3 and 5 mol%) somehow reduced the amount of surface and lattice oxygen removed from the catalyst., which show that 1 mol% Mo is the most appropriate doping concentration for Mo doped VPOs catalyst.

The TPR-H₂ result reveal that 0.1 mol% of Ga doped VPOs catalyst has the highest amount of oxygen removed, with the higher mobility oxygen species released associated with V⁴⁺, which greatly increased the oxidation of *n*-butane to maleic anhydride. VPOs-0.1%Ga gave the highest in *n*-butane conversion, i.e. 20 % with selectivity of 64 %. Hence, 0.1 mol% of Ga is found to be a good structural and electronic promoter as it increase the overall performances of VPOs catalysts.

For the series of Ga-Mo doped VPOs catalysts, XRD analyses revealed that all the catalysts showed similar characteristic reflection which comprised of well-crystallised (VO)₂P₂O₇ phase. The surface morphologies of the Ga-Mo doped catalysts with longer calcination time is shown to be agglomerates with bulky type of structure, which reduced in specific surface area as compared to its less calcined counterparts. TPR in H₂ results showed three peak maxima and no significantly changed was obtained in the total amount of reducible oxygen for the Ga-Mo doped catalysts, as calcined in different durations. However, the Ga-Mo doped catalyst calcined for 36 h has showed more oxygen can be removed from lattice and surface structure, which gave better lability of the lattice oxygen species that associated with V⁵⁺ and V⁴⁺ phases, which corresponding to the selectivity and activity of the VPO_s catalyst, respectively. The catalytic test shows that higher *n*-butane conversion and MA selectivity can be achieved from the 36 h calcined Ga-Mo doped catalyst synthesised via sesquihydrate route, i.e. 31 % and 69 %, respectively.

LIST OF REFERENCES

- Abdelouahab, F.B. et al., 1995. The role of Fe and Co dopants during the activation of the $\text{VO}(\text{HPO}_4) \cdot 0.5\text{H}_2\text{O}$ precursor of the vanadium phosphorus catalyst as studied by in Situ Laser Raman Spectroscopy. *Journal of Catalysis*, 157(2), pp. 687–697.
- Abon, M., Herrmann, J.M. and Volta, J.C., 2001. Correlation with the redox $\text{V}^{5+}/\text{V}^{4+}$ ratio in vanadium phosphorus oxide catalysts for mild oxidation of *n*-butane to maleic anhydride. *Catalysis Today*, 71 (1–2), pp. 121–128.
- Ai, M., 1986. Oxidation of propane to acrylic acid on V_2O_5 - P_2O_5 -based catalysts. *Journal of Catalysis*, 101, pp. 389–395.
- Ballarini, N., Cavani F. and Cortelli C., 2006. VPO catalyst for *n*-butane oxidation to maleic anhydride: A goal achieved, or a still open challenge? *Topic in Catalysis*, 38, pp. 1–3.
- Bartholomew, C.H. and Farrauto, R.J., 2006. Catalysts or industrial application. In: *Fundamentals of industrial catalytic processes*. New Jersey: John Wiley & Sons, Inc., pp. 1–49
- Batis, N.H., Batis, H. and Ghorbel, A., 1991. Synthesis and characterization of new VPO catalysts for partial *n*-butane oxidation to maleic anhydride. *Journal of Catalysis*, 128 (1), pp. 248–263.
- Bej, S.K. and Rao, M.S., 1991. Selective oxidation of *n*-butane to maleic anhydride. 3. Modelling studies. *Industrial and Engineering Chemistry Research*, 30 (8), pp. 1829–1832.

- Bej, S.K. and Rao, M.S. 1992a. Selective oxidation of *n*-butane to maleic anhydride. 4. Recycle reactor studies. *Industrial and Engineering Chemistry Research*, 31 (9),pp. 2075–2079.
- Bej, S.K. and Rao, M.S., 1992b. Selectivity oxidation of *n*-butane to maleic anhydride, a comparative study between promoted and unpromoted VPO catalysts. *Applied Catalysis A: General*, 83 (2), pp. 149–163.
- Ben Abdelouahab, F., Olier, R., and Ziyad, M., 1995. The role of Fr and Co dopants during the activation of the $\text{VO}(\text{HPO}_4)\cdot 0.5\text{H}_2\text{O}$ precursor of the vanadium phosphorus catalyst as studied by in situ laser raman-spectroscopy. *Journal of Catalysis*, 157, pp. 687-697.
- Bergeret, G., David, M., and Broyer, J.P., 1987. A contribution to the knowledge of the active sites of VPO catalysts for butane oxidation to maleic anhydride. *Catalysis Today*, 1 (1–2), pp. 37–47
- Bond, G.C., 1987. Basic principles of catalysts. In: *Heterogeneous Catalysis. Principle and Application*, 2nd (eds), Oxford Clarendon Press, pp. 1-11.
- Borders, E. and Courtine, P., 1979. Some selectivity criteria in mild oxidation catalysis: V-P-O phases in butane oxidation to maleic anhydride. *Journal of Catalysis*, 57, pp. 236-252.
- Borders, E., 1987. Crystallochemistry of V–P–O phases and application to catalysis. *Catalysis Today*, 1 (5), pp. 499–526.

- Bordes, E., Courtine, P. and Johnson, J.W., 1984. On the topotactic dehydration of $\text{VOHPO}_4 \cdot 0.5\text{H}_2\text{O}$ into vanadyl pyrophosphate. *Journal of Solid State Chemistry*, 55 (3), pp. 270–279.
- Bordes, E., 1993. Nature of the active and selective sites in vanadyl pyrophosphate, catalyst of oxidation of *n*-butane, butene and pentane to maleic anhydride. *Catalysis Today*, 16 (1), pp. 27–38.
- Brunauer, S., Emmett, P.H. and Teller, E., 1938. Adsorption of gases in multimolecular layers. *Journal of the American Chemical Society*, 60, pp. 309-319.
- Brutovsky, M., Kladekova, D., and Reiffova, K., 1997. Vanadium-phosphorus catalysts modified with magnesium, calcium and barium. *Collection of Czechoslovak Chemical Communications*, 62, pp. 392–396.
- Cavani, F., Centi, G. and Trifiro, F., 1984. The chemistry of catalysts based on vanadium-phosphorus oxides: Note IV: Catalytic behaviour of catalysts prepared in organic medium in the oxidation of C_4 fraction. *Applied Catalysis*, 9, pp. 191-202.
- Cavani, F., Centi, G., Trifiro, F. and Poli, G., 1985. Structure and reactivity of vanadium-phosphorus oxide. *Journal of Thermal Analysis*, 30, pp. 1241-1251.
- Cavani, F., Centi, G. and Trifiro, F., 1992. Redox properties of vanadium oxide based catalysts as key-factors for influencing the selectivity in C_4 oxidation to maleic anhydride and alkylaromatics ammoxidation to nitriles. *La Chimica & L'Industria, Milan*, 74, pp. 182-193.

- Cavani, F. and Trifiro, F., 1994. Catalysing butane oxidation to make maleic anhydride. *Chemtech*, 25 (34), pp. 18–25
- Centi, G., Fornasari, G. and Trifiro, F., 1984. On the mechanism of *n*-butane oxidation to maleic anhydride: Oxidation in oxygen-stoichiometry-controlled conditions. *Journal of Catalysis*, 89 (1), pp. 44–51.
- Centi, G., Trifiro, F. and Ebner, J.R., 1988. Mechanistic aspects of maleic anhydride synthesis from C₄ hydrocarbons over phosphorus vanadium oxide. *Chemical Reviews*, 88 (1), pp. 55–80.
- Centi, G., Golinelli, G. and Trifiro, F., 1989. Nature of the active sites of (VO)₂P₂O₇ in the selective oxidation of *n*-butane: Evidence from doping experiments. *Applied Catalysis*, 48 (1), pp. 13–24.
- Centi, G., 1993a. Selective heterogeneous oxidation of light alkanes. What differentiates alkane from alkene feedstocks. *Catalysis Letters*, 22, pp. 53–66.
- Centi, G., 1993b. Vanadyl Pyrophosphate—A Critical Overview. *Catalysis Today*, 24 (16), pp. 5–26.
- Centi, G., Cavani, F., and Trifiro, F., 2001a. New reactor technology options. In: *Selective oxidation by heterogeneous catalysis*. New York: Kluwer Academic/ Plenum Publishers, pp. 37–53.
- Centi, G. and Perathoner, S., 2001b. Site isolation in iron-molybdate-based catalysts for site chain oxidation of alkylaromatics. *Topics in Catalysis*, 15, pp. 145–152.

- Che, M. and Tench, A.J., 1982. Characterisation and reactivity of mononuclear oxygen species on oxide surface. *Advance Catalysis*, 31, pp. 77–133.
- Cheng, W. and Wang, W., 1997. Effect of calcinations environment on the selective oxidation of *n*-butane to maleic anhydride over promoted and unpromoted VPO catalyst. *Applied Catalysis A: General*, 156(1), pp. 57-69.
- Chorkendorff, I. and Niemantsverdriet, J.W., 2007. Introduction to catalysis. In: Concepts of modern catalysis and kinetics. 2nd Edition. Germany: WILEY-VCH Verlag GmbH & Co. KGaA., pp. 2–167.
- Contractor, R.M. and Sleight, A.W., 1987. Maleic anhydride from C-4 feedstocks using fluidized bed reactors. *Catalysis Today*, 1, pp. 587-607.
- Contractor, R.M., 1999. Dupont's CFB technology for maleic anhydride. *Chemical Engineering Science*, 54, pp. 5627-5632.
- Cornaglia, L.M., Caspani, C. and Lombardo, E.A., 1991. Physicochemical characterization and catalytic behaviour of VPO formulations. *Applied Catalysis*, 74, pp. 15-27.
- Cornaglia, L.M., Sanchez, C.A. and Lombardo, E.A., 1993. Chemistry of vanadium phosphorus oxide catalyst preparation. *Applied Catalysis A: General*, 95, pp. 117-130.
- Cornaglia, L.M., Carrare, C. and Petunchi, J.O., 1999. The role of cobalt as promoter of equilibrated vanadium-phosphorus-oxygen catalysts. *Applied catalysis A: General*, 183 (1), pp. 177–187.

- Cornaglia, L.M., Carrara, C.R. and Petunchi, J.O., 2000. Characterization of cobalt-impregnated VPO catalysts. *Catalysis Today*, 57, pp. 313-322.
- Cornaglia, L., Irusta, S., and Lombardo, E.A., 2003. The beneficial effect of cobalt on VPO catalysts. *Catalysis Today*, 78 (1– 4), pp. 291–301.
- Coulston, G.W., Thompson, E.A. and Herron, N., 1996. Characterization of VPO catalysts by x-ray photoelectron spectroscopy. *Journal of Catalysis*, 163, pp. 122-129.
- Ebner, J. and Gleaves, J., 1988. The vanadium phosphorus oxide catalyst. In: Martel, A. E. and Sawyer, D. T. (Eds.), Oxygen complexes and oxygen activation by transition metals. *New York and London: Plenum Press*, pp. 273–284.
- Ebner, J.R. and Thompson, M.R. 1993. An active site hypothesis for well-crystallized vanadium phosphorus oxide catalyst systems. *Catalysis Today*, 16, pp. 51-60.
- Ellison, I.J., Hutchings, G.J. and Sananes, M. T., 1994. Control of the composition and morphology of vanadium phosphate catalyst precursors from alcohol treatment of $\text{VOPO}_4 \cdot 2\text{H}_2\text{O}$. *Journal of the Chemical Society, Chemical Communications*, 8 (9), pp. 1093–1094.
- Ertl, G., 2002. Heterogeneous catalyst on atomic scale. *Journal of Molecular Catalysis A: Chemical*, 182-183, pp. 5-16.
- Fadoni, M. and Lucarelli, L., 1999. Temperature programmed desorption, reduction, oxidation and flow chemisorptions for the characterisation of

- heterogeneous catalysts-Theoretical aspects, instrumentation and applications. *Studies in Surface Science and Catalysis*, 120(a), pp. 177-255.
- Felthouse, T.R., Burnett, J. C. and Mitchell, S.F., 1995. In: *Encyclopedia of Chemical Technology*, 4th ed. New York: John Wiley & Sons Inc., pp. 893.
- Felthouse, T.R., Burnett, J.C. and Horrell, B., 2001. Maleic anhydride, maleic acid, and fumaric acid. In: Kirk-Othmer (Ed.). *Kirk-Othmerencyclopedia of chemical technology*. New York: John Wiley & Sons, Inc., pp. 893–928.
- Fisher, E. and Speier, A., 1895. Darstellung der Ester. *Chemische Berichte*, (28), pp. 3252-3258.
- Fumagalli, C. et al., 1993. Facile and not facile reactions for the production of maleic anhydride and phthalic anhydrides with vanadium mixed oxides based catalysts. *Catalysis Letters*, 21, pp. 19-26.
- Gai, P.L. and Kourtakos, K., 1995. Solid-state defect mechanism in vanadyl phosphosphate catalysts: Implications for selective oxidation. *Science*, 267 (5198), pp. 661-633.
- Garbassi, F., Bart, J.C.J. and Tassinari, R., 1986. Catalytic *n*-butane oxidation activity and physicochemical characterisation of vanadium-phosphorus oxides with variable P/V ratio. *Journal of Catalysis*, 98 (2), pp. 317–325.
- Geem, P.C. and Nobel, A.P.P., 1987. Influence of the P/V ratio on the oxidation of *n*-butane and trans-2-butene to maleic anhydride over phosphorus vanadium oxide catalysts. *Catalysis Today*, 1 (1–2), pp. 5–16.

- Gleaves, J., Yablonsky, G., and Zheng, X., 2010. Temporal analysis of products (TAP)-Recent advances in technology for kinetic analysis of multicomponent catalysts. *Journal of Molecular Catalysis A-Chemical*, 315, pp. 108-134.
- Goh, C.K., Taufiq-Yap, Y.H., and Hutchings, G.J., 2008. Influence of Bi-Fe additive on properties of vanadium phosphate catalysts for *n*-butane oxidation to maleic anhydride. *Catalysis Today*, 131 (1), pp. 408–412.
- Gopal, R. and Calvo, C., 1972. Crystal structure of β VPO₅. *Journal of Solid State Chemistry*, 5 (3), pp. 432–435.
- Guilhaume, M., Rouillet, M. and Pajonk, G., 1992. Butane oxidation to maleic anhydride on VPO catalyst: The importance of the preparation of the precursor on the control of the local superficial structure. *Studies in surface science and catalysis*, 72, pp. 255-265.
- Gulians, V.V. et al., 1996. The effect of the phase composition of model V–P–O catalysts for partial oxidation of *n*-butane. *Catalysis Today*, 28 (4), pp. 275–295.
- Gulians, V.V., 1999a. Structure-reactivity relationships in oxidation of C4 hydrocarbons on supported vanadia catalysts. *Catalysis Today*, 51, pp. 255-268.
- Gulians, V.V., Benziger, J.B. and Sundaresan, S., 1999b. Effect of promoters for *n*-butane oxidation to maleic anhydride over vanadium-phosphorus-oxide catalysts: comparison with supported vanadia catalysts. *Catalysis Letters*, 62, pp. 87-91.

- Guliants, V.V. et al., 2001. In situ studies of atomic, nano- and macroscale order during $\text{VOHPO}_4 \cdot 0.5\text{H}_2\text{O}$ transformation to $(\text{VO})_2\text{P}_2\text{O}_7$. *Journal of Molecular Catalysis A-chemical*, 172, pp. 265-276.
- Haber, J., Zazhigalov, V.A. and Stoch, J., 1997. Mechanochemistry: the activation method of VPO catalysts for *n*-butane partial oxidation. *Catalysis Today*, 33, pp. 39-47.
- Hartley, F.R., 1985. Catalysis. In: Supported metal complexes: *Catalysis by metal complexes*. Holland: D. Reidel Publishing Company, pp. 1–3.
- Herrmann, J.M. and Raulin, J., 2005. Heterogeneous photocatalysis: state of the art and present applications in honor of Pr. R. L. Burwell Jr. (1912-2003), former head of Ipatieff laboratories, Northwestern University, Evanston (Ill). *Topics in Catalysis*, 34, pp. 49-65.
- Hodnett, B.K., Permann, Ph. and Delmon, B., 1983. Influence of P/V ratio on the phase composition and catalytic activity of vanadium phosphate based catalysts. *Applied Catalysis*, 6 (2), pp. 231–244.
- Hodnett, B.K. and Delmon, B., 1984. Influence of calcination conditions on the phase composition of vanadium-phosphorus oxide catalysts. *Applied Catalysis*, 9 (2), pp. 203–211.
- Hodnett, B.K., 2000. Heterogeneous catalytic oxidation - Fundamental and technological aspect of the selective and total oxidation of organic compounds. Brisbane: John Wiley & Sons Ltd.

- Holmes, S. et al., 2000. Modifications of vanadium phosphorus oxides by aluminium phosphate for *n*-butane oxidation to maleic anhydride. *Studies in Surface Science and Catalysts*, 130, pp. 1709-1714.
- Horowitz, H.S., Blackstone, C.M. and Sleight, A.W., 1988. V-P-O catalysts for oxidation of butane to maleic anhydride: Influence of $(VO)_2H_2P_2O_9$ precursor morphology on catalytic properties. *Applied Catalysis*, 38, pp. 193-210.
- Hutchings, G.J., 1991. Effect of promoters and reactant concentration on the selective oxidation of *n*-butane to maleic anhydride using vanadium phosphorus oxide catalysts. *Applied Catalysis*, 72 (1), pp. 1–32.
- Hutchings, G.J. 1993. Vanadium phosphorus oxide catalysts for the selective oxidation of *n*-butane to maleic anhydride. *Catalysis Today*, 16 (1), pp. 139–146.
- Hutchings, G.J. and Higgins, R., 1996. Effect of promoters on the selective oxidation of *n*-butane with Vanadium-Phosphorus Oxide Catalysts. *Journal of Catalysis*, 162 (2), pp. 153–168.
- Hutchings, G.J. and Higgins, R., 1997. Selective oxidation of *n*-butane to maleic anhydride with vanadium phosphorus catalysts prepared by comminution in the presence of dispersants. *Applied Catalysis A: General*, 154 (1–2), pp. 103–115.
- Hutchings, G.J. et al., 1997. Improved method of preparation of vanadium phosphate catalysts. *Catalysis Today*, 33 (1–3), pp. 16–171.

- Hutchings, G.J., Kiely, C.J. and Sananes-Schulz, M.T., 1998. Comments on the nature of the active site of vanadium phosphate catalysts for butane oxidation. *Catalysis Today*, 40, pp. 273-286.
- Hutchings, G.J., 2004. Vanadium phosphate: A new look at the active components of catalysts for the oxidation of butane to maleic anhydride. *Journal of Materials Chemistry*, 14 (23), pp. 3385–3395.
- Hutchings, G.J., 2009. Heterogeneous catalysts-discovery and design. *Journal of Materials Chemistry*, pp. 19.
- Ieda, S., Phiyanalimat, S. and Komai, S., 2005. Involvement of active sites of promoted vanadyl pyrophosphate in selective oxidation of propane. *Journal of Catalysis*, 236, pp. 304-312.
- Inumaru, K., Misono, M. and Okuhara, T., 1997. Structure and catalysis of vanadium oxide overlayers on oxide supports. *Applied Catalysis A: General*, 149, pp. 133-149.
- Ishimura, I., Sugiyama, S. and Hayashi, H., 2000. Vanadyl hydrogen phosphate sesquihydrate as a precursor for preparation of $(VO)_2P_2O_7$ and cobalt incorporated catalysts. *Journal of Molecular Catalysis*, 158, pp. 559–565.
- Ji, W. et al., 2002. Effects of ball milling on the doped vanadium phosphorus oxide catalysts. *Catalysis Today*, 74 (1–2), pp. 101–110.

- Johnson, J.W., Johnston, D.C. and Jacobson, A.J., 1984. Preparation and characterization of vanadyl hydrogen phosphate hemihydrate and its topotactic transformation to vanadyl pyrophosphate. *Journal of the American Chemical Society*, 106 (26), pp. 8123–8128.
- Johnsson, J.E., Grace, J.R., and Graham, J.J., 1987. Fluidized-Bed reactor model verification on a reactor of industrial scale. *AIChE Journal*, 33 (4), pp. 619–627.
- Kiely, C.J. et al., 1995. Electron microscopy studies of vanadium phosphorus oxide catalysts derived from $\text{VOPO}_4 \cdot 2\text{H}_2\text{O}$. *Catalysis Letters*, 33, pp. 357-368.
- Kiely, C.J. et al., 1996. Characterisation of variations in vanadium phosphate catalyst microstructure with preparation route. *Journal of Catalysis*, 162 (1), pp. 31–47.
- Kirk and Othmer, 2013, *Maleic Anhydride: Demand Growth Trend* [Online]. Available at: http://en.wikipedia.org/wiki/Maleic_anhydride. [Accessed on 8th December 2013].
- Kourtakis, K., 2010. Direct grafting of alkoxide promoters on vanadium hydrogen phosphate precursor: Improved catalysts for the selective oxidation of *n*-butane. *Applied Catalysis A: General*, 376(1-2), pp. 40-46.
- Kung, H.H., 1986. Desirable catalyst properties in selective oxidation reactions. *Industrial and Engineering Chemistry Product Research and Development*, 25 (2), pp. 171–178.

- Ladwig, G., 1965. On the Constitution of the $VPO_5(nH_2O)$. *Journal of Inorganic and General Chemistry*, 338, pp. 266–278
- Lambardo, E.A., Sanchez, C.A. and Cornaglia, L.M., 1992. The effect of preparation methods and activation strategies upon the catalytic behavior of the vanadium-phosphorus oxides. *Catalysis Today*, 15, pp. 407-418.
- Lashier, M.E., Moser, T.P. and Schrader, G.L., 1990. In new development on selective oxidation. In: Centi, G. and Trifiro, F. (eds.), Amsterdam: Elsevier Science, pp. 156.
- Lawrie, L., 2011. Oxidation catalysts.in: Handbook of industrial catalysts. *Fundamental and Applied Catalysis*: Springer, pp. 119-167.
- Leong, L.K., Chin, K.S. and Taufiq-Yap, Y.H., 2011. The effect of Bi promoter on vanadium phosphate catalysts synthesized via sesquihydrate route. *Catalysis Today*, 164 (1), pp. 341–346.
- Leonowicz, M.E., Johnson, J.W. and Brody, J.F., 1985. Vanadyl hydrogen phosphate hydrates: $VO(HPO_4) \cdot 4H_2O$ and $VO(HPO_4) \cdot 0.5H_2O$. *Journal of Solid State Chemistry*, 56, pp. 370-378.
- Liang, H. and Ye, D., 2005. Selective oxidation of *n*-butane over VPO catalyst modified by different additives. *Journal of Natural Gas Chemistry*, 14, pp. 177-180.
- Ma, L. et al., 2012. Influence of calcination temperature on Fe/HBEA catalyst for the selective catalytic reduction of NO_x with NH_3 . *Catalysis Today*, 184(1), pp. 145-152.

- Mars, P. and van Krevelen, D.W., 1954. Oxidations carried out by means of vanadium oxide catalysts. *Special Supplement to Chemical Engineering Science*, 3 (1), pp. 41–59.
- Martin, V., Millet, J.M.M. and Volta, J.C., 1998. Thermogravimetric analysis of vanadium phosphorus oxide catalysts doped with cobalt and iron. *Journal of Thermal Analysis and Calorimetry*, 53, pp. 111-121.
- Matsuura, I. and Yamazaki, M., 1990. Reactivity and structure of vanadyl pyrophosphate as a butane oxidation catalyst. In: Centi, G. and Trifiro, F. (eds.), *Studies in surface science and catalysis*, Amsterdam: Elsevier Science, pp. 563–572.
- Matsuura, I., Ishimura, T. and Kimura, N., 1995. Preparation and characterization of vanadyl hydrogen phosphate hydrates; $\text{VO}(\text{HPO}_4)\cdot 1.5\text{H}_2\text{O}$ and $\text{VO}(\text{HPO}_4)\cdot 0.5\text{H}_2\text{O}$. *Chemistry Letters*, 9, pp. 769–770.
- Misono, M. et al., 1990. In new developments in selective oxidation. In: Centi, G. and Trifiro, F. (eds.), Amsterdam: Elsevier Science, pp. 605.
- Misono, M., 2002. Selective oxidation of butanes toward green/sustainable chemistry. *Topics in Catalysis*, 21 (1–3), pp. 89–96.
- Mizuno, N., Hatayama, H. and Misono, M., 1997. One-pot synthesis of $\text{VOHPO}_4\cdot 0.5\text{H}_2\text{O}$ with high growth of the (0 0 1) plane: An important catalyst precursor of $(\text{VO})_2\text{P}_2\text{O}_7$. *Chemistry of Materials*, 9, pp. 2697-2698.

- Morishige, H., Tamaki, J. and Miura, N., 1990. Amorphous V–P mixed oxide with P/V = 2.0 as active phase for butane oxidation. *Chemistry letters*, (9), pp. 1513–1516.
- Mota, S., Abon, M. and Volta, J.C., 2000. Selective oxidation of *n*-butane on a VPO catalyst: Study under fuel-rich conditions. *Journal of Catalysis*, 193 (2), pp. 308–318.
- O'Connor, M., Dason, F. and Hodnett, B.K., 1990. Preparation of vanadium phosphorus oxide catalysts: Influence of macroscopic P:V ratio in determining phase composition after calcination. *Applied Catalysis*, 64, pp. 161-171.
- Okuhara, T. and Misono, M., 1993. Key reaction steps and active surface phase of vanadyl pyrophosphate for selective oxidation of butane. *Catalysis Today*, 16, pp. 61-67.
- O'Mahony, L., Zemlyanov, D., Mihov, M., Curtin, T. and Hodnett, B.K., 2005. In situ X-ray diffraction analysis of the crystallisation of $\text{VOHPO}_4 \cdot 0.5\text{H}_2\text{O}$. *Journal of Crystal Growth*, 275, pp. 1793-1798.
- Pepera, M.C. et al., 1985. Fundamental study of the oxidation of butane over vanadyl pyrophosphate. *Journal of the American Chemical Society*, 107 (17), pp. 4883–4892.
- Pierini, B.T. and Lombardo, E.A., 2005. Cr, Mo and W used as VPO promoters in the partial oxidation of *n*-butane to maleic anhydride. *Catalysis Today*, 107-108, pp. 323-329.

- Poli, G., Resta, I. and Ruggeri, O., 1981. The chemistry of catalysts based on vanadium-phosphorus oxides: Note II The role of the preparation method. *Applied Catalysis*, 1, pp. 395-404.
- Rodemerck, U., Kubias, B. and Zanthoff, H.W., 1997. The reaction mechanism of the selective oxidation of butane on $(VO)_2P_2O_7$ catalysts: The influence of the valence state of vanadium. *Applied Catalysis: General*, 153, pp. 217-231.
- Rothenberg, G., 2008. Catalyst/substrate interactions and Sabatier's principle. In: *Catalysis: Concepts and green applications*. Netherlands: WILEY-VCH Verlag GmbH & Co. KGaA., pp. 11-66.
- Rownaghi, A.A., Taufiq-Yap, Y.H. and Rezaei, F., 2009. Influence of rare-earth and bimetallic promoters on various VPO catalysts for partial oxidation of *n*-butane. *Catalysis Letters*, 130, pp. 504-516.
- Ruiz, P. and Delmon, B., 1987. The role of mobile oxygen species in the selective oxidation of isobutene. *Catalysis Today*, 1 (1-2), pp. 1-4.
- Ruiz, P. et al., 1993. New aspects of the cooperation between phases in vanadium phosphate catalysts. *Catalysis Today*, 16, pp. 99-111.
- Ryumon, N., Imai, H. and Kamiya, Y., 2006. Effect of water vapor on the transformation of $VOHPO_4 \cdot 0.5H_2O$ into $(VO)_2P_2O_7$. *Applied Catalysis A: General*, 297, pp. 73-80.

- Sajip, S. et al., 2001. Structural transformation sequence occurring during the activation under *n*-butane air of a cobalt-doped vanadium phosphate hemihydrate precursor for mild oxidation to maleic anhydride. *Physical Chemistry Chemical Physics*, 11, pp. 2143-2147.
- Sajip, S. et al., 2001. Structure-activity relationships for Co and Fe-promoted vanadium phosphorus oxide catalysts. *New Journal of Chemistry*, 25, pp. 125-130.
- Sakakini, B.H., Taufiq-Yap, Y.H. and Waugh, K.C., 2000. A study of a kinetics and mechanism of the adsorption and anaerobic partial oxidation of *n*-butane over a vanadyl pyrophosphate catalyst. *Journal of Catalysis*, 189, pp. 253-262.
- Sananes-Schulz, M.T., Petunchi, J.O. and Lambardo, E.A., 1992. The effect of Zn, Ti and Zr used as additives in VPD formulations. *Catalysis Today*, 15, pp. 527-535.
- Sananes-Schulz, M.T., Hutchings, G.J. and Volta, J.C., 1995. On the role of the VO(H₂PO₄)₂ precursor for *n*-Butane Oxidation into Maleic Anhydride. *Journal of Catalysis*, 154 (2), pp.253–260.
- Sananes-Schulz, M.T., Ben Abdelouahab, F. and Hutchings, G.J., 1996. On the role of Fe and Co dopants during the activation of the VO(HPO₄)·0.5H₂O precursor of the vanadium phosphorus catalyst as studied by in situ laser raman spectroscopy. *Journal of Catalysis*, 163, pp. 346-353.

- Sananes-Schulz, M.T., Tuel, A. and Hutching, G.J., 1997. The V^{4+}/V^{5+} balance as a criterion of selection of vanadium phosphate oxide catalysts for *n*-butane oxidation to maleic anhydride: A proposal to explain the role of Co and Fe dopants. *Journal of Catalysis*, 166, pp. 388-392.
- Sanchez, J.C., Lopez-Sanchez, J.A. and Wells, R.P.K., 2001. Effect of group 13 compounds and bulky organic oxygenates as structural promoter for the selective oxidation of *n*-butane with vanadium oxide catalysts. *New Journal of Chemistry*, 25, pp. 1528-1536.
- Sartoni, L. et al., 2004. Promotion of vanadium phosphate catalysts using gallium compounds: effect of low Ga/V molar ratios. *Journal of Molecular Catalysis A: Chemical*, 220, pp. 85-92.
- Satsuma, A. et al., 1989. Surface active sites of vanadium pentoxide-molybdenum trioxide catalysts. *Journal of Physical Chemistry*, 93, pp. 1484-1490.
- Satsuma, A., Kijima, Y. and Komai, S., 2001. Insertion of iron-complex to lamellar vanadyl benzylphosphate for preparation of well-defined catalyst. *Catalysis Today*, 71, pp. 161-167.
- Sharp D.W.A., 2003. *The Penguin Dictionary of Chemistry*, pp. 56-98.
- Shen, S., Zhou, J. and Zhang, F., 2002. Effect of the Ce-Fe oxides on performance of VPO catalyst for *n*-butane oxidation to maleic anhydride in the absence of gas-phase oxygen. *Catalysis Today*, 74, pp. 37-43.

- Shimoda, T., Okuhara, T. and Misono, M., 1985. Preparation of vanadium-phosphorus mixed oxide (P/V = 1) catalysts and their application to oxidation of butane to maleic anhydride. *Bulletin of the Chemical Society of Japan*, 58, pp. 2162-2171.
- Solsona, B., Zazhigalov, V.A. and Lopez Nieto, J.M., 2003. Oxidative dehydrogenation of ethane on promoted VPO catalysts. *Applied Catalysis A-general*, 249, pp. 81-92.
- Somorjai G.A., 1994. Introduction to Surface Chemistry and Catalysis. Wiley, New York. Sons, Inc., pp. 1-49.
- Tamaki, J., Morishita, T. and Morishige, H., 1992. Promotion of V-P mixed oxide catalyst for butane oxidation by metal additives. *Chemistry Letters*, 1, pp. 13-16.
- Taufiq-Yap, Y.H., Sakakini, B.H. and Waugh, K.C., 1997a. On the mechanism of the selective oxidation of *n*-butane, but-1-ene and but-1,3-diene to maleic anhydride over a vanadyl pyrophosphate catalyst. *Catalysis Letters*, 46, pp. 273-277.
- Taufiq-Yap, Y.H., Sakakini, B.H. and Waugh, K.C., 1997b. Investigation of the nature of the oxidant (selective and unselective) in/on a vanadyl pyrophosphate catalyst. *Catalysis Letters*, 48, pp. 105-110.
- Taufiq-Yap, Y.H. et al., 2001. The effect of the duration of *n*-butane/air pretreatment on the morphology and reactivity of (VO)₂P₂O₇ catalysts. *Catalysis Letters*, 74 (1), pp. 99-104.

- Taufiq-Yap, Y.H., Looi, M.H. and Waugh, K.C., 2002. Investigation of vanadyl pyrophosphate catalysts synthesized from three different routes. *Asian Journal of Chemistry*, 14, pp. 1494-1502.
- Taufiq-Yap, Y.H. et al., 2003. Bismuth-modified vanadyl pyrophosphate catalyst. *Catalysis Letters*, 89, pp. 87-93.
- Taufiq-Yap, Y.H., Leong, L.K. and Hussein, M.Z., 2004a. Synthesis and characterization of vanadyl pyrophosphate catalysts via vanadyl hydrogen phosphate sesquihydrate precursor. *Catalysis Today*, 93, pp. 715–722
- Taufiq-Yap, Y.H., Waugh, K. C. and Ho, C.P., 2004b. TPD and TPR studies of vanadyl pyrophosphate catalysts derived from $\text{VOPO}_4 \cdot 2\text{H}_2\text{O}$ precursor. *Eurasian Chemico-Technological Journal*, 6, pp. 201-203.
- Taufiq-Yap, Y.H. and Mohd. Hasbi, A.R., 2005. Hydrothermal synthesis of vanadium phosphate. *Eurasian Chemico-Technological Journal*, 7, pp. 261-265.
- Taufiq-Yap, Y.H. et al., 2006a. Synthesis of vanadium phosphate catalysts by hydrothermal method for selective oxidation of *n*-butane to maleic anhydride. *Catalysis Letters*, 106 (3–4), pp. 177–181.
- Taufiq-Yap, Y.H., Goh, C. K. and Hutching, G.J., 2006b. Effects of mechanochemical treatment to the vanadium phosphate catalysts derived from $\text{VOPO}_4 \cdot 2\text{H}_2\text{O}$. *Journal of Molecular Catalysis A: Chemical*, 260 (1–2), pp. 24–31.

- Taufiq-Yap, Y.H., Kamiya, Y. and Tan, K.P., 2006c. Promotional effect of bismuth as dopant in Bi-doped vanadyl pyrophosphate catalysts for selective oxidation of *n*-butane to maleic anhydride. *Journal of Natural Gas Chemistry*, 15, pp. 297-302.
- Taufiq-Yap, Y.H. and Saw, C.S., 2008. Effect of Different Calcination Environments on the Vanadium Phosphate Catalysts for Selective Oxidation of Propane and *n*-Butane. *Catalysis Today*, 131, pp. 285-291.
- Taufiq-Yap, Y.H., 2009. Catalysis for a sustainable world, *Universiti Putra Malaysia Press*.
- Taufiq-Yap, Y.H., Goh, C.K. and Hutchings, G.J., 2009. Dependence on *n*-butane activation on active site of vanadium phosphate catalysts. *Catalysis Letters*, 130, pp. 327-332.
- Taufiq-Yap, Y.H., Lee H.V. and Wong Y.C., 2012. Effect of different calcination duration on physicochemical properties of vanadium phosphate catalysts. *E-Journal of Chemistry*, 9(3), pp. 1440-1448.
- Torardi, C.C. and Calabrese, J.C., 1984. Ambient- and low-temperature crystal structure of vanadyl pyrophosphate (VO)₂H₄P₂O₉. *Inorganic Chemistry*, 23 (10), pp. 1308–1310.
- Trifiro, F., 1993. Key properties of V-P mixes oxides in selective oxidation of C₄ and C₅ -paraffins. *Catalysis Today*, 16, pp. 91-98.
- Trivedi, B.C. and Culbertson, B.M., 1982. Maleic anhydride. New York: Plenum Press.

- Védrine, J.C., Hutchings, G.J., and Kiely, C.J., 2013. Molybdenum oxide model catalysts and vanadium phosphates as actual catalysts for understanding heterogeneous catalytic partial oxidation reactions: A contribution by Jean-Claude Volta. *Catalysis Today*, pp. 1–8.
- Volta, J.C., 1996. Dynamic process on vanadium phosphorus oxides for selective alkane oxidation. *Catalysis Today*, 32, pp. 29-36.
- Volta, J.C., 2000. Vanadium phosphorus oxides, a reference catalyst for mild oxidation of light alkanes: A review. *Chemistry*, 3, pp. 717-723.
- Waugh K.C. and Taufiq-Yap Y.H., 2003. The effect of varying the duration of the butane/air pretreatment on the morphology and reactivity of $(VO)_2P_2O_7$ catalysts. *Catalysis Today*, 81, pp. 215-225.
- Ye, D., Satsuma, A. and Hattori, T., 1990. Enhanced activity of promoted $(VO)_2P_2O_7$ by preferential exposure of the (0 2 0) plane. *Journal of the Chemical Society, Chemical Communications*, pp. 1337-1338.
- Ye, D., Satsuma, A. and Hattori, A., 1993. Effect of additives on the active sites of $(VO)_2P_2O_7$ catalysts. *Catalysis Today*, 16, pp. 113-121.
- Zazhigalov, V.A. et al., 1993. Properties of cobalt-promoted $(VO)_2P_2O_7$ in the oxidation of butane. *Applied Catalysis A-General*, 96, pp. 135-150.
- Zazhigalov, V.A. et al., 1996. *n*-Butane Oxidation on VPO catalysts. influence of alkali and alkaline-earth metal ions as additions. *Applied Catalysis A: General*, 134 (2), pp. 225–137.

Zazhigalov, V.A., Haber, J. and Stoch, J., 2001. The mechanism of *n*-pentane partial oxidation on VPO and VPBiO catalysts. *Catalysis Communications*, 2, pp. 375-378.

Zazhigalov, V.A., 2002. Effect of bismuth additives on the properties of vanadium-phosphorus oxide catalyst in the partial oxidation of *n*-pentane. *Kinetics and Catalysis*, 43, pp. 514-521.

Zeyss, S., Wendt, G. and Hallmeier, K.H., 1996. Influence of zirconium phosphate on the properties of $(VO)_2P_2O_7$ catalysts for the selective oxidation of *n*-butane to maleic anhydride. *Journal of the Chemical Society, Faraday Transactions*, 92, pp. 3273-3279.

List of Seminars/Conferences Participated:

- i. 1st seminar on Catalysis for A Sustainable World, Universiti Putra Malaysia, Serdang, Malaysia, August 7, 2009.
- ii. Malaysian Science and Technology Congress (MSTC) 2010, Crystal Crown Hotel, Petaling Jaya, Selangor, November 9, 2010 (Oral Presentation).
- iii. Shell Inter-Varsity Student Paper Presentation Contest (S-Spec) 2012, University Technology Malaysia, Johor, May 17-18, 2012.
- iv. 7th World Congress on Oxidation Catalysis (WCOC) 2013, Saint Louis, Missouri, U.S., June 9-12, 2013 (Poster and Oral Presentation).

APPENDICES

Appendix A

Calculation for the Gallium Dopant Used

$$\text{Molecular weight of VOPO}_4 \cdot 2\text{H}_2\text{O} = 197.9426 \text{ g mol}^{-1}$$

$$\begin{aligned} 10 \text{ g of VOPO}_4 \cdot 2\text{H}_2\text{O} &= \frac{10 \text{ g}}{197.9426 \text{ g mol}^{-1}} \\ &= 0.0505 \text{ mol} \end{aligned}$$

$$\begin{aligned} \text{Molecular weight of Ga(C}_5\text{H}_7\text{O}_2\text{)}_3 &= 69.723 \text{ g mol}^{-1} + 3 \times [(5 \times 12.0107 \text{ g mol}^{-1}) + (8 \times 1.0079 \text{ g mol}^{-1}) + \\ &\quad (2 \times 15.9994 \text{ g mol}^{-1})] \\ &= 370.0695 \text{ g mol}^{-1} \end{aligned}$$

Example of calculation:

For VPO_s-0.1% Ga

Since $\text{Ga} / \text{V} = 0.001$; $\text{V} = 0.0505 \text{ mol}$

Thus, the concentration of Ga = 0.0000505 mol

$$\begin{aligned} \text{Total mass of Ga needed} &= \text{No. of mole of Gallium needed} \times \\ &\quad \text{Molecular weight of Gallium(III) acetylacetonate} \\ &= 0.0000505 \text{ mol} \times 370.0695 \text{ g mol}^{-1} \\ &= 0.018689 \text{ g} \\ &= 18.689 \text{ mg} \end{aligned}$$

Thus, 10 g VOPO₄•2H₂O was added with 18.689 mg of Ga(acac)₃ to 150 cm³ of 1-butanol and reflux at 353 K.

Calculation for the Molybdenum Dopant Used

Molecular weight of VOPO₄•2H₂O = 197.9426 g mol⁻¹

$$\begin{aligned} 10 \text{ g of VOPO}_4 \cdot 2\text{H}_2\text{O} &= \frac{10 \text{ g}}{197.9426 \text{ g mol}^{-1}} \\ &= 0.0505 \text{ mol} \end{aligned}$$

$$\begin{aligned} \text{Molecular weight of MoO}_2 &= 95.94 \text{ g mol}^{-1} + (2 \times 15.999 \text{ g mol}^{-1}) \\ &= 127.94 \text{ g mol}^{-1} \end{aligned}$$

Example of calculation:

For VPO_s-1% Mo

Since Mo / V = 0.01 ; V = 0.0505 mol

Thus, the concentration of Mo = 0.000505 mol

Total mass of Mo needed = No. of mole of Molybdenum needed ×

$$\begin{aligned} &\text{Molecular weight of Molybdenum(IV) Oxide} \\ &= 0.000505 \text{ mol} \times 127.94 \text{ g mol}^{-1} \\ &= 0.06461 \text{ g} \\ &= 64.61 \text{ mg} \end{aligned}$$

Thus, 10 g VOPO₄•2H₂O was added with 64.61 mg of MoO₂ to 150 cm³ of 1-butanol and reflux at 353 K.

APPENDIX B

X-ray Diffraction (XRD) Analyses

Calculation of Crystallite Size by Using Powder XRD Technique

$$FWHM \text{ (rad)} = FWHM \text{ (}^\circ\text{)} \times \left(\frac{\pi}{180^\circ} \right)$$

According to Scherrer's formula,

$$\text{Crystallite size, } T \text{ (}\text{\AA}\text{)} = \frac{0.89 \lambda}{FWHM \times \cos \theta}$$

Given $\lambda_{\text{Cu K}\alpha} = 1.54 \text{ \AA}$

Example of calculation steps to determine the crystallite size are shown as below by using VPOs-Undoped data.

Plane	2θ	θ	FWHM ($^\circ$)	FWHM (rad)
(020)	22.8237	11.4119	1.3697	0.0239
(204)	28.4030	14.2015	0.7492	0.0131
(221)	29.6748	14.8374	1.1097	0.0194

Peak appears at $2\theta = 22.8237$ correspond to (020) plane.

$$FWHM \text{ (rad)} = 1.1754^\circ \times \left(\frac{\pi}{180^\circ} \right)$$

$$= 0.0205$$

$$T \text{ (}\text{\AA}\text{)} = \frac{0.89 \times 1.54 \text{ \AA}}{0.0205 \times \cos 11.4119}$$

$$= 58.4898 \text{ \AA}$$

Peak appears at $2\theta = 28.4030$ correspond to (204) plane.

$$T \text{ (}\text{\AA}\text{)} = \frac{0.89 \times 1.54 \text{ \AA}}{0.0205 \times \cos 14.2015} = 108.1224 \text{ \AA}$$

For VPOs-0.1% Ga

Plane	2 θ	θ	FWHM (°)	FWHM (rad)
(020)	22.8606	11.4303	1.1754	0.0205
(204)	28.4356	14.2178	0.7382	0.0129
(221)	29.8842	14.9421	0.7664	0.0134

For VPOs-0.3% Ga

Plane	2 θ	θ	FWHM (°)	FWHM (rad)
(020)	22.9477	11.4739	0.9760	0.0170
(204)	28.4664	14.2332	0.7592	0.0133
(221)	29.9507	14.9754	0.6734	0.0118

For VPOs-0.5% Ga

Plane	2 θ	θ	FWHM (°)	FWHM (rad)
(020)	22.9486	11.4743	1.0212	0.0178
(204)	28.4664	14.2332	0.7476	0.0130
(221)	29.9507	14.9754	0.7127	0.0124

For VPOs-1% Mo

Plane	2 θ	θ	FWHM (°)	FWHM (rad)
(020)	22.8634	11.4317	1.2283	0.0214
(204)	28.4619	14.2310	0.7217	0.0126
(221)	29.9200	14.9600	0.6934	0.0121

For VPOs-3% Mo

Plane	2 θ	θ	FWHM (°)	FWHM (rad)
(020)	22.9201	11.4600	1.1779	0.0206
(204)	28.5910	14.2955	0.7274	0.0127
(221)	29.9200	14.9600	0.7786	0.0136

For VPOs-5% Mo

Plane	2 θ	θ	FWHM (°)	FWHM (rad)
(020)	22.8883	11.4442	1.0406	0.0182
(204)	28.4400	14.2200	0.7180	0.0125
(221)	29.2400	14.6200	1.9334	0.0337

For VPOs-0.1%Ga1%Mo-18

Plane	2 θ	θ	FWHM (°)	FWHM (rad)
(020)	22.6705	11.3353	1.7840	0.0311
(204)	28.4171	14.2086	0.7081	0.0124
(221)	29.8392	14.9196	0.7251	0.0127

For VPOs-0.1%Ga1%Mo-36

Plane	2 θ	θ	FWHM (°)	FWHM (rad)
(020)	22.9109	11.4555	1.1513	0.0201
(204)	28.4815	14.2408	0.7598	0.0133
(221)	29.9510	14.9755	0.7633	0.0133

For VPOs-0.1%Ga1%Mo-54

Plane	2 θ	θ	FWHM (°)	FWHM (rad)
(020)	22.8872	11.4436	1.1497	0.0201
(204)	28.4464	14.2232	0.7845	0.0137
(221)	29.9340	14.9670	0.7880	0.0138

For VPOs-0.1%Ga1%Mo-72

Plane	2 θ	θ	FWHM (°)	FWHM (rad)
(020)	22.8139	11.4070	1.1671	0.0204
(204)	28.3865	14.1933	0.7257	0.0127
(221)	29.8650	14.9325	0.7412	0.0129

APPENDIX C

Preparation of Solutions Used in ICP-OES

Preparation of 8 M HNO₃

$$\begin{aligned}\text{Molarity for 65 \% of HNO}_3 &= \frac{\text{Density of HNO}_3}{\text{Molecular Weight of HNO}_3} \times \frac{65}{100} \times 1000 \\ &= \frac{1.4090 \text{ g cm}^{-3}}{63.0130 \text{ g mol}^{-1}} \times \frac{65}{100} \times 1000 \\ &= 14.5343 \text{ mol L}^{-1} \\ &= 14.5343 \text{ M}\end{aligned}$$

$$M_1V_1 = M_2V_2$$

where,

M_1 = concentration of 65 % of HNO₃ (14.5343 M)

V_1 = volume of 65 % of HNO₃

M_2 = concentration of 8 M HNO₃

V_2 = volume of 8 M HNO₃

$$M_1V_1 = M_2V_2$$

$$(14.5343 \text{ M}) V_1 = (8 \text{ M})(250 \text{ mL})$$

$$\begin{aligned}V_1 &= \frac{(8 \text{ M})(250 \text{ mL})}{14.5343 \text{ M}} \\ &= 137.65 \text{ mL}\end{aligned}$$

Thus, 137.65 mL of 65 % of HNO₃ was diluted to 250 mL with deionised water.

Preparation of Stock Solution of Phosphorus, P

Molecular weight of $\text{NH}_4\text{H}_2\text{PO}_4$

$$= (14.0067 + 10079 \times 4 + 30.9738 + 15.9994 \times 4) \text{ g mol}^{-1}$$

$$= 115.0255 \text{ g mol}^{-1}$$

Atomic weight of P = $30.9738 \text{ g mol}^{-1}$

50 ppm of stock solution for P = 50 mg L^{-1}

$$= 0.05 \text{ g L}^{-1}$$

$$\text{Number of mole of P} = \frac{0.05 \text{ g L}^{-1}}{30.9738 \text{ g mol}^{-1}}$$

$$= 1.6145 \times 10^{-3} \text{ mol L}^{-1}$$

Mass of $\text{NH}_4\text{H}_2\text{PO}_4$ = $1.6145 \times 10^{-3} \text{ mol L}^{-1} \times 115.0255 \text{ g mol}^{-1}$

$$= 0.1857 \text{ g L}^{-1}$$

Thus, 0.1857 g of $\text{NH}_4\text{H}_2\text{PO}_4$ was transferred into 1000 mL volumetric flask and top up with deionised water.

Preparation of standard solution of phosphorus, P

$$M_1V_1 = M_2V_2$$

where,

M_1 = concentration of stock solution (50 ppm)

V_1 = volume of stock solution

M_2 = concentration of standard solution

V_2 = volume of standard solution (250 mL)

Example of calculation for standard solution of 20 ppm

$$M_1V_1 = M_2V_2$$

$$(50 \text{ ppm}) V_1 = (20 \text{ ppm})(250 \text{ mL})$$

$$V_1 = \frac{(20 \text{ ppm})(250 \text{ mL})}{50 \text{ ppm}}$$

$$= 100 \text{ mL}$$

Thus, 100 mL of stock solution for phosphorus was dissolved in 8 M HNO₃ then diluted to 250 mL with deionised water to produce 20 ppm standard solution of phosphorus.

Preparation of Stock Solution of Vanadium, V

Molecular weight of NH_4VO_3

$$= (14.0067 + 10079 \times 4 + 50.9415 + 15.9994 \times 3) \text{ g mol}^{-1}$$

$$= 116.9780 \text{ g mol}^{-1}$$

Atomic weight of V = $50.9415 \text{ g mol}^{-1}$

50 ppm of stock solution for V = 50 mg L^{-1}

$$= 0.05 \text{ g L}^{-1}$$

Mass of $\text{NH}_4\text{VO}_3 = 9.8155 \times 10^{-4} \text{ mol} \times 116.9780 \text{ g mol}^{-1}$

$$= 0.1148 \text{ g L}^{-1}$$

Thus, 0.1148 g of NH_4VO_3 was transferred into 1000 mL volumetric flask and top up with deionised water.

Preparation of standard solution of vanadium, V

$$M_1V_1 = M_2V_2$$

where,

M_1 = concentration of stock solution (50 ppm)

V_1 = volume of stock solution

M_2 = concentration of standard solution

V_2 = volume of standard solution (250 mL)

Example of calculation for standard solution of 10 ppm

$$M_1V_1 = M_2V_2$$

$$(50 \text{ ppm}) V_1 = (10 \text{ ppm})(250 \text{ mL})$$

$$V_1 = \frac{(10 \text{ ppm})(250 \text{ mL})}{50 \text{ ppm}}$$
$$= 50 \text{ mL}$$

Thus, 50 mL of stock solution for phosphorus was dissolved in 8 M HNO₃ then diluted to 250 mL with deionised water to produce 10 ppm standard solution of phosphorus.

Preparation of Stock Solution of Gallium, Ga

Molecular weight of Ga(acac)₃ / Ga(C₅H₈O₂)₃

$$= 69.723 \text{ g mol}^{-1} + 3 \times [(5 \times 12.0107 \text{ g mol}^{-1}) + (8 \times 1.0079 \text{ g mol}^{-1}) + (2 \times 15.9994 \text{ g mol}^{-1})]$$
$$= 370.0695 \text{ g mol}^{-1}$$

Atomic weight of Ga = 69.723 g mol⁻¹

50 ppm of stock solution for V = 50 mg / L

$$= 0.05 \text{ g / L}$$

$$\text{Number of mole of Ga} = \frac{0.05 \text{ g L}^{-1}}{69.723 \text{ g mol}^{-1}}$$

$$= 7.1712 \times 10^{-4} \text{ mol L}^{-1}$$

Mass of Ga(acac)₃ = 7.1712 × 10⁻⁴ mol L⁻¹ × 370.0695 g mol⁻¹

$$= 0.2654 \text{ g L}^{-1}$$

Thus, 0.2654 g of Ga(acac)₃ was transferred into 1000 mL volumetric flask and top up with deionised water.

Preparation of standard solution of gallium, Ga

$$M_1V_1 = M_2V_2$$

where,

M₁ = concentration of stock solution (50 ppm)

V₁ = volume of stock solution

M₂ = concentration of standard solution

V₂ = volume of standard solution (250 mL)

Example of calculation for standard solution of 5 ppm

$$M_1V_1 = M_2V_2$$

$$(50 \text{ ppm}) V_1 = (5 \text{ ppm})(250 \text{ mL})$$

$$V_1 = \frac{(5 \text{ ppm})(250 \text{ mL})}{50 \text{ ppm}}$$

$$= 25 \text{ mL}$$

Thus, 25 mL of stock solution for phosphorus was dissolved in 8 M HNO₃ then diluted to 250 mL with deionised water to produce 5 ppm standard solution of phosphorus.

Preparation of Stock Solution of Gallium, Mo

$$\begin{aligned} \text{Molecular weight of MoO}_2 &= 95.94 \text{ g mol}^{-1} + (2 \times 15.9994 \text{ g mol}^{-1}) \\ &= 127.94 \text{ g mol}^{-1} \end{aligned}$$

Atomic weight of Mo = 95.94 g mol⁻¹

50 ppm of stock solution for V = 50 mg / L

$$= 0.05 \text{ g / L}$$

$$\text{Number of mole of Mo} = \frac{0.05 \text{ g L}^{-1}}{95.94 \text{ g mol}^{-1}}$$

$$= 5.2116 \times 10^{-4} \text{ mol L}^{-1}$$

Mass of MoO₂ = 2.2116 × 10⁻⁴ mol L⁻¹ × 127.94 g mol⁻¹

$$= 0.067 \text{ g L}^{-1}$$

Thus, 0.067 g of MoO₂ was transferred into 1000 mL volumetric flask and top up with deionised water.

Preparation of standard solution of molybdenum, Mo

$$M_1V_1 = M_2V_2$$

where,

M₁ = concentration of stock solution (50 ppm)

V₁ = volume of stock solution

M₂ = concentration of standard solution

V₂ = volume of standard solution (250 mL)

Example of calculation for standard solution of 5 ppm

$$M_1V_1 = M_2V_2$$

$$(50 \text{ ppm}) V_1 = (5 \text{ ppm})(250 \text{ mL})$$

$$V_1 = \frac{(5 \text{ ppm})(250 \text{ mL})}{50 \text{ ppm}}$$

$$= 25 \text{ mL}$$

Thus, 25 mL of stock solution for phosphorus was dissolved in 8 M HNO₃ then diluted to 250 mL with deionised water to produce 5 ppm standard solution of phosphorus.

Preparation of 100 ppm sample solution

$$\begin{aligned} 0.025 \text{ g sample in } 250 \text{ mL} &= \frac{0.025 \text{ g}}{250 \text{ mL of HNO}_3} \\ &= \frac{0.1 \text{ g}}{1000 \text{ mL of HNO}_3} \\ &= 0.1 \times 10^3 \text{ mg L}^{-1} \\ &= 100 \text{ ppm} \end{aligned}$$

Thus, 0.0250 g of sample was transferred into 250 mL volumetric flask and dissolved by 10 mL of 8 M HNO₃. Then, top up to 250 mL with deionised water to produce 100 ppm sample solution.

APPENDIX D

Inductively Coupled Plasma-Optical Emission Spectrometry (ICP-OES)

Calculation of P/V and Ga/V mole ratio by using ICP-OES analysis

$$\frac{P}{V} = \frac{\text{Concentration of P/Atomic Weight of P}}{\text{Concentration of V/ Atomic Weight of V}}$$

$$\frac{Ga}{V} = \frac{\text{Concentration of Ga/Atomic Weight of Ga}}{\text{Concentration of V/ Atomic Weight of V}}$$

Example of calculation

For VPO_s-Ga0.1%

$$\begin{aligned} \frac{P}{V} &= \frac{12.53 \text{ mgL}^{-1}/30.9738 \text{ mgL}^{-1}}{15.74 \text{ mgL}^{-1}/ 50.9415 \text{ mgL}^{-1}} \\ &= 1.3093 \end{aligned}$$

The P/V atomic ratio for VPO_s-0.1% Ga is 1.31.

APPENDIX E

Preparation of Solutions Used in Redox Titration

Preparation of 2M sulphuric acid, H₂SO₄ solution

Concentrated H₂SO₄ (95-98 %)

$$1 \text{ L} = 1.84 \text{ kg} = 1840 \text{ g} / 1000 \text{ cm}^3$$

$$= 1.84 \text{ g} / \text{cm}^3$$

M_r of H₂SO₄ = 98.07 g/mol

$$\text{Concentration of 95-98 \% H}_2\text{SO}_4 = \frac{1.84 \text{ g} / \text{cm}^3}{98.07 \text{ g} / \text{mol}} \times \frac{95}{100} \times 1000 = 17.82 \text{ M}$$

$$M_1V_1 = M_2V_2$$

where M₁ = concentration of 95-98 % H₂SO₄

M₂ = concentration of diluted H₂SO₄ (2 M)

V₁ = volume of 95-98 % H₂SO₄

V₂ = volume of diluted H₂SO₄ (2 M)

$$(17.82 \text{ M})(V_1) = (2 \text{ M})(1000 \text{ cm}^3)$$

$$V_1 = 112.23 \text{ cm}^3$$

Preparation of 0.1 M sulphuric acid, H₂SO₄ solution

$$M_1V_1 = M_2V_2$$

where M₁ = concentration of 95-98 % H₂SO₄

M₂ = concentration of diluted H₂SO₄ (0.1 M)

V₁ = volume of 95-98 % H₂SO₄

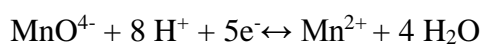
V₂ = volume of diluted H₂SO₄ (0.1 M)

$$(17.82 \text{ M})(V_1) = (0.1 \text{ M})(1000 \text{ cm}^3)$$

$$V_1 = 5.61 \text{ cm}^3$$

Preparation of 0.01 N potassium permanganate, KMnO_4

$$\text{Normality, } N \text{ (eq/L)} = M \text{ (mol/L)} \times n \text{ (eq/mol)}$$



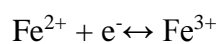
$$\begin{aligned} \text{Molarity, } M \text{ (mol/L)} &= \frac{N \text{ (eq/L)}}{n \text{ (eq/mol)}} \\ &= \frac{0.01}{5} \\ &= 0.002 \text{ M} \end{aligned}$$

$$M_r \text{ of } \text{KMnO}_4 = 158.04 \text{ g/mol}$$

$$\begin{aligned} \text{Weight for } \text{KMnO}_4 \text{ in } 1000 \text{ cm}^3 \text{ diluted (0.1 M) H}_2\text{SO}_4 &= 0.002 \times 158.04 \\ &= 0.3161 \text{ g} \end{aligned}$$

Preparation of 0.01 N ammonium iron (II) sulphate, $(\text{NH}_4)_2\text{Fe}(\text{SO}_4)_2 \cdot 6\text{H}_2\text{O}$

$$\text{Normality, } N \text{ (eq/L)} = M \text{ (mol/L)} \times n \text{ (eq/mol)}$$



$$\begin{aligned} \text{Molarity, } M \text{ (mol/L)} &= \frac{N \text{ (eq/L)}}{n \text{ (eq/mol)}} \\ &= \frac{0.01}{1} \\ &= 0.01 \text{ M} \end{aligned}$$

$$M_r \text{ of } (\text{NH}_4)_2\text{Fe}(\text{SO}_4)_2 \cdot 6\text{H}_2\text{O} = 391.99 \text{ g/mol}$$

$$\begin{aligned} & \text{Weight for } (\text{NH}_4)_2\text{Fe}(\text{SO}_4)_2 \cdot 6\text{H}_2\text{O} \text{ in } 1000 \text{ cm}^3 \text{ diluted } (0.1 \text{ M}) \text{ H}_2\text{SO}_4 \\ & = 0.01 \times 391.99 \\ & = 3.9199 \text{ g} \end{aligned}$$

Preparation of Diphenylamine, Ph₂NH, indicator

1 g of diphenylamine was weighed and dissolved in a few ml of concentrated sulphuric acid, H₂SO₄. Then the solution was transferred to a 100 ml volumetric flask and further top up with concentrated H₂SO₄.

APPENDIX F

Calculation of Average Oxidation State of Vanadium (V_{AV})

According to Niwa and Murakami (1982),

$$V^{4+} + 2V^{3+} = 20 [\text{MnO}_4^-] V_1$$

$$V^{5+} + V^{4+} + V^{3+} = 20 [\text{Fe}^{2+}] V_2$$

$$V^{5+} = 20 [\text{Fe}^{2+}] V_3$$

$$[\text{MnO}_4^-] = 0.01$$

$$[\text{Fe}^{2+}] = 0.01$$

$$V^{4+} + 2V^{3+} = 0.2 V_1 \quad (1)$$

$$V^{5+} + V^{4+} + V^{3+} = 0.2 V_2 \quad (2)$$

$$V^{5+} = 0.2 V_3 \quad (3)$$

(2)-(3),

$$V^{4+} + V^{3+} = 0.2 V_2 - 0.2 V_3 \quad (4)$$

$$V^{4+} = 0.2 V_2 - 0.2 V_3 - V^{3+} \quad (5)$$

Substitute (5) to (1),

$$0.2 V_2 - 0.2 V_3 - V^{3+} + 2V^{3+} = 0.2 V_1$$

$$V^{3+} = 0.2 V_1 - 0.2 V_2 + 0.2 V_3 \quad (6)$$

Substitute (6) to (5),

$$V^{4+} = 0.4 V_2 - 0.4 V_3 - 0.2 V_1$$

Therefore;

$$V^{5+} = 0.2V_3$$

$$V^{4+} = 0.4 V_2 - 0.4 V_3 - 0.2 V_1$$

$$V^{3+} = 0.2 V_1 - 0.2 V_2 + 0.2 V_3$$

Average Oxidation State:

$$V_{AV} = \frac{3 V^{3+} + 4 V^{4+} + 5 V^{5+}}{V^{3+} + V^{4+} + V^{5+}}$$

Calculation steps to determine the average oxidation state of vanadium are shown as below by using VPO_s-0.1% Ga catalyst:

$$V_1 = 11.13 \quad V_2 = 14.73 \quad V_3 = 3.30$$

$$\begin{aligned} \text{From (5): } V^{3+} &= 20 (0.01) V_1 - 20 (0.01) V_2 + 20 (0.01) V_3 \\ &= 0.2 V_1 - 0.2 V_2 + 0.2 V_3 \\ &= 0.2 (11.13 \text{ cm}^3) - 0.2 (14.73 \text{ cm}^3) + 0.2 (3.30 \text{ cm}^3) \\ &= -0.06 \text{ cm}^3 \end{aligned}$$

$$\begin{aligned} \text{From (6): } V^{4+} &= 40 (0.01) V_2 - 40 (0.01) V_3 - 20 (0.01) V_1 \\ &= 0.4 V_2 - 0.4 V_3 - 0.2 V_1 \\ &= 0.4 (14.73 \text{ cm}^3) - 0.4 (3.30 \text{ cm}^3) - 0.2 (11.13 \text{ cm}^3) \\ &= 2.35 \text{ cm}^3 \end{aligned}$$

$$\begin{aligned}
\text{From (7): } V^{5+} &= 20 (0.01) V_3 \\
&= 0.2 V_3 \\
&= 0.2 (3.30 \text{ cm}^3) \\
&= 0.66 \text{ cm}^3
\end{aligned}$$

The average oxidation state of vanadium is calculated as

$$V_{AV} = \frac{3V^{3+} + 4V^{4+} + 5V^{5+}}{V^{3+} + V^{4+} + V^{5+}}$$

Since the value for V^{3+} was negative, it was negligible,

$$\begin{aligned}
V_{AV} &= \frac{3(0) + 4(2.35 \text{ cm}^3) + 5(0.66 \text{ cm}^3)}{0 + (2.35 \text{ cm}^3) + (0.66 \text{ cm}^3)} \\
&= 4.2196
\end{aligned}$$

Since V_{AV} of $VPO_5-0.1\% \text{ Ga} = 4.2196$

$$\begin{aligned}
\text{Thus } V^{5+} (\%) &= 21.96 \% \\
V^{4+} (\%) &= (100-21.96) \% \\
&= 78.04 \%
\end{aligned}$$

APPENDIX G

Calculation of TPR in H₂ Analysis

Total oxygen removed (atom g⁻¹)

$$= \text{Amount of oxygen removed } (\mu \text{ mol g}^{-1}) \times 6.022 \times 10^{23} \text{ atom mol}^{-1}$$

$$= \text{Amount of oxygen removed (atom g}^{-1}\text{)}$$

Example of calculation

For VPOs-0.1% Ga

$$\text{Total oxygen atom removed} = (903.8556 + 2600.4750) \mu\text{mol/g}$$

$$= 3.5043 \times 10^{-3} \text{ mol/g}$$

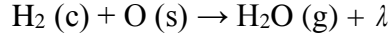
$$= 3.5043 \times 10^{-3} \text{ mol/g} \times 6.022 \times 10^{23} \text{ atom/mol}$$

$$= 2.1103 \times 10^{21} \text{ atom/g}$$

Appendix H

Calculation of Reduction Activation Energy (E_r) for TPR in H_2 Analysis

Calculation step to obtain reduction activation energy, E_r



where (s) = surface or lattice oxygen species; (c) = chemisorbed species

(g) = gaseous species; λ = oxygen vacancy

$$\text{Rate} = k[H_2]_m[O_s]$$

$$-\frac{d[H_2]}{dt} = A \exp\left(\frac{-E_r}{RT_m}\right) [H_2]_m [O_s] \quad (1)$$

Setting the derivative of equation (1) to zero at T_m gives the modified version of Redhead (1962) equation:

$$\frac{E_r}{RT_m^2} = \left(\frac{A_r}{\beta}\right) [H_2]_m \exp\left(\frac{-E_r}{RT_m}\right) \quad (2)$$

From the Arrhenius (1889) equation,

$$k_1 = A \exp\left(\frac{-E_r}{RT_m}\right) \quad (3)$$

Therefore from equation (2),

$$k_2 = A[H_2]_m \exp\left(\frac{-E_r}{RT_m}\right) \quad (4)$$

Since k_1 and k_2 are the same at T_m and let $k = \chi$ at T_m

$$\frac{\chi}{A[H_2]_m} = \exp\left(\frac{-E_r}{RT_m}\right) \text{ or } \frac{A[H_2]_m}{\chi} = \exp\left(\frac{E_r}{RT_m}\right)$$

$$\frac{E_r}{RT_m} = \ln\left(\frac{A[H_2]_m}{\chi}\right)$$

$$E_r = RT_m \ln\left(\frac{A[H_2]_m}{\chi}\right)$$

where, R = 0.001987 kcal K⁻¹ mol⁻¹; 82.056 cm³ atm K⁻¹ mol⁻¹

A = 10¹³ s⁻¹

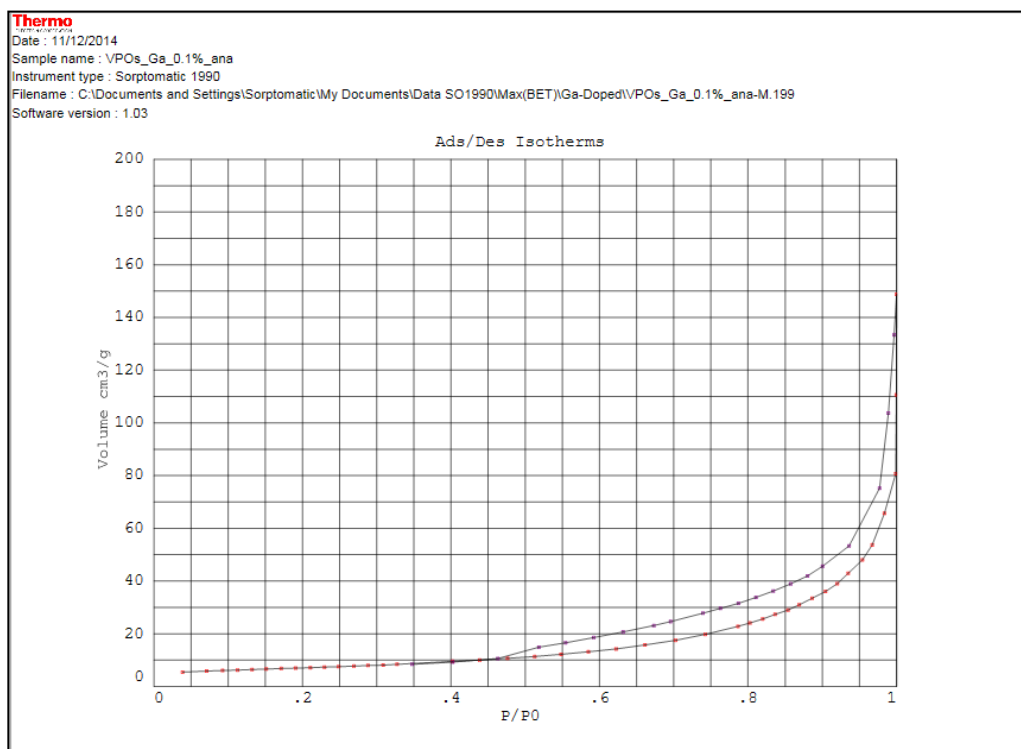
T_m = maxima temperature of the peak

E_r = reduction activation energy

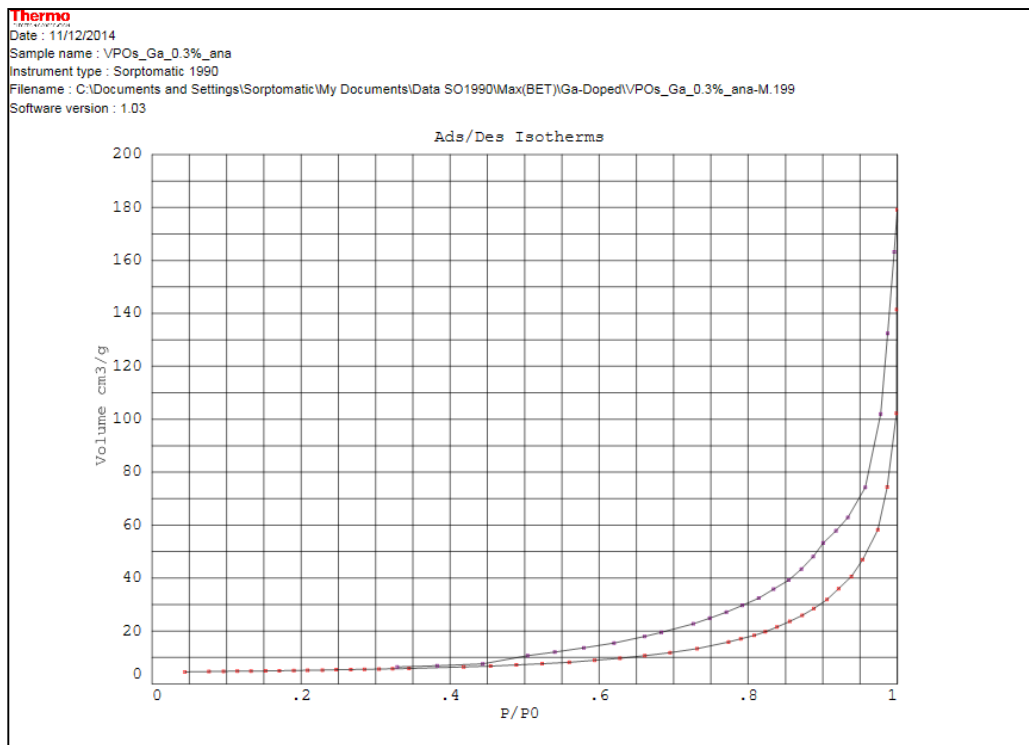
APPENDIX I

BET Analysis: Nitrogen Adsorption Curves

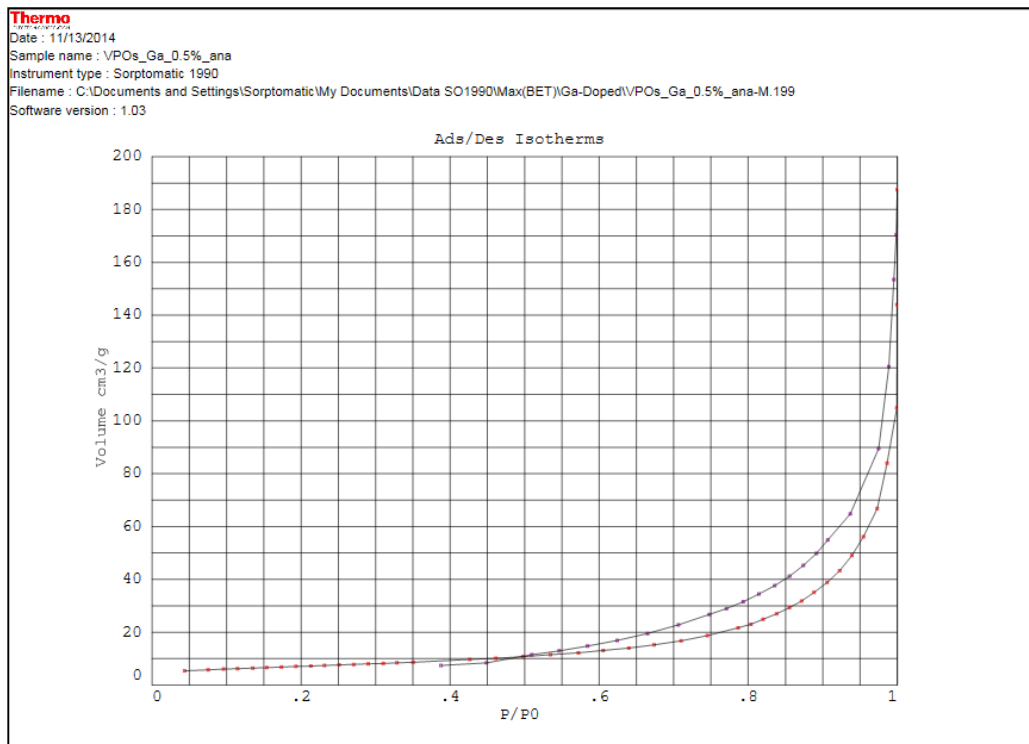
For VPOs-0.1% Ga



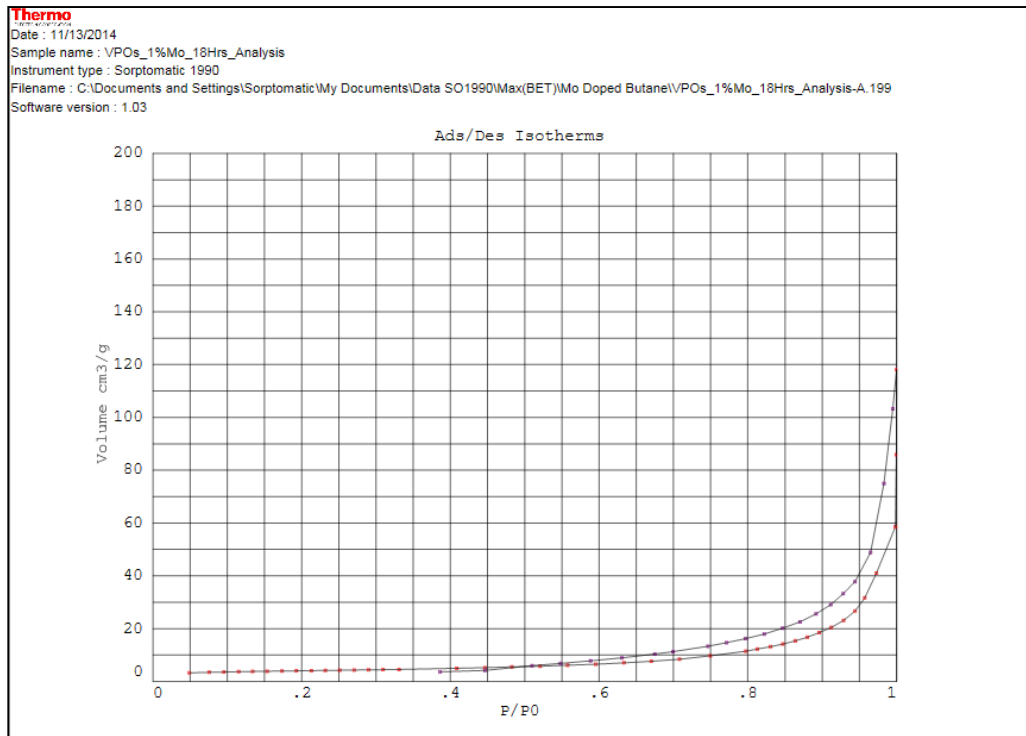
For VPOs-0.3% Ga



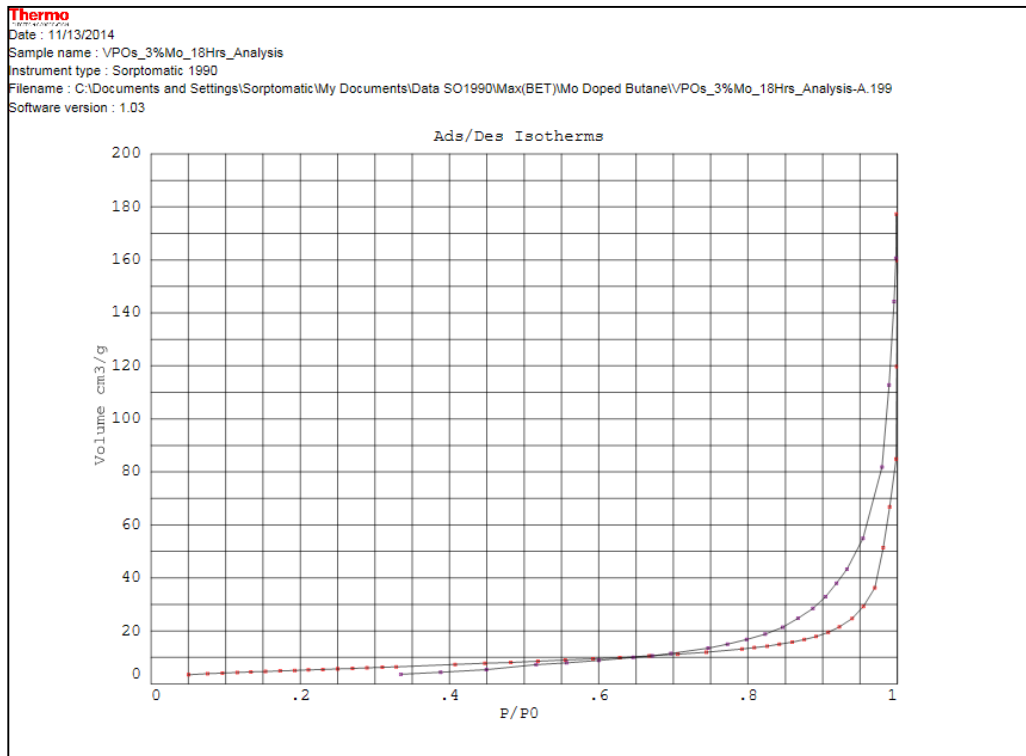
For VPOs-0.5% Ga



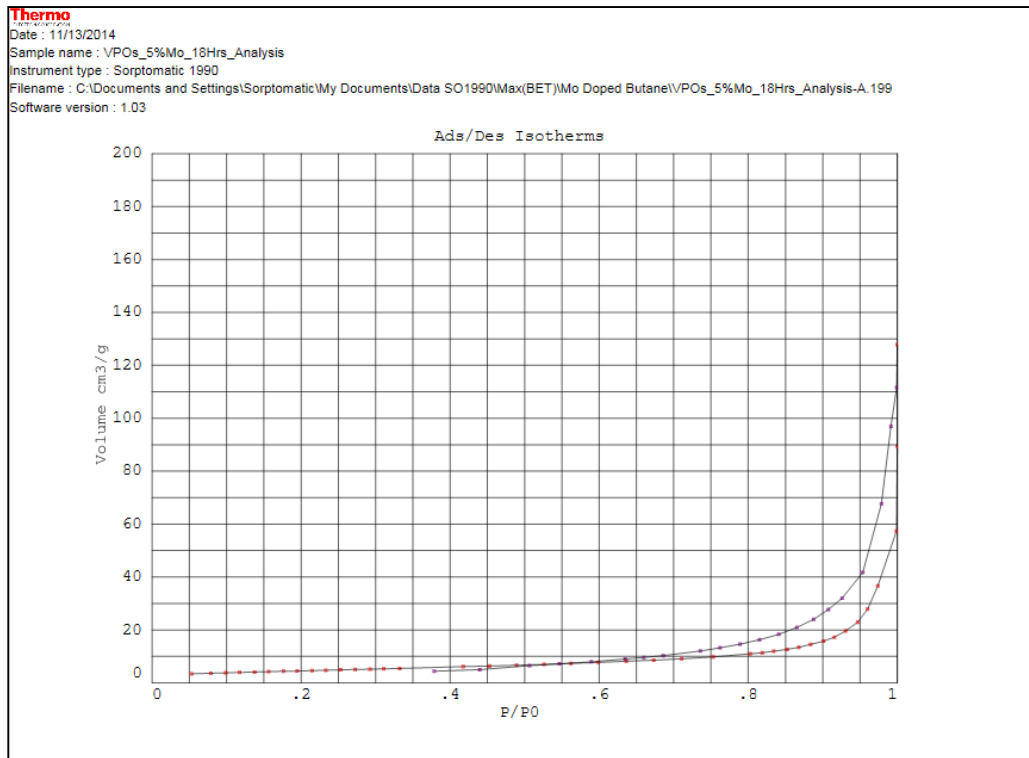
For VPOs-1% Mo



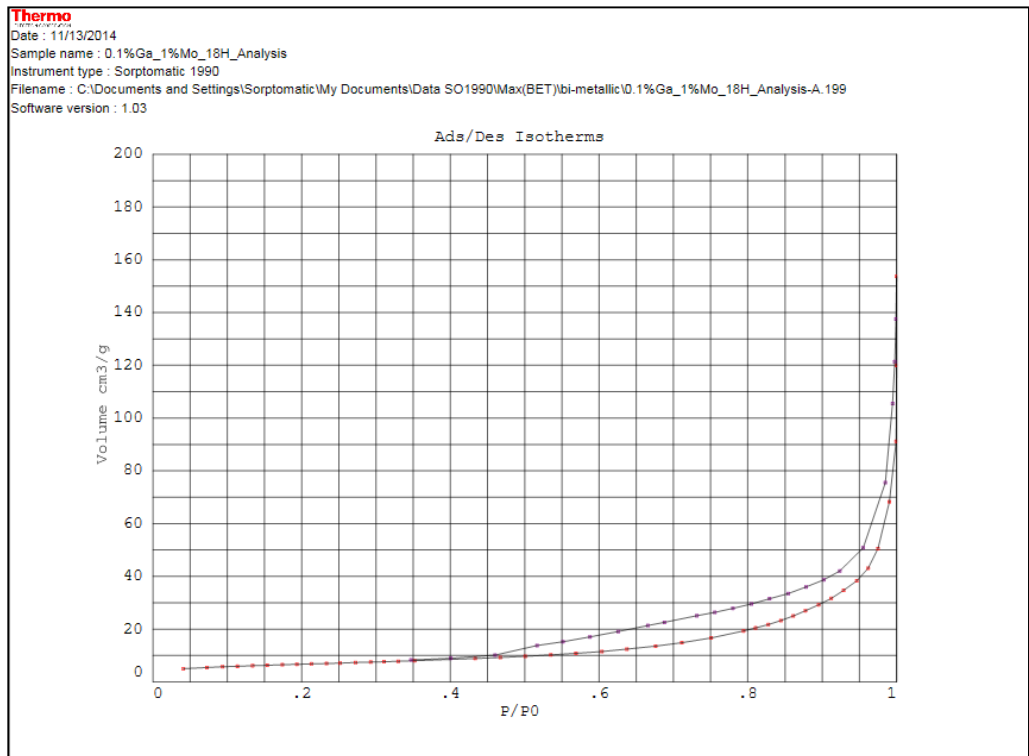
For VPOs-3% Mo



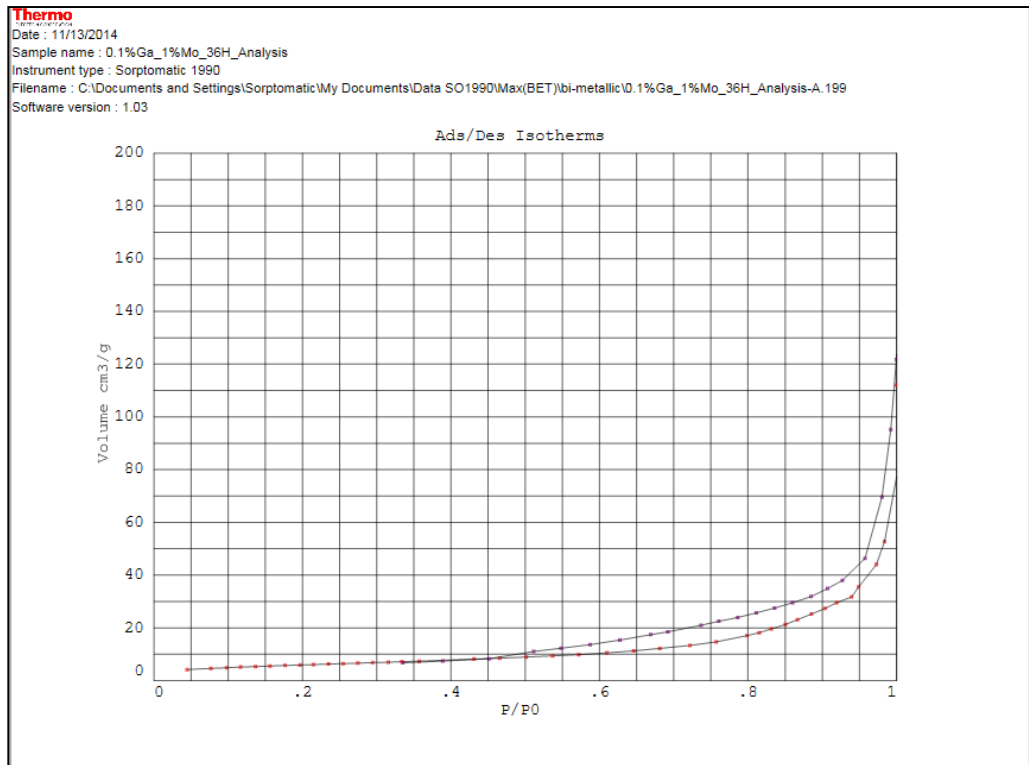
For VPOs-5% Mo



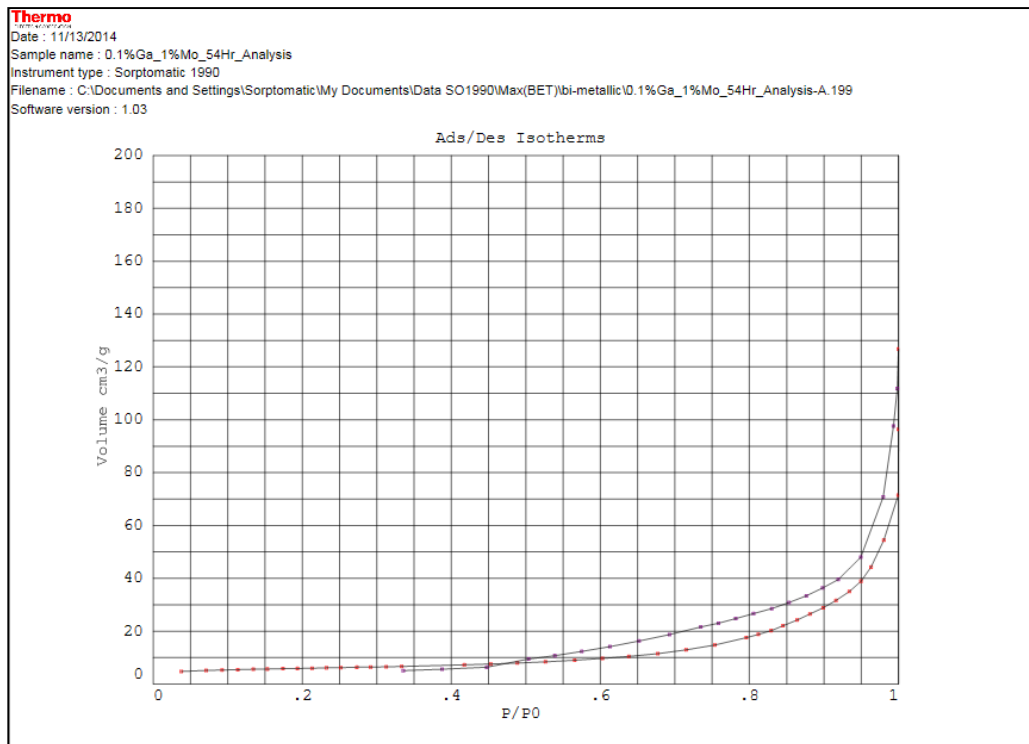
For VPOs-0.1% Ga 1% Mo-18



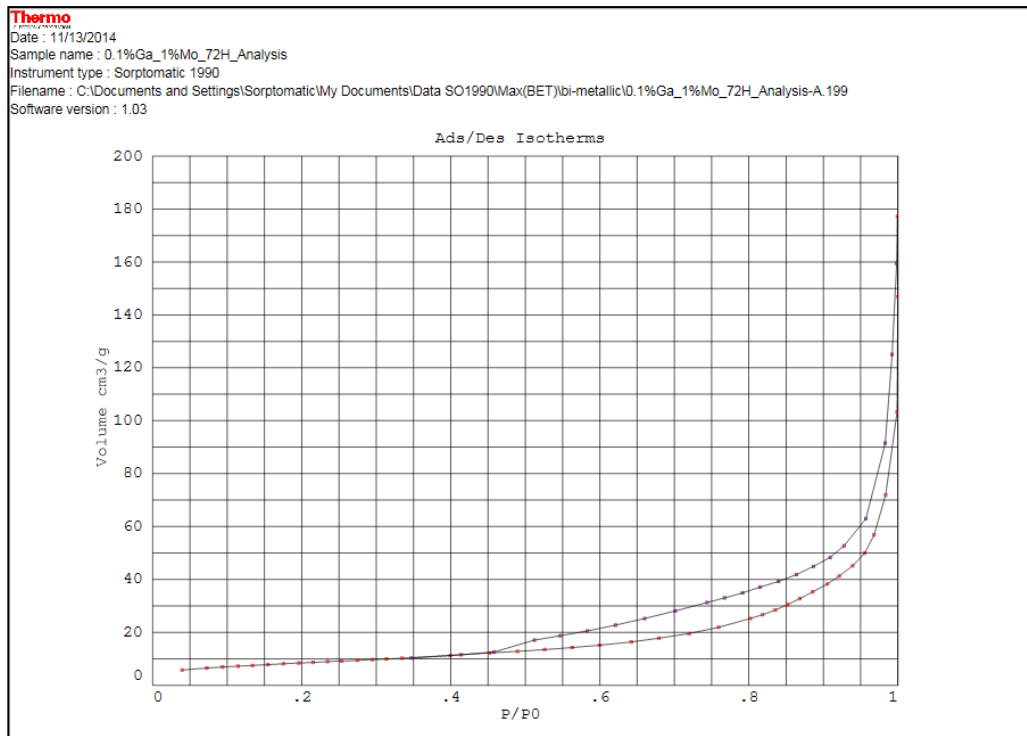
For VPOs-0.1%Ga1%Mo-36



For VPOs-0.1%Ga1%Mo-54



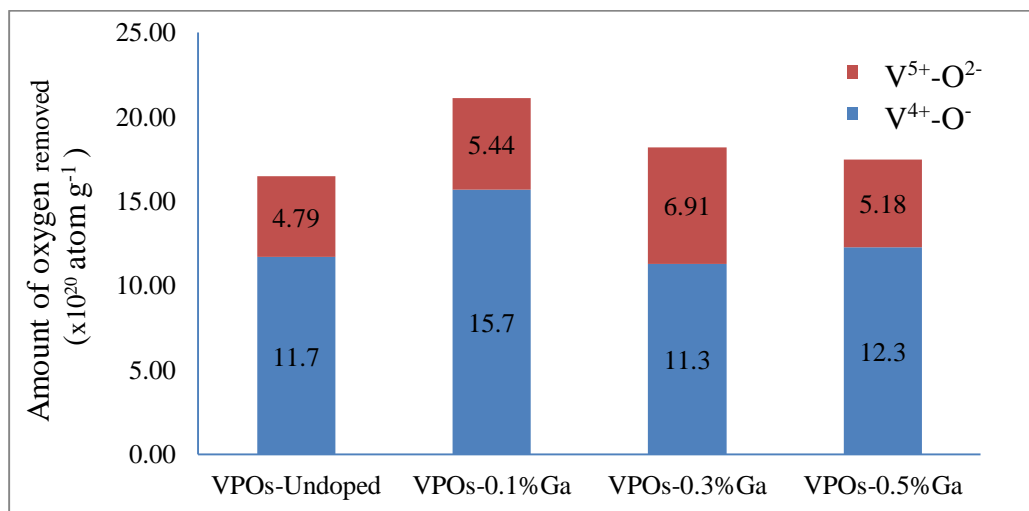
For VPOs-0.1%Ga1%Mo-72



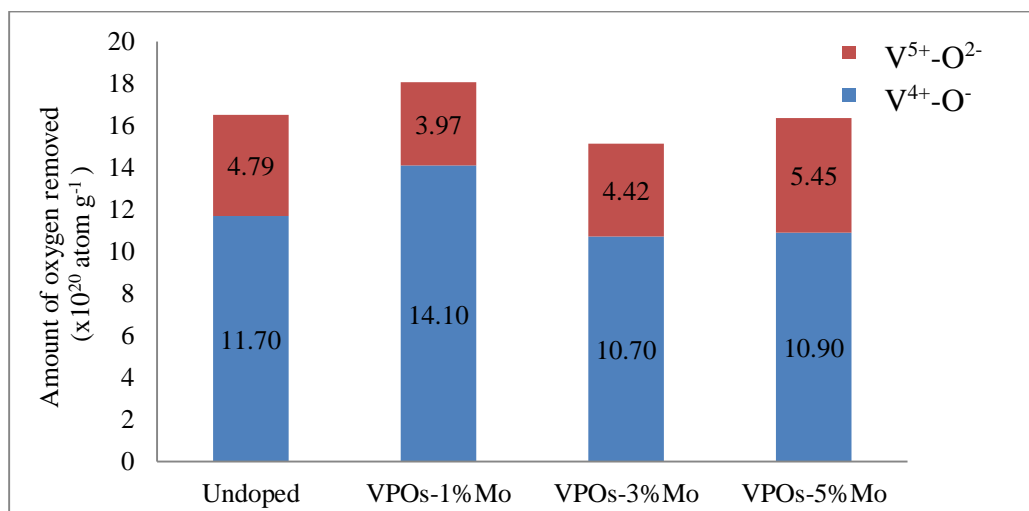
APPENDIX J

The summaries of total amount of oxygen removed by TPR in H_2

For Ga doped VPOs catalysts



For Mo doped VPOs catalysts



For Ga-Mo doped VPOs catalysts

